MASTER THESIS

Comparison of limit finite element analysis and strength reduction techniques

Ivo Raissakis, B.Sc.

Institute of Soil Mechanics and Foundation Engineering
Graz University of Technology

Advisors:

Ao.Univ.-Prof. Dipl.-Ing. Dr.techn. M.Sc. Helmut Schweiger
Institute of Soil Mechanics and Foundation Engineering
Graz University of Technology

Dipl.-Ing. Franz Tschuchnigg
Institute of Soil Mechanics and Foundation Engineering
Graz University of Technology

Graz, August 2012

Declaration

I hereby declare that this submission is my own work and that, to the best of my knowledge and belief, it contains no material previously published or written by another person nor material which to a substantial extent has been accepted for the award of any other degree or diploma of the university or other institute of higher learning, except where due acknowledgment has been made in the text.

Graz, August 2012 Ivo Raissakis

Acknowledgements

Firstly, I like to take this opportunity to thank the people who provided scientific and financial support to make this work possible. I thank Prof. Helmut Schweiger who initiated the thesis and gave me the opportunity to pursue parts of the work at the University of Newcastle in Australia. I must also thank Prof. Scott Sloan and his research group who offered me a warm welcome and generously provided all the information and assistance I needed.

My sincere thanks go to many friends and colleagues, not only for scientific discussion, also for the great and challenging times we shared throughout our studies. I only name a few of them with whom I spent a considerable amount of time working on projects and studying for exams. These are, Hans Georg Leitinger, Hanns Schinner und Peter Joachim Heinrich.

I must gratefully acknowledge other close personal friends, like Philipp Römer, Stefan Tödtling and many more, for the great times and memorable moments we had. I believe my joyful free time during University was a necessity to stay focused and fully energized while studying and researching. A very special thanks belongs to the people, especially the Family Dube, who made my stay in Australia an everlasting memory.

Last but by no means least, I like to thank my whole family for general education and the support provided over all these years. In particular, I thank my parents who set the framework for my life and academic education, intellectually and temperamentally. I also thank Arno Lerchbaumer for his ongoing support and assistance in every aspect.

Abstract

Strength reduction techniques are often applied in displacement based finite element methods to analyse the stability of geotechnical structures. In this approach, the loads are kept constant and the material strength is reduced until excessive deformation takes place. Stability may also be accessed using limit finite element analysis methods, which are based upon the limit theorems of plasticity, that predict failure by optimising the applied loads with consideration of the stress equilibrium equations, the stress-strain relationship and the kinematic compatibility of the problem.

Several case studies have been performed to evaluate the outcomes of the two finite element methods. The comparison is based on a Factor of Safety in terms of material strength. Thus, a strength reduction approach is required in limit finite element analysis as well. This was done by varying the strength until the obtained failure loads equal the given loads of the stability problem. The case studies consider stability problems under drained and undrained conditions. The analysed problems are, a simple homogenous slope, a tunnel excavation and a pile.

In case of drained conditions, special emphasis was put on the influence of the flow rule. The limit theorems of plasticity are so far only proved for an associated flow rule. Consequently, the limit finite element analysis outcomes were compared to results obtained from the displacement based finite element – strength reduction analysis, using an associated flow rule. Additionally, Davis argued (Davis E. H., 1968), that one should use reduced strength values with an associated approach, if the dilatancy is less than implied by an associated flow rule. The argument is based on velocity characteristics, which are considered in limit finite element analysis. His approach was used in limit finite element analysis and compared to results of non-associated finite element analysis.

Under undrained conditions, the different available calculation methods were analysed in more detail. Furthermore, it is presented that a strength reduction approach generally provides higher Safety Factors for an undrained effective stress analysis than obtained from a total stress analysis. The related fundamentals are discussed and results of the study are provided to give evidence of this issue.

Kurzfassung

Limit Analysis ist ein Verfahren dass verwendet wird um Grenztragfähigkeitszustände von Festkörpern zu untersuchen. Das Verfahren basiert auf den Grenzwertsätzen der Plastizitätstheorie und setzt sich aus der *Lower Bound* und *Upper Bound* Methode zusammen. Gekoppelt mit der Finiten Elemente Methode können Obere und Untere Schranken von Bruchlasten numerisch ermittelt werden. Ein andere übliche Methode um Grenztragfähigkeitszustände mittels eines numerischen Berechnungsverfahrens (FEM) zu analysieren ist die *Strength Reduction Method*. Dabei werden die Lasten konstant gehalten und die Festigkeiten des Materials schrittweise reduziert bis ein Versagen des Körpers eintritt.

Mehrere Probleme wurden mit beiden numerischen Berechnungsverfahren auf ihre Grenztragfähigkeit untersucht. Der Vergleich der Methoden erfolgt anhand der berechneten Sicherheitsfaktoren, wobei die Sicherheit als Verhältnis zwischen vorhandener Materialfestigkeit und Materialfestigkeit im Grenztragfähigkeitszustand definiert ist. Folglich, wurden auch im Limit Analysis Verfahren die Festigkeiten reduziert. Die untersuchten Probleme sind, eine homogene Böschung, eine stabilisierte Ortsbrust und eine Pfahl.

Neben dem generellen Vergleich, wurde der Einfluss der Fließregel genauer untersucht. Die Grenzwertsätze der Plastizitätstheorie sind nur für eine assoziierte Fließregel erfüllt. Es wurden daher die Limit Analysis Ergebnisse mit den Ergebnissen der SRM-FEM unter Verwendung einer assoziierten Fließregel verglichen. Zum Vergleich von Materialien mit nicht assoziierten Fließregeln wurden in den Berechnungen nach dem Verfahren der Limit Analysis die Festigkeitsparameter nach Davis (Davis E. H., 1968) verwendet.

Bei der Untersuchung der Grenztragfähigkeit unter undrainierten Verhältnissen werden die Berechnungen in totalen und effektiven Spannungen durchgeführt und verglichen. Es wird gezeigt dass die mittels einer SRM ermittelten Sicherheitsfaktoren einer effektiven Spannungsberechnung, verglichen mit einer totalen Spannungsberechnung, allgemein zu höheren Sicherheitsfaktoren führen.

Abbreviations

FEM	Finite element method
FEA	Finite element analysis
SRM	Strength reduction method
LFEA	Limit finite element analysis
FoS	Factor of Safety
SF	Safety Factor
UB	Upper Bound
LB	Lower Bound
φ'	Effective friction angle
c'	Effective cohesion
ψ'	Dilatancy angle
s_u	Undrained shear strength
$s_{u.limit}$	Limit state undrained shear strength
$\bar{\varphi}$	Friction angle after Davis
$\bar{c}$	Cohesion after Davis
τ	Shear stress
s	Shear strength
s_{limit}	Limit state shear strength
p'	Effective hydrostatic pressure
q	Deviatoric pressure
u	Horizontal displacements
v	Vertical displacements

Table of contents

1 Introduction

Designing and building safe structures is at the core of civil engineering. In the last decades, more complex and sophisticated methods became available to analyse engineering structures. At the same time, cost pressures drive structural designs closer to their bearing capacity and Safety Factors are sought to be as low as possible. However, the economic and social cost of failure can be devastating.

Consequently, research has to comply with the needs of society and the community expectations, that engineers can handle and design cost effective complex structures. A powerful tool in this context is the finite element method, which enabled engineers to solve far more complex problems as it is possible with analytical methods. However, major failures continue to occur and validations of available analysis methods certainly remain necessary.

Based on these circumstances, a comparison between two different numerical approaches using finite elements, is presented in this work. In general, these methods can be used to analyse any kind of solid body. However, the considered applications are intended for geotechnical stability analysis. One method is based on the limit theorems of plasticity, combining a lower and upper bound analysis. The other method is a strength reduction approach implemented in a displacement based finite element formulation.

At first, relevant general fundamentals are discussed, followed by basics and differences about the two finite element formulations. Additionally, undrained effective stress and total stress analysis are compared at the initial and limit state respectively. The main part consists of a case study of 3 stability problems. The considered problems are a simple homogenous slope, a supported tunnel face and a pile. The slope represents an unconfined problem, which is analysed under drained and undrained conditions. The stability of the tunnel face is solely evaluated under undrained conditions. At last, the pile is included to compare the results of the two methods for a relatively constraint problem. However, the analysis is plane strain due to the current limitations of the limit finite element formulations.

Apart from the general comparison, the influence of the flow rule is investigated for drained analysis and under undrained conditions, the difference between effective and total stress analysis is evaluated.

2 Fundamentals

2.1 Soil failure

2.1.1 Basics

Soil failure, like failure in many other solid materials, can either be caused by tension or by shearing. Whereby, in soils, tension of minor importance is. It may develop soil cracks, for example at the top of a slope and should therefore be considered. However, in most practical problems, soil fails primarily in shear. In general, failure occurs if a combination of shear and normal stress reach its corresponding shear resistance. Once this is the case along a whole surface through the soil body, failure occurs.

Unfortunately, shear failure in soils is more complex than it is for many other construction materials (e.g. steel, concrete, etc.) First, soil as a material is not manufactured. Thus, its properties are not as well known. Its characteristics and behaviour are affected throughout the whole history of its development. Second, water plays a crucial role in soil failure. Regardless of fully or partly saturated, water simply affects soil failure. Furthermore, different soil types with different grain sizes, distributions and mineral compositions behave differently if subjected to shear stress. Finally, pre consolidation and initial density also affect the development of failure in soil. As a result, the shear parameters of soils, which mainly govern failure, are not a material constant.

However, since its complexity, a numerical approach that copes with all these influences is yet not in practical use. In most analysis a Coulomb failure criterion is used, whereby the cohesion c' and the friction angle φ' are assumed as material constants. The two considered methods in this work, LFEA and SRM-FEM, are no exception.

2.1.2 Failure criteria

The most common failure criterion in soil mechanics is the Coulomb failure criterion. It was first introduced by Coulomb in 1773 (A., 1773). This failure criterion splits the material strength in 2 components, a stress independent and a stress dependent part. The stress independent strength is called cohesion c'. The second component, the friction angle φ', takes the stress dependency into account. Namely, φ' governs the strength increase in accordance to the normal stress.

Equation (1) shows the Coulomb failure equation for a given plane and a given normal stress σ_n acting on it. s stands for the resultant shear strength.

$$s = \sigma_n * \tan\varphi' + c' \quad (1)$$

Unfortunately, within a soil body, the failure plane is not explicitly given as assumed in Equation (1). The direction of the plane and the corresponding normal stress are dependent on the major and minor effective stresses σ'_1 and σ'_3 respectively. However, Mohr's circle of stress provides an arithmetic relationship to derive the angle of the critical failure plane. Figure 1 illustrates this relationship. The critical failure plane is the plane at which the shear stress first reaches the soil strength.

$$\alpha = 45° + \frac{\varphi'}{2} \quad (2)$$

$$\sigma_n = \frac{1}{2}(\sigma'_1 + \sigma'_3) + \frac{1}{2}(\sigma'_1 - \sigma'_3) * \cos(2\alpha) \quad (3)$$

The plane is inclined at the angle α to the direction of the effective minor stress σ'_3 and is solely dependent on the friction angle (see Equation (2)). Furthermore, Equation (3) can be used to calculate the normal stress. Thus, the soil shear strength s is known.

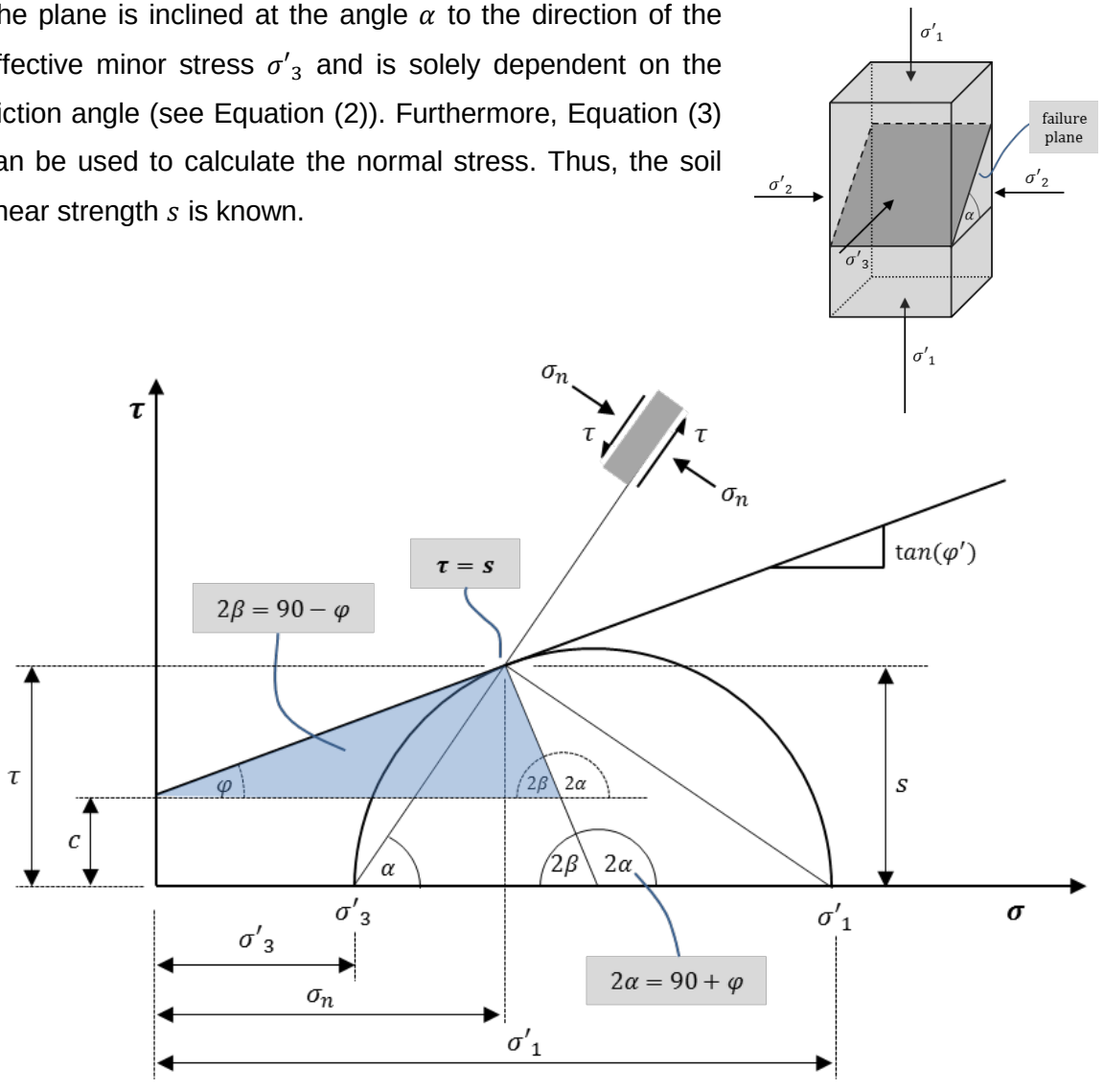

Figure 1: Mohr's circle of stress and Coulomb's failure criterion illustrated in a $\sigma - \tau$ diagram.

2.1.3 Drained/ undrained failure

It is important to distinguish between drained and undrained conditions. If the soil pores are saturated with water, failure, depending on the soil pore size, the degree of water saturation and time involved, can take place drained or undrained. The smaller the pores and the faster the loads are applied the more likely it is that the failure characteristics are undrained.

To explain this in more detail, water, compared to air or unsaturated soils, has a very high bulk modulus. In fact, from a soil engineering point of view, water can be seen as incompressible. If the soil pore volume is filled with air, an increase in stress generally results in a compression of air and therefore a total volume change. This is the case for elastic as well as plastic deformation. The volume can either increase or decrease and the term used to define this is drained. On the other hand, if the soil is fully saturated with water and there is not enough time or no possibility for the water to be displaced, the volume stays constant. Only deviatoric volume changes are possible. This means, the soil can purely be deformed but the volume remains constant. For such conditions, the term undrained is used.

To calculate the undrained shear strength for Coulomb´s failure criteria and plane strain conditions one can use the following Equation:

$$s_u = c' * \cos(\varphi') + \frac{\sigma'_1 + \sigma'_3}{2} * \sin(\varphi') \quad (4)$$

Two of today's common failure criteria that assume constant shear strength are the Tresca failure criterion (H., 1868) and von Mises failure criterion (R., 1928). The difference between the two criteria is in the load angle. The von Mises criterion is load angle independent, whereas the Tresca criterion takes the load angle into account. Thus, for soils, the Tresca criterion is preferable. Figure 2 illustrates the Tresca criterion in a $\sigma - \tau$ diagram. Additionally, the relationship between s_u and the drained strength parameters is shown (plane strain). Furthermore, the 2 stress circles represent an effective and total stress state respectively.

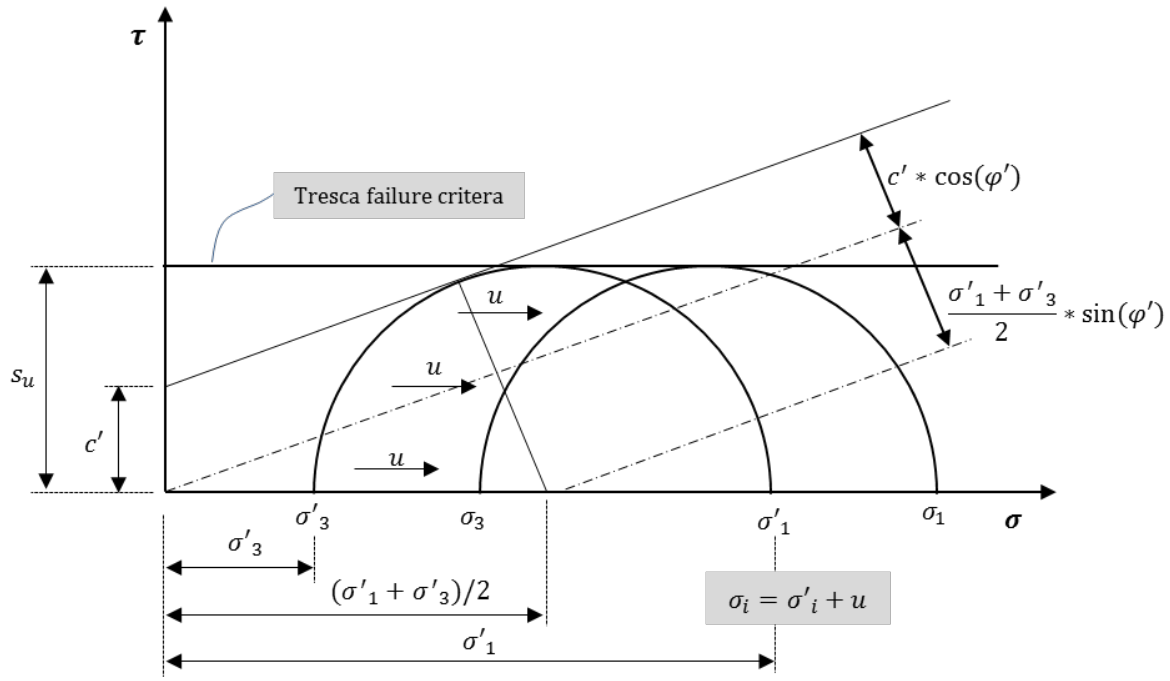

Figure 2: Mohr's circle of stress and Tresca failure criterion in a $\sigma - \tau$ diagram

Both, the LFEA and SRM-FEA codes have a Tresca failure criterion implemented.

2.2 Factor of Safety

2.2.1 Basics

The Factor of Safety or Safety Factor is used to describe the bearing capacity of a problem (system). The actual state of the problem is compared to the limit state, and generally expressed as a ratio of capacity. It is common practice in engineering to design a system with a greater capacity than needed to consider uncertainty and to take the error between the modelled and the real system into account. Engineering design codes and standards require certain Factors of Safety for certain problems and the actual design of the engineer needs to comply with the required (minimum) Factor of Safety.

A Safety Factor can be applied to any key parameter (feature) separately or to the total capacity at once. It is common in soil mechanics to express the Factor of Safety either in terms of loads or material strength. Which definition is more applicable is depending on the analysis method. A limit equilibrium method, that assumes a failure mechanism and then equates the loads, is only capable to provide the Factor of Safety based on the loads. Whereas other methods, like strength reduction techniques are solely able to define a Factor of Safety based on the material strength.

2.2.2 Load based

A Factor of Safety based on the load capacity is defined as limit loads over actual loads. Equation (5) shows the formulation in a general form.

$$FoS = \frac{limit\ loads}{actual\ loads} \tag{5}$$

This definition is probably the simplest as well as the oldest one to describe the Safety of a geotechnical application. However, a disadvantage is for example the fact that some geotechnical problems behave differently depending on the value of the loads. Namely, a greater load can possibly create a different failure surface with a different shear resistance. Furthermore, loads are relatively certain compared to soil properties. Thus, it might be advisable to consider the uncertainty of the strength parameters more directly by applying a Factor of Safety on the material strength.

2.2.3 Strength based

The Factor of Safety based on the material strength is defined as actual material strength over limit material strength. Equation (6) shows the formulation in its general form and with Coulomb´s failure criterion implied.

$$FoS = \frac{actual\ mat.strength}{limit\ mat.strength} = \frac{\tau}{\tau_{limit}} = \frac{c'}{c'_{limit}} = \frac{\tan(\varphi')}{\tan(\varphi'_{limit})} \tag{6}$$

The Safety Factor is derived via a reduction of the strength properties under constant loads.

2.3 Methods to estimate soil failure

2.3.1 Limit equilibrium methods

Limit equilibrium methods are the oldest approaches among stability analysis in soils. The methods are used to obtain approximate solutions of stability problems. Various failure mechanisms are assumed and the driving forces are equated to the resistant forces. The assumed failure mechanisms primarily consist of a combination of simple shapes, such as planes, circles or log spirals. The critical mechanism is the one with the smallest difference between driving and resistant forces.

Note that, the resultant failure surface of the method may not be the real one (due to simplifications), but provides in many cases reasonable approximations of the true failure mechanism. However, the advantage of its simplicity is offset by the fact that one cannot

be sure that the assumed failure mechanism is the critical one. Furthermore, the method does not fulfil the stress distribution, boundary or yield criterion requirements throughout the soil body. Hence, the obtained loads are not necessarily true collapse loads of the given problem.
Examples of limit equilibrium approaches are, Bishop's, Spencer's and Morgenstern's and Price's methods for slopes, and many other methods for different geotechnical structures.

2.3.2 Limit analysis

The method is used to analyse the limit state of solid bodies. Basically, it can be split into two parts that are based on the theorems of plasticity, namely the lower and upper bound theorem. Other than limit equilibrium methods, the approach considers the stress equilibrium equations, the stress-strain relationship and the kinematical compatibility throughout the whole soil body. Hence, the approach calculates true collapse loads, or in most cases, bracketed collapse loads with a known error for the assumed material.
The lower bound analysis looks at equilibrium and the yield criterion. A stress distribution is considered where; (i) the equilibrium equations, (ii) stress boundary conditions, and (iii) the yield criterion are satisfied. Any loads which produce a stress distribution that fulfils these requirements is a lower bound and equal or lower than the actual collapse loads.
The upper bound analysis on the other hand, looks at velocities and energy dissipation. The external work, resultant form applied loads and deformations, are equated to the internal energy dissipation. A velocity field (deformation) is sought that satisfies; (i) the velocity boundary conditions and (ii) the strain and velocity compatibility conditions. Any loads which produce a velocity field that satisfies these requirements is an upper bound and equal or greater than the actual collapse loads. By maximising the lower bound (choice of stress field) and minimising the upper bound (choice of velocity field) the collapse load can be bracketed in between the lower and upper bound. (Chen W.F., 2008)

2.3.3 Strength reduction techniques – FEM

A strength reduction technique coupled with a displacement based finite element method is a common numerical approach to perform stability analysis of geotechnical applications. There are several advantages that make this technique a powerful tool. First, the method needs no assumption of a critical failure surface. The reduction in material strength combined with constant loads results in increasing shear strains, which subsequently form a critical failure surface. Second, it is applicable to complex problems. Third, fewer simplifications are required, which yields a closer representation of the real problem. Finally, service-ability and limit state are not completely decoupled. In other words, material stiffness is considered as well and affects the limit state results. However,

strength parameters remain the primary factors. In contrast to most limit equilibrium approaches the strength reduction method results in a Factor of Safety based on material strength.

2.4 Flow rule

2.4.1 Basics

If a solid body is subjected to loading the geometry generally changes. This change is either elastic or plastic. An elastic deformation is one that is removable whereas plastic deformation is permanent. During elastic deformation the rate and the magnitude are governed by elastic stiffness parameters.

In case of plastic deformation, the flow rule defines the rate of deformation. It governs the relative ratio between the strain rate components. Since these components coincide with the stress components (shear stress and normal stress), the flow rule sets the rate between volumetric and shear deformation. Basically, the flow rule is solely important for drained soil behaviour. Since undrained soil behaviour, per definition, assumes no volume change during deformation. Thus, the ratio is already set.

In soil mechanics, the flow rule is often liked with the dilatancy angle of the material, which is observed via soil tests. Simply speaking, the dilatancy angle ψ governs the volume change during plastic shearing. A dilatancy angle $\psi = 0$ means no volume change. $\psi > 0$ implies a volume increase (expansion) and $\psi < 0$ results in a volume decrease (compaction). Two terms are used to describe the flow rule further. The flow rule is either termed associated or non-associated.

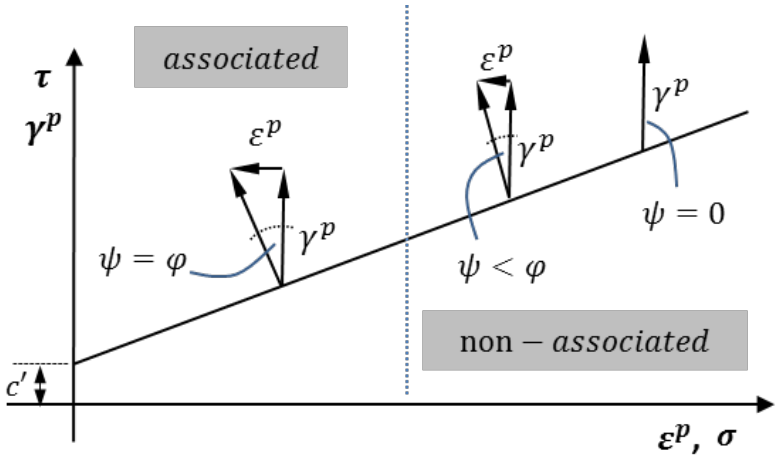

Figure 3: Associated and non-associated flow in a $\sigma - \tau$ diagram.

2.4.2 Associated flow rule

An associated flow rule assumes that the plastic strain rate is normal to the yield curve. This implies, in case of Coulomb's failure criterion, that the dilatancy angle equals the friction angle ($\psi = \varphi$) of the material. Figure 3 shows this in a $\sigma - \tau$ diagram (on the left site). It is often observed in the laboratory that the volume increase of soil is less than implied by an associated flow rule and that it might differ considerably from real soil behaviour. However, there are advantages in assuming an associated behaviour. For example, the limit theorems of plasticity have yet only been proved for an associated flow rule. Furthermore, the velocity (deformation) and stress characteristics coincide solely with an associated flow rule. (Davis E. H., 1968)

2.4.3 Non-associated flow rule

A non-associated flow rule is one where the plastic strain rate is other than normal to the yield curve. In general, the dilatancy angle is assumed to be less than the friction angle of the material. Two examples of non-associated flow rules are shown in Figure 3. In one case the dilatancy angle is set to 0, which means no volume change. The other case shows a flow rule with a dilatancy angle greater than 0 but less than the actual friction angle. A non-associated flow rule provides a possibility to model the real soil behaviour more closely, since many soils tend to dilate with a dilatancy angle $\psi < \varphi$.

2.4.4 Davis approach

Davis (Davis E. H., 1968) argued that, on a velocity characteristic, the shear and normal stress ($\bar{\tau},\ \bar{\sigma}$) do not satisfy Coulomb´s failure criterion and instead, are governed by

$$\bar{\tau} = \bar{c} + \bar{\sigma} * \cos\bar{\varphi} \tag{7}$$

where $\bar{c}$ and $\bar{\varphi}$ are defined as follows

$$\bar{c} = c' * \frac{\cos(\psi') * \cos(\varphi')}{1 - \sin(\psi') * \sin(\varphi')} \tag{8}$$

$$\bar{\varphi} = tan^{-1}\left[\frac{\cos(\psi') * \sin(\varphi')}{1 - \sin(\psi') * \sin(\varphi')}\right] \tag{9}$$

On his basis one should use $\bar{c}$ and $\bar{\varphi}$ as the cohesion and friction angle on slip planes (failure surfaces) instead of c' and φ' which are based (and obtained) on stress characteristics. This is due to the fact that, only with $\psi = \varphi$ it is justified that the stress characteristics are similar to the velocity characteristics.

Davis strength parameters may provide a closer representation of the real soil behaviour for an approach with an associated flow rule if the observed soil shows less dilatancy than implied by an associated flow rule. Since the limit theorems of plasticity are so far only proven for an associated flow rule, the reduced strength parameters can be used to model materials with little to no dilatancy.

If $\bar{c}$ and $\bar{\varphi}$ are used in a stability analysis, the Factor of Safety definition needs to be adapted as well. The equation looks as follows.

$$FoS = \frac{\bar{c}}{\bar{c}_{limit}} = \frac{\tan(\bar{\varphi})}{\tan(\bar{\varphi}_{limit})} \tag{10}$$

Basically, the whole problem is simply shifted from one which is characterised by c', φ' and ψ' to one that is defined by $\bar{c}$ and $\bar{\varphi}$.

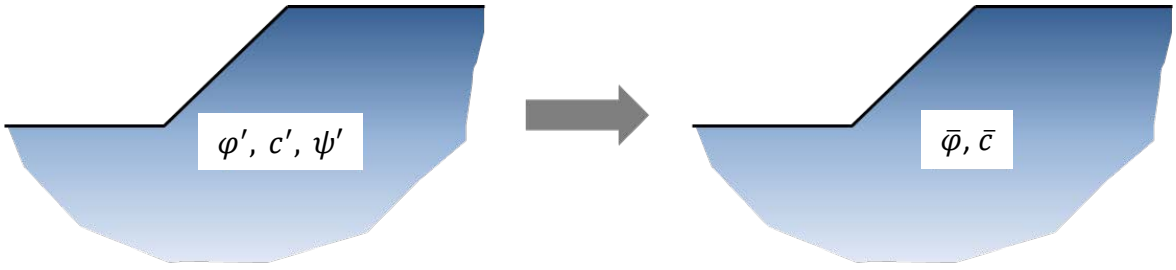

$\tau = c' + \tan(\varphi')$ $\qquad$ $\bar{\tau} = \bar{c} + \tan(\bar{\varphi})$

Figure 4: Transformation of strength parameters after Davis

3 Limit analysis

3.1 Introduction

Limit analysis is a technique to analyse the limit state of solid bodies. The approach is based on the limit theorems of plasticity and takes the stress equilibrium equations, the stress-strain relationship and the kinematic compatibility into account. The problem is generally accessed by two methods, the lower bound and the upper bound method. By combining these two methods, the approach is capable to bracket the true collapse load from above (upper bound) and below (lower bound). Before the two methods are explained in more detail, some basic assumptions that apply to both methods are stated. These assumptions simplify the real soil (material) behaviour, but are necessary to formulate a rigorous approach based on the limit theorems of plasticity (Drucker D.C. G. H., 1951).

First, the material is assumed as an elastic – perfectly plastic material. Strain softening or hardening is ignored. Thus, for soils, the shear strength has to be set on a basis to best represent the real behaviour of the material. Second, a simplified yield criterion is needed to model the material strength. For soils, Coulomb´s or Teresa's failure criterion are primarily used. Third, an assumption about the flow rule, which defines the behaviour of plastic deformation, is required. To prove the lower and upper bound theorems in general, an associated flow rule is necessary (Drucker D.C. G. H., 1952). Hence, for a frictional material, a dilatancy angle equal to the friction angle is automatically implied. Last, it must be assumed that the deformations are only small. Large deformations prior to the ultimate state of failure change the characteristics of the problem. The possible changes in stress and a deformation of the soil-body cannot be taken into account. Limit analysis considers the undeformed geometry.

3.2 Upper-bound theorem

The upper bound theorem is based on work equations. The power expended by all external loads (e.g. soil weight, surcharge, etc.) is equated to the power dissipated by internal plastic deformation. Any external loads which are determined by the internal power dissipation of a kinematically admissible (deformation mechanism) velocity field are an upper bound. The obtained loads (upper bound) are not less than the true failure loads of the problem. The term kinematically admissible refers to the following criteria:

- Velocity boundary conditions

- Strain and velocity compatibility conditions (associated flow rule)

Both criterions must be satisfied for an assumed deformation mode to be termed as kinematically admissible. Furthermore, the stresses must satisfy the yield conditions. The stress distribution, on the other hand, need not to be in equilibrium. By minimizing the internal power dissipation, namely varying kinematically admissible velocity fields, the least upper bound can be found. The lower the internal power dissipation, the closer is the upper bound to the true limit load.

3.3 Lower-bound theorem

The lower-bound theorem is grounded on a stress field calculation. Any loads, which produce a stress field that, (a) satisfies the equilibrium conditions (b) does not violate the yield criterion and (c) fulfils the boundary conditions, are a lower bound on the true failure loads of the problem. A stress field that complies with all these conditions is termed statically admissible stress field. A lower bound is always lower than the actual failure load. By varying statically admissible stress fields, the highest lower bound can be found.

3.4 Application on a simple stability problem

3.4.1 Problem definition

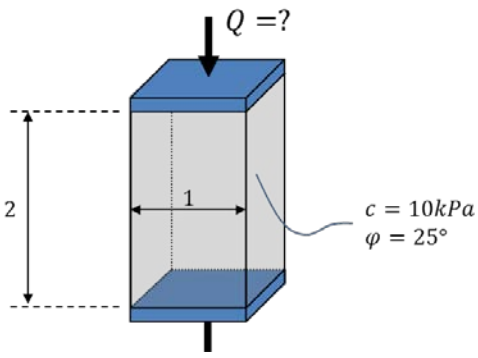

Figure 5: one-axial compression test properties

The considered problem is a uniaxial compression test, with a given material strength and an unknown bearing capacity. The strength properties are a cohesion of 10 kPa and a friction angle of 25°. The soil is assumed to be weight less and the boundaries at the top and bottom are smooth (for simplicity). Figure 6 shows the dimensions of the stability problem.

3.4.2 Upper-bound analysis

Let us first assume a kinematically admissible failure mechanism (velocity field) to derive an upper bound. The assumed failure mode consists of two rigid zones and an inclined plastic zone between them (see Figure 10). Furthermore, we assume that shear strength is fully mobilized along the failure plane (perfectly plasticity) and any power dissipation

takes place in this (narrow) plastic zone. The deformation mode is a combination of shear flow parallel (δu) to the failure surface and extension normal (δw) to it. The ratio between these movements is governed by the friction angle (associated flow rule). The resulting velocity field is shown in Figure 10.

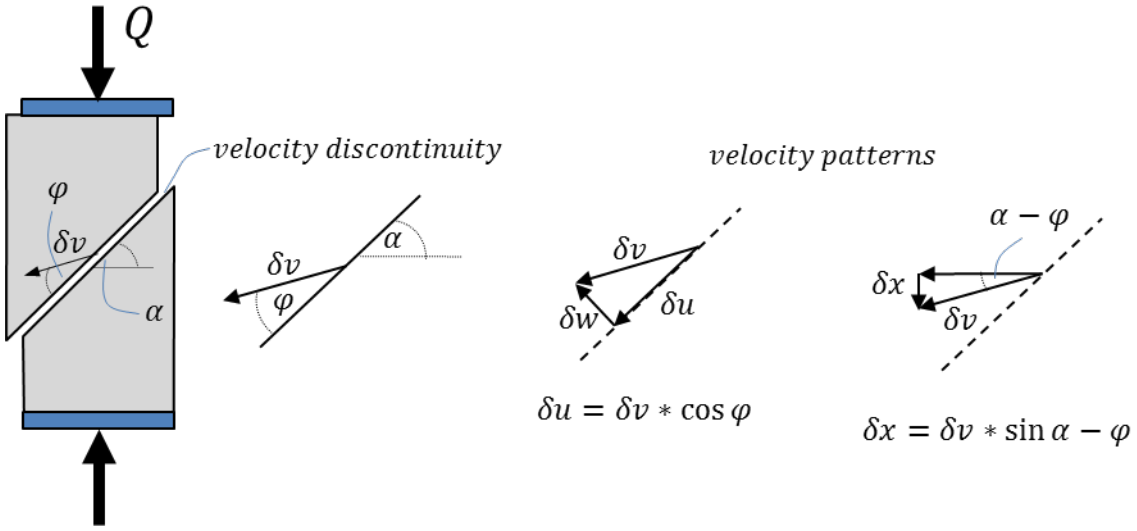

Figure 6: Assumed failure mode (velocity field) and relevant velocity patterns

The energy dissipation (per unit) in the plastic zone is a combination of shearing ($\tau * \delta u$) and lateral expansion ($-\sigma * \delta w$, compression is taken positive).

$$D = \tau * \delta u - \sigma * \delta w \tag{11}$$

Since the yield function must be satisfied, it follows from Equation (1) that:

$$D = c * \delta u = c * \delta v * \cos\varphi \tag{12}$$

The total internal power dissipation is then:

$$D = \int c * \delta v * \cos\varphi * dl = c * \delta v * \cos\varphi * \frac{1}{\cos\alpha} \tag{13}$$

Equated to the external power $W_{ext.} = Q * \delta v * \sin(\alpha - \varphi)$ gives:

$$Q = \frac{c * \delta v * \cos\varphi}{\cos\alpha * \delta v \sin(\alpha - \varphi)} \tag{14}$$

If we for example assume $\alpha = 40°$ we obtain $Q = 45.71\ kN$ as an upper bound. However, the desired least upper bound can be found by varying α.

$\frac{dQ}{d\alpha} = 0$ provides $\alpha = 57.5°$

The least upper bound for this problem is therefore $Q = 31.394\ kN$. However, note that this is only the least upper bound for the assumed velocity field. There might be a different failure mode which provides a lower solution.

3.4.3 Lower-bound analysis

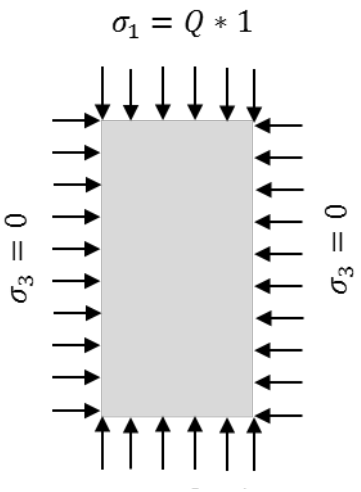

Figure 7: stress field for the lower bound calculation

Now, a statically admissible stress field must be assumed to calculate a lower bound. In this case, the stress field is a simple homogeneous one and no stress discontinuities are required (smooth boundaries). See Figure 11.
It follows from the yield criterion, that:

$$\sigma_1 = \sigma_3 * \frac{1 + \sin\varphi}{1 - \sin\varphi} + \frac{2c * \cos\varphi}{1 - \sin\varphi}$$

As a result, the lower bound for this stress field is $Q = 31.394\ kN$. Since this is the only statically admissible stress field, the obtained lower bound is automatically the least one.Thus, the true failure load is now bracketed between the lower and the upper bound, $31.394\ kN \leq Q \leq 31.394\ kN$. Since both bounds provide the same solution for this problem, the outcome $Q = 31.394\ kN$ is the exact one.

4 Limit finite element analysis

4.1 Introduction

As discussed previously, the lower and upper bound methods are a powerful tool to assess the stability of geotechnical applications. However, an analytical approach is limited to rather simple problems. Deriving adequate stress and velocity fields by hand is often too complicated. To use the lower and upper bound methods in engineering practice, a numerical approach is needed. This enables one to solve more complex geometry, material, boundary and load conditions. Fortunately, finite element formulations have been recently developed based on the limit theorems of plasticity. These formulations are capable to perform two and three dimensional analysis and can be applied to a wide range of stability problems.
The following sections outline some facts about limit finite element analysis. The formulations are thoroughly discussed in (Lyamin A. V. S. S., 2002a), (Lyamin A. V. S. S., 2002b), (Lyamin A. V. S. S., 2005) and other works done by the Geotechnical Research Group – University of Newcastle (Australia).

4.2 Program codes

The program codes are very general and can deal with layered soil profiles, anisotropic strength characteristics, complicated boundary conditions and complex loading in both two and three dimensions (Sloan S. W., 2004).
The codes that are used in this work were all developed at the Centre of Geotechnical and Materials Modelling – University of Newcastle. (Sloan S. L. A., 2007)

4.3 Key features

The key features of limit finite element analysis, are as follows:

- *"The limit load is given directly, without the need to perform a complete incremental analysis. This is a major advantage in large scale three-dimensional applications, where stability analysis using the conventional finite element method is both difficult and time consuming*
- *For the material model assumed, the loads obtained are rigorous upper and lower bounds on the true collapse load. This means that the difference between the*

bounds gives a direct measure of the mesh discretisation error in the solution. For many practical problems it is often sufficient to base a design on the lower bound solution, with the upper bound solution providing an accuracy check as well as insight into the failure mechanism.

- *Apart from providing an accuracy check, the bounding property of the methods provides some insurance against operator error.*
- *The methods can handle complex boundary and loading conditions, as well as anisotropic and inhomogeneous soil properties*
- *No assumptions are needed in advance about the shape of the failure surface (unlike limit equilibrium calculations).*
- *The methods permit discontinuities in the stress and velocity fields. This means that they can model jointed media and soil-structure interfaces in a natural manner. It also means that, even with a modest number of elements, the computed solutions are often quite accurate.*
- *Compared with traditional incremental finite element method, the procedures are very fast and straightforward to use".* (Sloan S. W., 2004)

4.4 Elements

Linear simplex finite elements are used in LFEA. The upper bound analysis is based on linear velocity elements and the lower bound analysis is based on linear stress elements. Each of the element nodes is unique, which means, the nodes of two adjacent elements can have different values although they share the same coordinates. However, the resultant discontinuities are restricted to statically admissible stresses in lower bound analysis and kinematically admissible velocities in upper bound analysis respectively. This formulation ensures accurate, rigorous lower and upper bounds on the true collapse loads. Figure 8 shows the finite elements and the discontinuity formulations of both, the lower (left side) and upper bound method (right side).

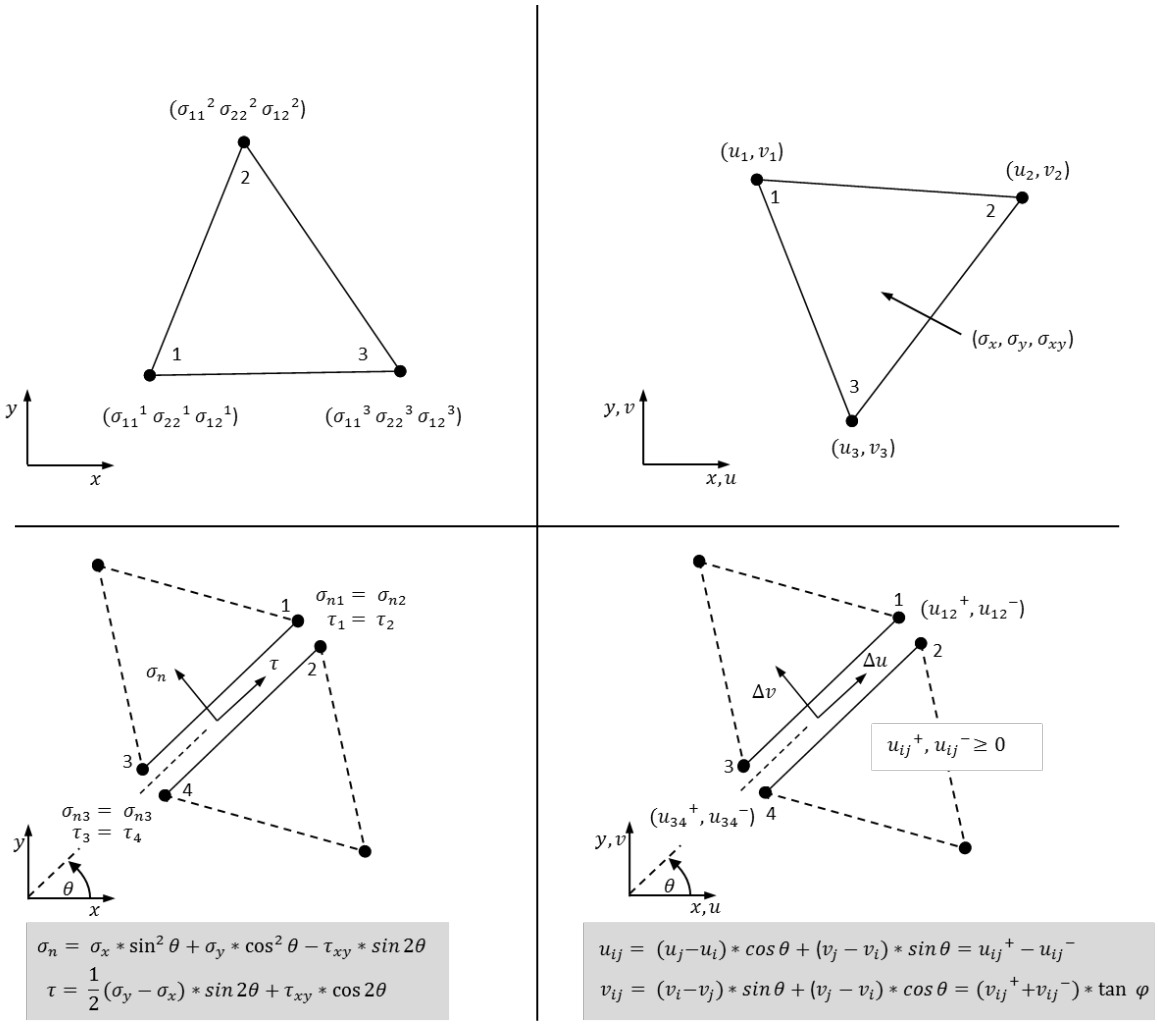

Figure 8: LFEA – statically admissible stress discontinuity (left side) and kinematically admissible velocity discontinuity (right side)

Higher order elements, which are often effective in conventional finite element analysis, are not an option since they lead to stress fields which may not be statically admissible (Sloan S. W., 2004).

4.5 Mesh

4.5.1 General

The limit finite element mesh consists of triangular linear finite elements with unique nodes and statically admissible discontinuities between these nodes. Both meshes lower and upper bound, can be produced with an adaptive remeshing method. This procedure generates adequate meshes for any problem and can be used for complex conditions. The boundary conditions can be set to zero velocities, (displacements) normal, tangential,

or in both directions to the boundary. Furthermore, fan points can be set at certain points, to generate fan shaped meshes to cope with stress singularities (e.g strip footings).
In general, upper and lower bound meshes are produced independently. Different control variables in the refinement procedure are used, to best create adequate meshes. On closer look, the difference becomes apparent (see for example Figure 21 and Figure 22 in section 6.4.2). However, since the refinement primarily takes place around the failure surface, the difference between the lower and upper bound meshes has to be considerably low.

4.5.2 Discretization influence

Unfortunately, the finite element discretization introduces an error in the upper and lower bound analysis. The UB calculation computes higher failure loads and the LB analysis achieves lower solutions respectively. Thus, the calculated lower and upper bounds drift away from the true collapse load. Although this is a disadvantage, the upper and lower bounds still bracket the true failure load with a known maximal error. The error decreases the more accurate the problem discretization becomes. In commonly done stability analysis the actual collapse load can be predicted with less than 5% error. (Lyamin A. V. S. S., 2005)

4.5.3 Adaptive mesh refinement

The mesh refinement procedure starts with a homogeneous equally sized element distribution and automatically refines the mesh in accordance to a control variable. The control variable can be the value, gradient or hessian of, for example, the plastic multiplier in a LB calculation or the power dissipation in an UB analysis. Based on the user's inputs, the element number, size and distribution vary during the adaptive mesh refinement due to pre-defined end values.
The mesh refinement is a stepwise procedure, based on previous calculation results. Hence, LB and UB analysis with adaptive remeshing run several times for one problem, each time with a further refined mesh. Generally, 3 - 4 steps (calculations) are sufficient to achieve precise solutions.

4.6 Material Input parameters

The material input parameters are the material weight and the strength parameters of the material. Stiffness parameters are not required since limit analysis only consider the limit

sate.

4.7 Factor of Safety estimation

The Estimation procedure is depending on the definition of the Factor of Safety. If a Safety Factor based on loads is desired, in other words actual load over limit load (Equation (5)), a solution can be obtained fast. One analysis is sufficient to calculate the FoS.

However, if the Safety Factor needs to be expressed in terms of material strength, that is actual material strength over limit material strength (Equation (6)), a strength reduction must be performed. Therefore, several upper and lower bound analyses are required, each with different strength parameters. Once a state is found where the obtained collapse load equals the actual load, the limit strength parameters are derived.

Since the SRM-FEA calculates a FoS in terms of material strength, the load based FoS is inadequate for a comparison. Figure 9 shows the general procedure of the strength based FoS estimation.

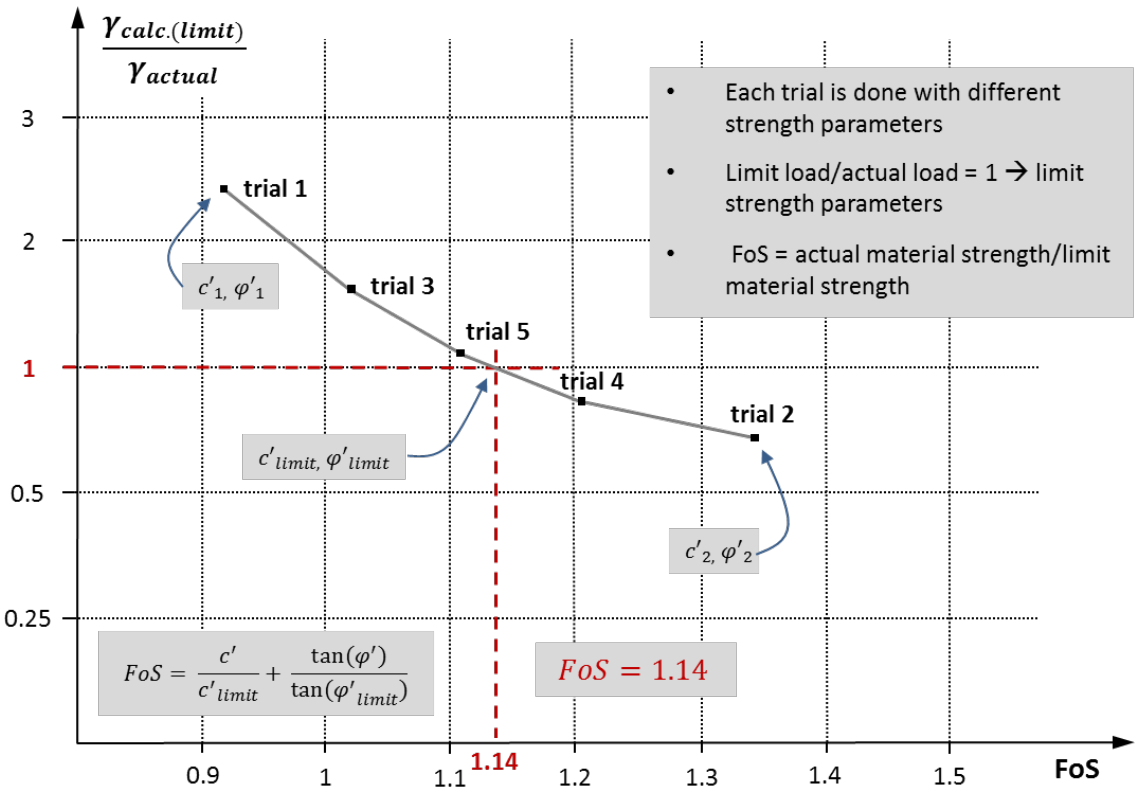

Figure 9: Factor of Safety estimation in LFEA

5 Strength reduction technique – FEM

5.1 Introduction

There are two ways to access the stability of a problem with a displacement based finite element method. One possibility is to increase the loads until failure occurs. The other way is to weaken the material until it collapses. If the loads are increased the analysis is generally performed with a stepwise procedure. The stepwise added loads subsequently increase the stress in the material. Deformation and stress distribution evolves until the full load is either applied or total bearing capacity is reached. In the latter case, the loads lead to a stress-strain distribution where total equilibrium is no longer satisfied. This represents a state above the limit state. Therefore, the last load step can be taken as the bearing load of the problem.

In contrast, the loads in a strength reduction are kept constant. The strength reduction procedure commonly follows the loading stage, since the actual loads need to be applied first. The material strength is then reduced step by step. The reduction leads to an increase of plastic regions (points). As a result, stress redistribution and deformation takes place. At one point, the deformation becomes excessive without a further reduction of the strength properties. This state can be seen as soil failure. The related strength parameters are the limit strength parameters.

5.2 Software code

The program used in this comparison is PLAXIS 2D 2010. The software is developed by the company PLAXIS bv incorporated in Delft, Netherlands and is intended for 2D analysis of deformation and stability of soil structures, as well as groundwater and heat flow, in geo-engineering applications such as excavations, foundations, embankments and tunnels (Brinkgreve R.B.J., 2010).

The software with all its capabilities, features and limitations is thoroughly discussed in the published manuals available at the company's website: http://www.plaxis.nl/. The following comments primarily point out some relevant facts and differences relevant for the comparison with LFEA.

5.3 Elements

5.3.1 Basics

There are a number of different elements used in PLAXIS 2D 2010. The types range from structural over to area elements. However, the following stability analyses are primarily modelled with area (soil) elements. These are triangular, higher order elements with either 6 or 15 nodes. Linear area elements with 3 nodes are not available. The primary unknowns in a stability analysis are the displacements. Each node has 2 unknowns corresponding to the displacement components (u_x, u_y). The displacement distribution throughout the elements is obtained from the nodal displacement components and the distribution functions (shape functions).
The presented stability problems in this work are mostly modelled with 15 node elements. However, in some cases 6 node elements are used. In these instances, the total element number is increased to ensure precise solutions.

5.3.2 Discretization influence

The model discretization, represented by the element number and the element type, affects the results of a stability analysis. Thus, it is desirable to keep the discretization error considerable low. The error is generally greater with coarser meshes and decreases with a higher element number. However, once a certain element number is reached, the Factor of Safety remains almost constant and higher element numbers have insignificant influence on the precision of the strength reduction. This state is sought and the mesh should therefore always be evaluated.
Furthermore, the element number has to be high where stresses and strains gradients are high. Areas further away from particular failure surfaces can have coarser mesh properties. By running several strength reductions, starting with a coarse mesh and subsequently refining the model, it is possible to determine an adequate mesh for a given problem.

5.4 General Analysis properties

5.4.1 Calculation settings

The calculation settings are mainly kept at standard settings. Exceptions are made for the step number in the safety calculation stage. The number of additional steps is increased to at least 250. If the calculation settings are adjusted to achieve more stable results, a

note is provided in the section considered.

5.4.2 Constitutive model

The Mohr-Coulomb model is used for all soil elements. More sophisticated constitutive models are not considered, since the software automatically switches to the Mohr-Coulomb, once a strength reduction (Safety analysis) is started.

5.4.3 Calculation stages

PLAXIS 2D 2010 offers the engineer a possibility to model the load history or the construction of an application in a stepwise procedure. The initial phase is either performed with a K0-procedure or with gravity loading. In case of the K0-procedure the lateral loads are based on the vertical loads multiplied with the K0 value. In the latter case the initial stresses are calculated based on the soil weight. Additional stage construction phases are discussed individually in the adequate sections of the considered problems.

5.5 Drained stability analysis and the flow rule

The user has a choice, ranging from a non-associated approach with no dilatancy up to an associated flow rule. Depending on the problem and the engineer's assumptions and judgments, a suitable approach should be considered. The governing parameter in this matter is the dilatancy angle ψ. If set equal to the friction angle φ the approach is associated. On the contrary, if the dilatancy angle ψ is set to a value between 0 and φ the approach is non-associated.

Note that the dilatancy angle cannot exceed the friction angle of the material. This must remain true during a strength reduction. Therefore, the dilatation angle ψ is reduced in line with the friction angle φ. For the non-associated cases, where the initial dilatancy angle is smaller than the friction angle, the value of ψ, is constant until the reduced friction angle reaches the same value. From that point onwards, both, the friction and the dilatancy angle are reduced by the simultaneously.

This feature implies that the limit problem might differ from the initial problem. In other words an initially defined non-associated approach can become associated in the limit case. This is especially relevant for high Factors of Safety.

5.6 Undrained stability analysis

5.6.1 General

There are 3 available methods to perform an undrained analysis in Plaxis 2D 2010. Undrained A, B and C. In short, the 3 methods can be summarised as follows:

- Undrained A: Undrained effective stress analysis with effective strength parameters. The undrained shear strength is dependent on the effective stress state and effective strength parameters.
- Undrained B: Undrained effective stress analysis with undrained strength parameters. The undrained shear strength is explicitly defined by the user and independent of the effective stress state.
- Undrained C: Undrained total stress analysis with undrained strength parameters. All parameters are specified in undrained terms.

In method A the input parameters of the material strength are c' and φ' and the actual undrained shear strength s_u is always derived from these parameters. Method B and C on the other hand, directly operate with the undrained shear strength itself. Therefore, the input parameters are $s_{u,ref}$, that is the undrained shear strength at a specific point and $s_{u,inc}$ which specifies a gradient in accordance to $s_{u,ref}$.
In general, one might expect the same Factors of Safety from a strength reduction if the initially defined undrained shear strength of the methods is equivalent. However, this is not the case. The next 2 sections explain the methods in more detail and point out the difference of the Factor of Safety estimation. Finally, a comparative example provides further evidence for this issue.

5.6.2 Method A

Figure 10 shows the calculation of the undrained shear strength for the initial and the limit state. For plane strain conditions equation (4) is used to derive s_u. At the surface, the shear strength is governed by the cohesion c'. With increasing depth, (hydrostatic pressure) the undrained shear strength increases as well.
During a strength reduction, the drained parameters c' and φ' are reduced until failure takes place. Figure 10 illustrates the initial and limit state calculation of the undrained shear strength for one point at the surface and one in the soil body.

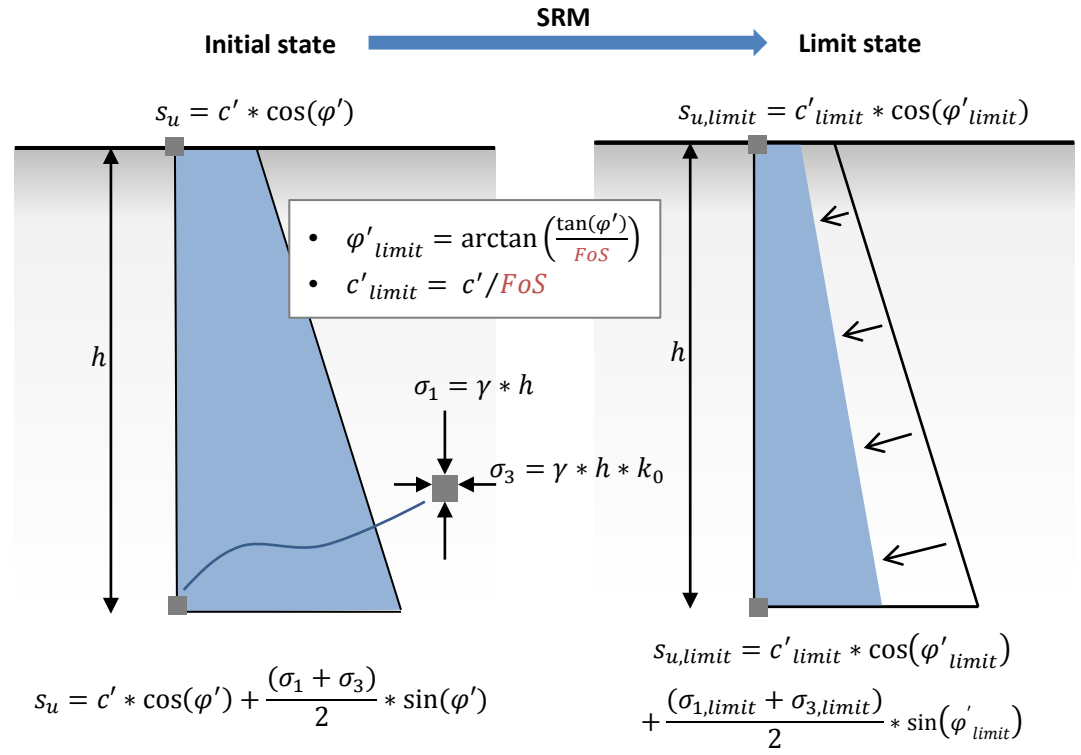

Figure 10: Undrained shear strength in method A – initial state and limit state.

Although, the material strength is governed by the undrained shear strength, the Factor of Safety is defined as initial drained strength parameters over limit drained strength parameters (see Equation (6)). Figure 11 shows the reduction of the strength parameters in a $\sigma - \tau$ diagram.

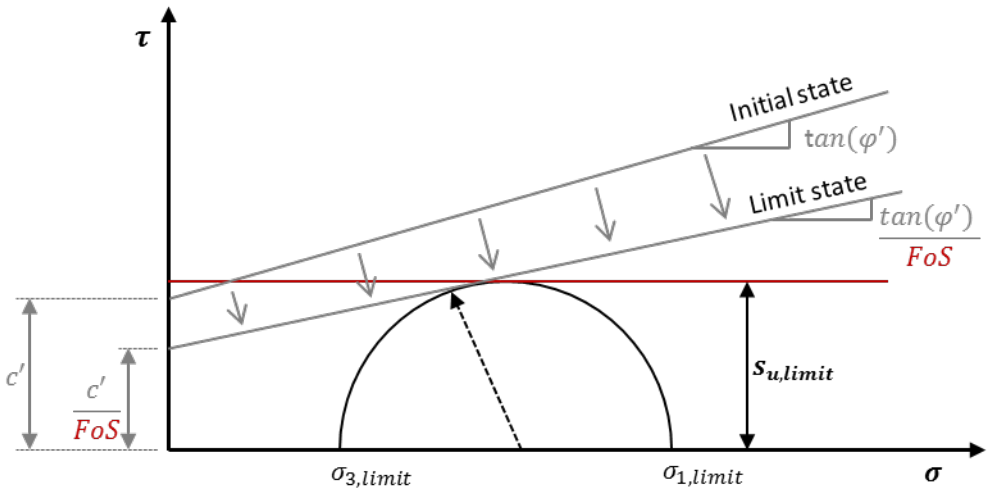

Figure 11: Undrained shear strength in method A – $\sigma - \tau$ diagram.

5.6.3 Method B & C

In Method B and C the input parameters for the material strength are $s_{u,ref}$ and $s_{u,inc}$. Thus, undrained strength parameters can be entered directly or if drained parameters available, Equation (4) can be used to derive them. Figure 12 illustrates the calculation of the undrained shear strength of a point on the surface and one within the soil body before and after the strength reduction.

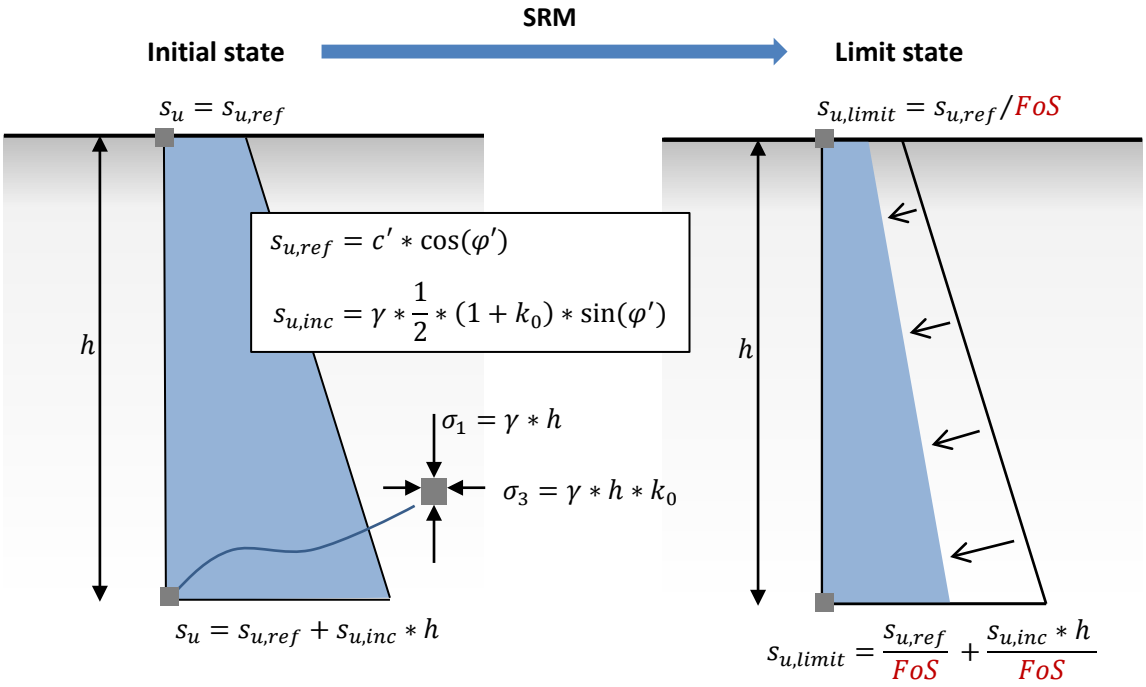

Figure 12: Undrained shear strength in method B & C – initial state and limit state.

The Factor of Safety is defined as initial undrained shear strength over limit undrained shear strength.

$$FoS = \frac{s_{u,ref} + s_{u,inc} * h}{s_{u,ref,limit} + s_{u,inc,limit} * h} \tag{15}$$

Hence, the undrained strength parameters are reduced during a strength reduction. Figure 13 shows the principles of the procedure in the $\sigma - \tau$ plane.

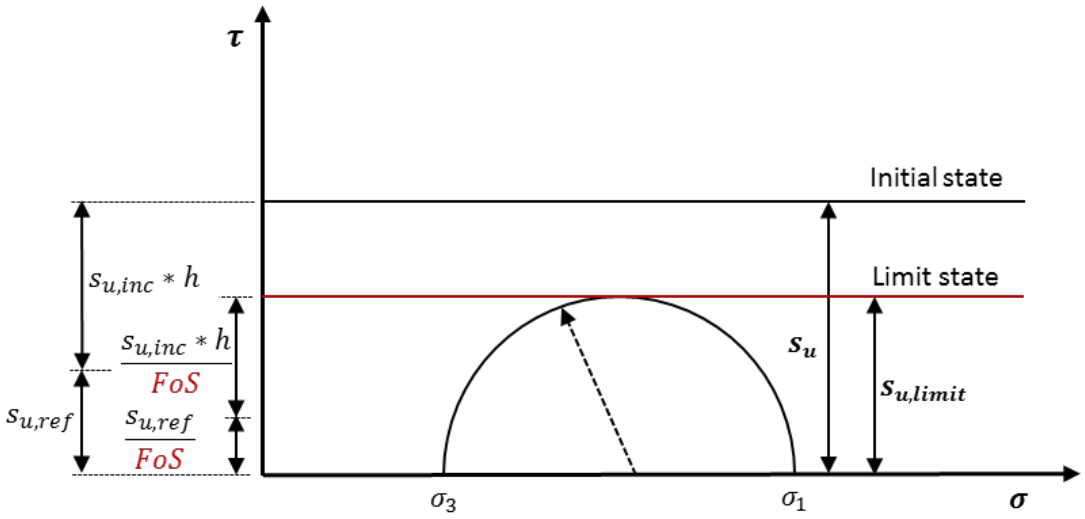

Figure 13: Undrained shear strength in method B & C – $\sigma - \tau$ diagram.

Besides this difference between method A compared to B and C, the methods B and C can be distinguished by their elastic stiffness parameters. In Method B the elastic input values are the drained parameters E and ν whereas in method C undrained elastic parameters E_u and ν_u are required.

5.6.4 Comparative Example

The stability of a vertical slope with a height of 5 m is analysed to illustrate the difference between the methods. The soil material in this example is similar to the cohesive-frictional material in the stability analysis of the homogeneous slope. Thus, see Table 5 for the Plaxis material set parameters or additionally Table 3 (cohesive-frictional material) for the underlying material properties.

The FE-Model is shown in Figure 14. The boundary conditions are set to total fixities at the bottom and horizontal fixities at the right side. The total element number is 1996 and 15-node elements are used. The analysis is divided into two steps. First, a K_o-procedure and afterwards, a strength reduction method is performed. Hence, the initial (drained) stress conditions and the undrained shear strength in all methods should be equivalent.

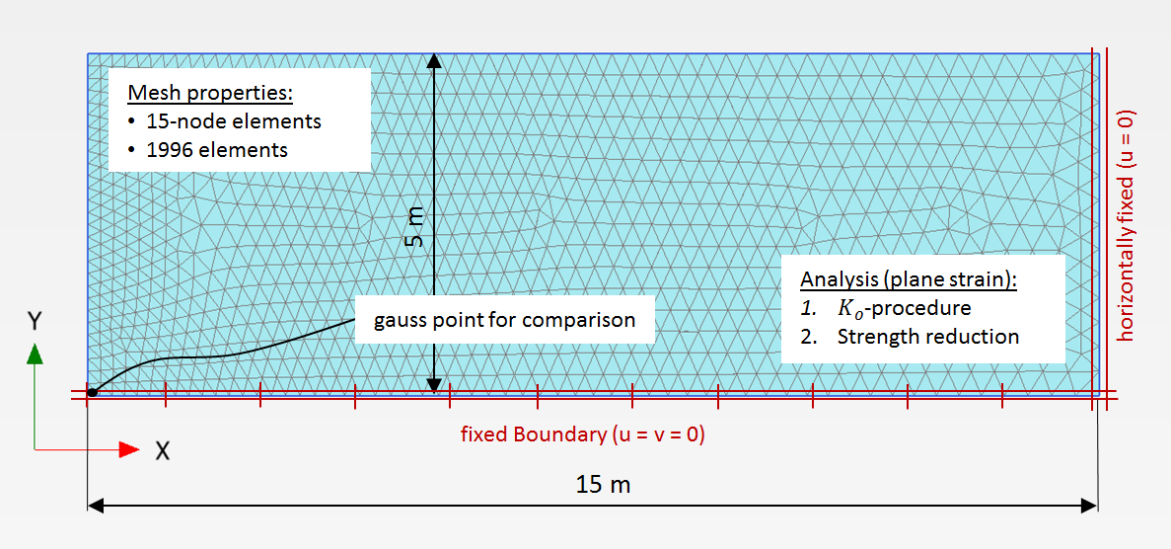

Figure 14: Comparative example – FE-Modell

Additionally, a gauss point close to the bottom of the vertical slope is analysed. The data of the point is exported to compare the undrained shear strength. Table 1 and Table 2 show the relevant information for the initial and limit state. Furthermore, a column $s_{u,calculated}$ is added, where the undrained shear strength is calculated as explained in the 2 previous sections. Finally, results obtained with LFEA are included and compared with the Plaxis results (Table 2).

Table 1: Undrained shear strength in [kPa] under initial conditions (Method A/B/C)

INITIAL STATE	$x\ [m]$	$y\ [m]$	$\frac{\sigma'_1+\sigma'_3}{2}$	τ_{max}	s_u	$s_{u\,(calculated)}$
Method A	0.011	0.011	-74.76	49.72	-	49.72
Method B	0.011	0.011	-74.76	-	49.72	49.72
Method C	0.011	0.011	-74.76	-	49.72	49.72

Table 2: Undrained shear strength in [kPa] after a strength reduction (Method A/B/C)

LIMIT STATE	$\frac{\sigma'_1+\sigma'_3}{2}$	τ_{max}	s_u	$s_{u\,(calculated)}$ [1]	FoS_{Plaxis}	FoS_{LB}	FoS_{UB}
Method A	-74.41	34.20	-	34.24	1.53	1.41	1.43
Method B	-74.24	-	34.97	34.94	1.42	1.41	1.43
Method C	-102.03	-	52.46	52.47	0.95	1.41	1.43
Method C (max itr. 100)	-102.52	-	47.34	47.35	1.05	1.41	1.43
Method C (arc length off)	-344.64	-	13.61	13.62	3.65	1.41	1.43
Method C (desired min/max)	-75.60	-	39.80	39.80	1.25	1.41	1.43

[1] $s_{u\,(calculated)}$ is based on the exact FoS

Method A and B behave as expected and their obtained FoS's are different. However, more importantly the undrained shear strength of both methods is virtually equivalent (32.24 kPa and 34.94 kPa). Note that this small difference is not a result of the different

Safety Factor´s. The undrained shear strength in Method A is dependent on the actual drained stress state during the strength reduction. Thus, the slight difference (2%) in this gauss point might be offset in other gauss points along the failure surface. Furthermore, the difference, due to the formulation of the FoS, varies between points in the soil. Namely, the gradient of the limit undrained shear strength is not equivalent as initially defined.

The upper bound (1.41) and lower bound (1.43) bracket the FoS of Method B. This is desirable since the FoS definition and undrained shear strength calculation of Method B and LFEA are defined identically. However, unfortunately, Method C with a similar undrained shear strength definition shows a different figure. The calculated FoS (with standard settings) is 0.95 compared to 1.42 from Method B and 1.53 from Method A. Consequently, an additional study with different calculation settings under Method C is performed to see if this difference can be overcome. The results are included in Table 2. Figure 15 illustrates the outcomes of the strength reductions plotted against the (normalised) displacements. The red lines show the behaviour using Method C with different calculation settings. The 2 blue lines are Method A and B respectively. The calculation settings of the study include:

- Standard → no changings in settings
- Arc length off → arc length controll is switched off
- Max iter. 100 → The number of maximum itnerations is set to 100
- Desired min/max → The number of desired maximum iteration is set to 60 (equal to maximum interations)

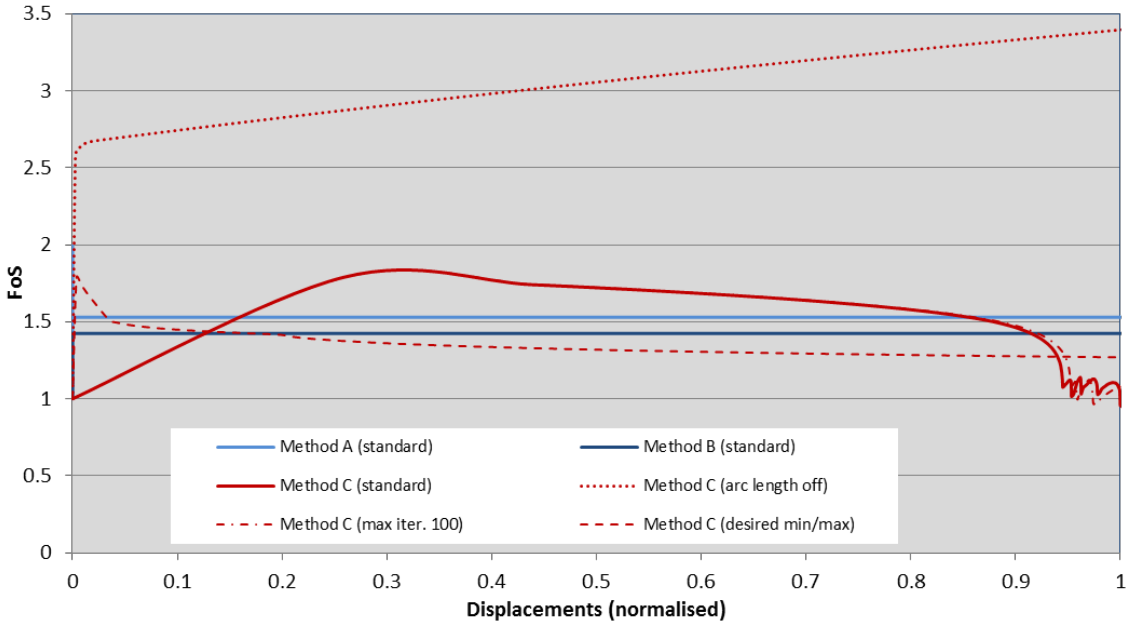

Figure 15: SRM - Output for Method A/B/C, FoS vs. displacements

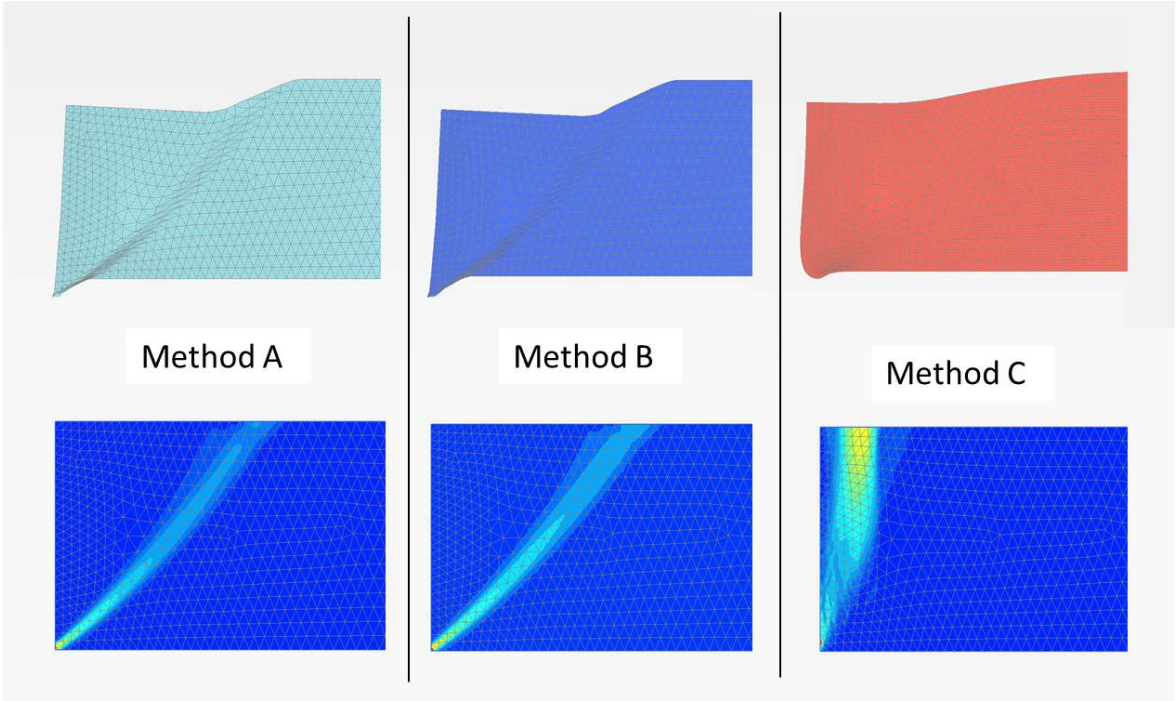

Figure 16: Failure mechanisms of the vertical slope - Method A/B/C (standard settings)

Figure 16 illustrates the obtained failure mechanisms of the 3 methods. The displacements and deviatoric strains are shown at the top and bottom respectively. Method A and B result in a similar failure mechanism whereas Method C (standard settings) shows a different behaviour.

6 Homogeneous slope

6.1 Problem description

This first example is a simple homogenous slope with a slope height H equal to 10m and a varying slope angle β of 15°, 30°, 45° and 60°. Additionally, 2 depth factors $D = 1$ and $D = 4$ which quantify the distance to a firm base (bedrock) are considered. Figure 17 shows the geometry.

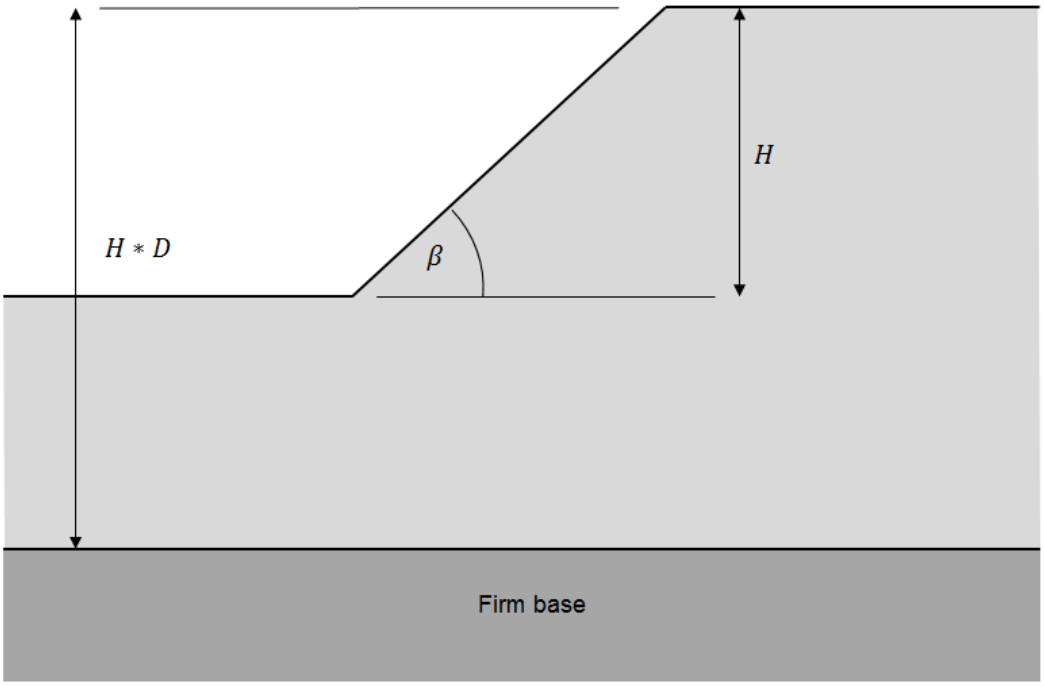

Figure 17: Homogeneous slope geometry

The dimensions of the slope are based on a previously done stability analysis (Yu H. S., 1988) using limit finite element analysis.

6.2 Parameter description

The analysis considers drained and undrained conditions. The material sets include 2 different soil types, a frictional material (no cohesion) and a cohesive-frictional material. However, the undrained analysis is solely done with the cohesive-frictional material. Table 3 shows the underlying material parameters upon both methods (LFEA and SRM-FEM) are based. Additionally, specific input parameters for the individual calculation methods of Plaxis are given in Table 4 and Table 5 respectively.

Table 3: General material properties

		frictional material (drained)	Cohesive-frictional material (drained)	Cohesive-frictional material (undrained)
γ_{unsat}	[k/m^3]	17	19	19
γ_{sat}	[k/m^3]	20	21	21
E	[k/m²]	40000	20000	20000
ν '	[-]	0.3	0.3	0.3
c'	[k/m²]	0	20	-
φ'		35	25	-
ψ	[°]	0	0	-
$s_{u,ref}$	[k/m²]	-	-	18.13
$s_{u,inc}$	[k/m²/m]	-	-	6.333

The drained material sets of Table 4 represent the frictional material with no cohesion (drained 1) and the cohesive-frictional (drained 2). Additionally, both materials are considered with an associated (_A) and non-associated (_NA) approach.

Table 4: drained material set properties for the SRM-FEA (Plaxis)

		drained 1_NA	drained 1_A	drained 2_NA	drained 2_A
γ_{unsat}	[k/m^3]	17	17	19	19
γ_{sat}	[k/m^3]	20	20	21	21
E	[k/m²]	40000	40000	20000	20000
ν '	[-]	0.3	0.3	0.3	0.3
c'$_{ref}$	[k/m²]	0	0	20	20
φ'		35	35	25	25
ψ	[°]	0	35	0	25

The undrained material sets are derived from the cohesive-frictional material and adjusted for the three available undrained analysis methods in Plaxis.

Table 5: undrained material set properties for the SRM-FEA (Plaxis)

		undrained A	undrained B	undrained C
γunsat	[k/m^3]	19	19	19
γsat	[k/m^3]	21	21	21
E	[k/m²]	20000	20000	-
ν'	[-]	0.3	0.3	-
Eu	[k/m²]	-	-	23076
νu	[-]	-	-	0.495
c' $_{ref}$	[k/m²]	20	-	-
φ'	[°]	25	-	-
$s_{u,ref}$	[k/m²]	-	18.13	18.13
$s_{u,inc}$	[k/m²/m]	-	6.333	6.333

6.3 SRM – FEA Properties

6.3.1 Model

A representative finite element model ($D = 4$ and $\beta = 45°$) is shown in Figure 18. The boundary conditions are defined by standard fixities. Consequently, the horizontal displacements u on each side of the model are set to 0 and the vertical and horizontal displacements at the firm base are 0. Furthermore, the horizontal model dimension is extended by $3 * H$ from the top of the slope and bottom of the slope respectively.

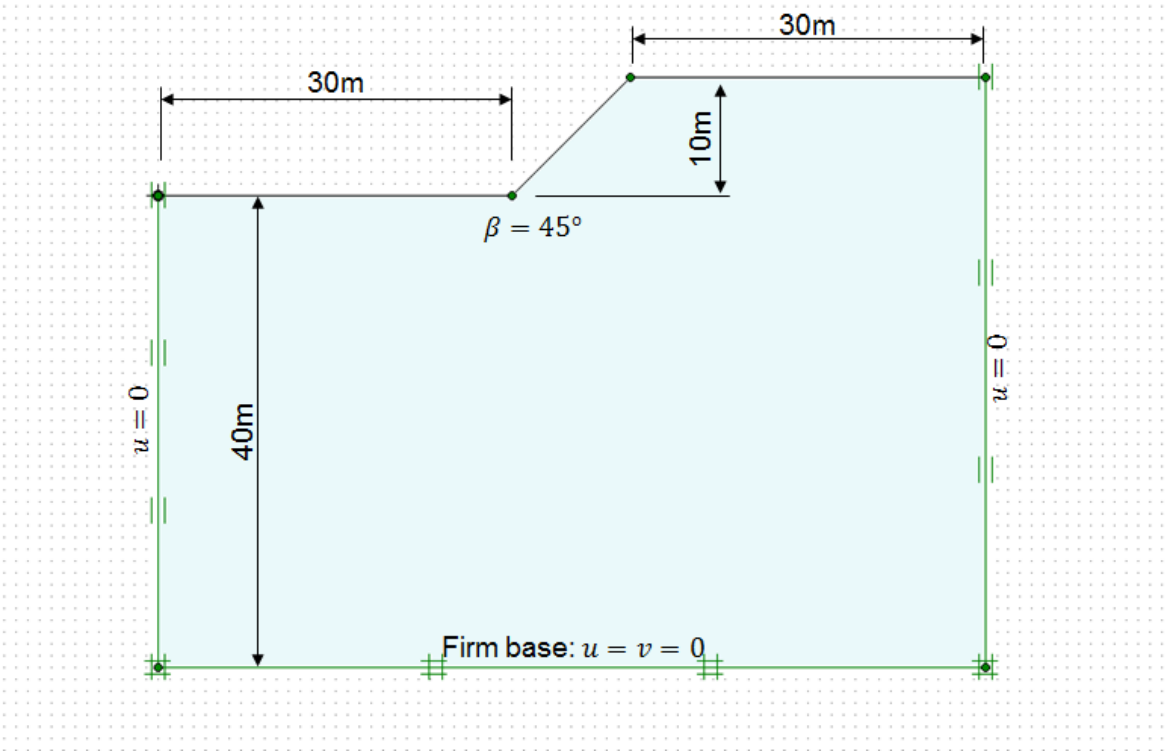

Figure 18: Homogeneous slope model dimensions in Plaxis

6.3.2 Mesh

The properties of the finite element mesh affect the SRM (see section 5.1). Thus, it is necessary to evaluate this influence and to reduce the introduced error to a negligible extend. In case of the slope, the evaluation is done for $\beta = 45°$ with $D = 1$ and $= 4$. The models with other slope angels are then set to similar mesh properties obtained from these examples. Furthermore, additional mesh refinement is done where required. Table 6 and Figure 19 show results of the mesh evaluation procedure for the case $D = 4$ (material = drained_2_NA).

Table 6: FoS and calculation time using different element numbers

Elements	FOS	Time (sec)
127	1.564	20
253	1.500	42
626	1.440	76
1292	1.420	168
1542	**1.414**	**208**
2445	1.413	292

The solutions calculated with element numbers above 1200 differ in a negligible range and are therefore acceptable. However, taking into account the failure mechanisms of the purely frictional material, the mesh properties (1542 elements, Figure 20) with an additional refinement along the slope line are required. Hence, the underlying standard mesh properties for the analysis are set to an element number of 1542.

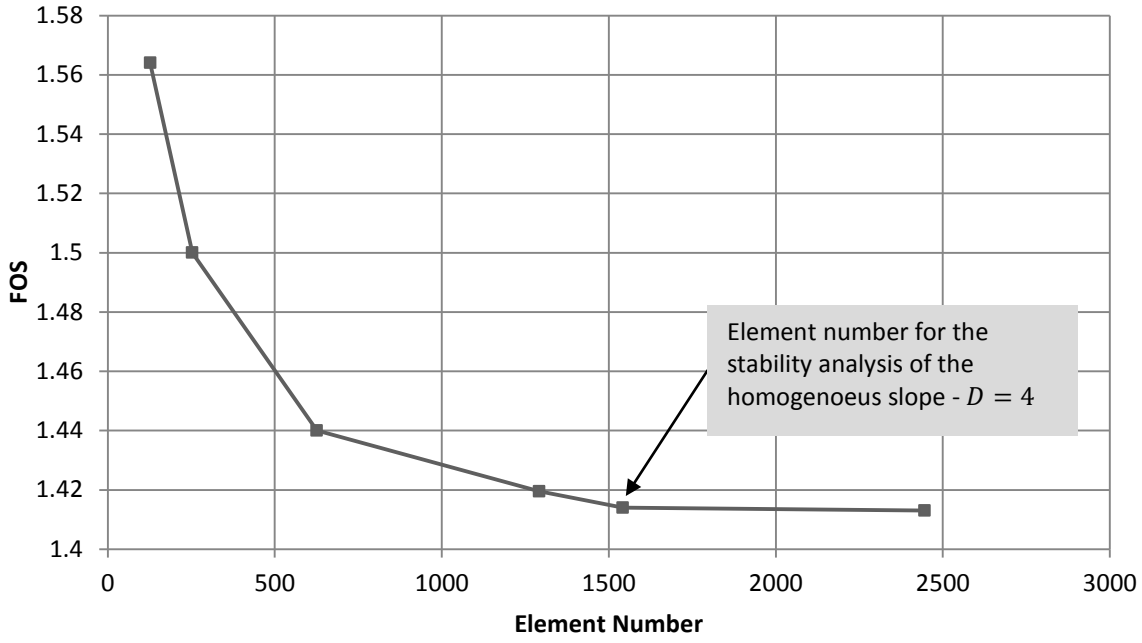

Figure 19: FoS obtained with different element numbers. ($D = 4$, $\beta = 45°$, material: drained_2_NA)

If the SRM does not provide precise solutions or the shear failure occurs in too coarse mesh areas, the mesh is adapted to achieve more accurate results.

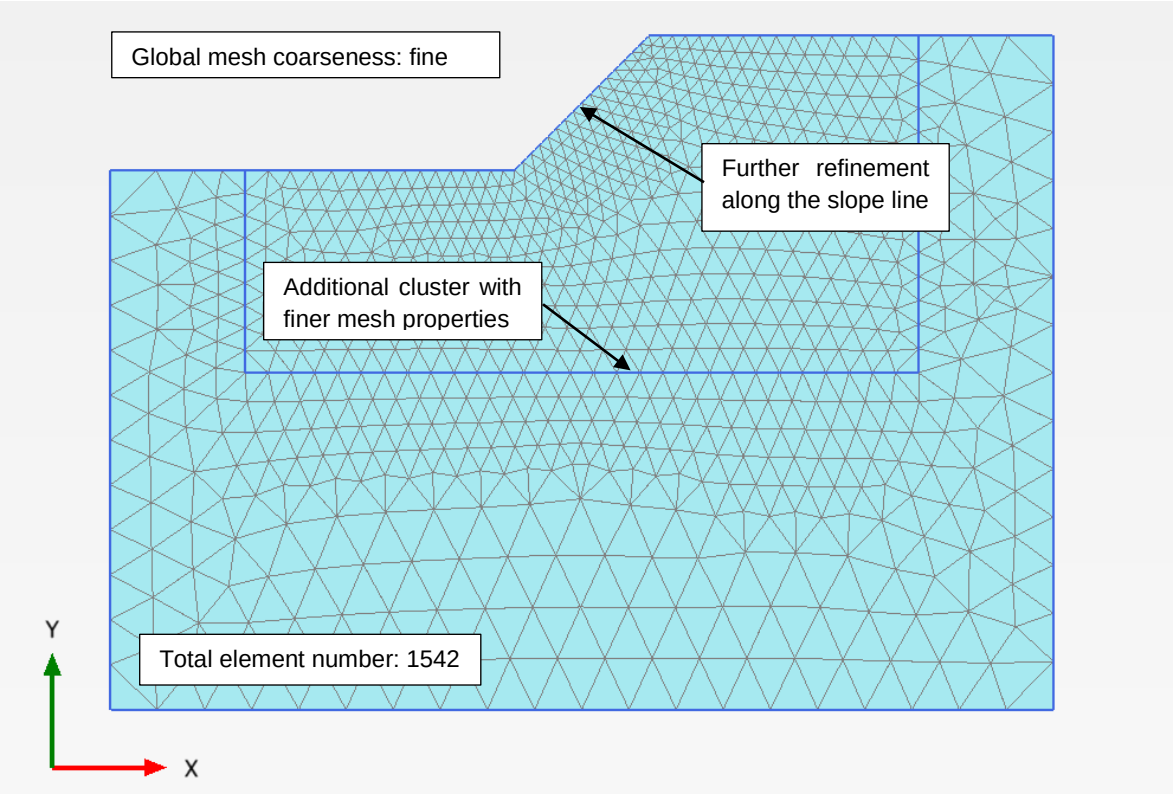

Figure 20: Mesh properties of the homogeneous slope model ($D = 4$ and $\beta = 45°$)

Figure 4 shows a mesh with the defined standard mesh properties. The global coarseness is set to *fine* and an additional cluster is defined to keep the overall element number lower. Furthermore, the mesh is refined once more along the face of the slope.

6.3.3 Initial undrained stress conditions

The initial effective stress situation of an undrained stability problem is of major importance. The effective stress level combined with the effective strength parameters (c', φ') determin the undrained shear strength of the material. Further stress developments (increase/decrease) do not effect the shear strength under undrained conditions. However, in Method A the shear strength is defined in effective terms where as in Method B and C it is defined in undrained terms. The Initial stress conditon, or more accurately, the initial strength profils of all methods have to be equvialent to analyse similar problems. Therefore, an excavation of the slope is simulated (stage construction under undrained conditions) for Method A. This provides similar undrained shear strength profiles prior to the stability analysis.

6.4 LFEA Properties

6.4.1 Model

The LFEA model dimensions equal the model dimensions used in the SRM-FEA (see Figure 18). The velocities (upper bound) and displacements (lower bound) at the bottom of the model are set to zero in all directions. Additionally, the vertical boundaries are restricted to zero velocity and zero displacements normal to the boundary, respectively.

6.4.2 Mesh

Figure 21 and Figure 22 show typical lower and upper bound finite element meshes for the homogeneous slope. The illustrated meshes represent the final steps of the adaptive procedure. In general, three steps are performed for this analysis. The refinement starts with 1000 elements and ultimately produces a mesh with 3000 elements. In some cases, where the error between upper and lower bound remains greater than 5%, the adaptive procedure is set to 4 calculation steps. Furthermore, a fan shape mesh condition at the top of the slope is used to ensure precise results with the cohesion-less material.

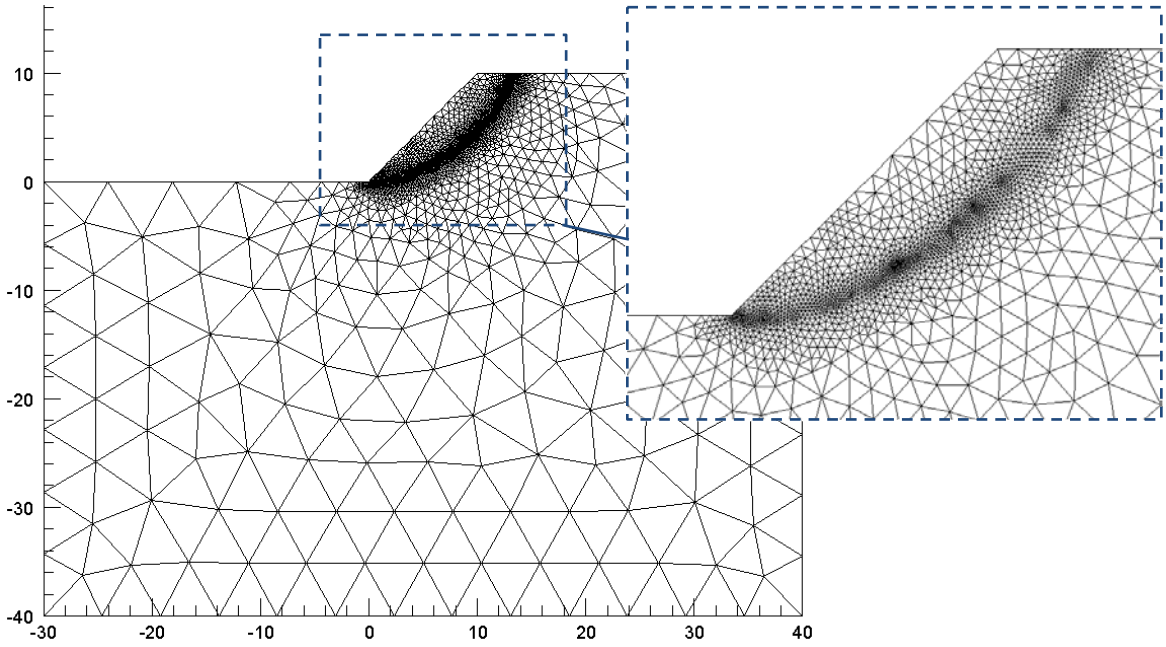

Figure 21: LFEA lower bound mesh for the homogeneous slope ($D = 4,\ \beta = 45°$, drained_2)

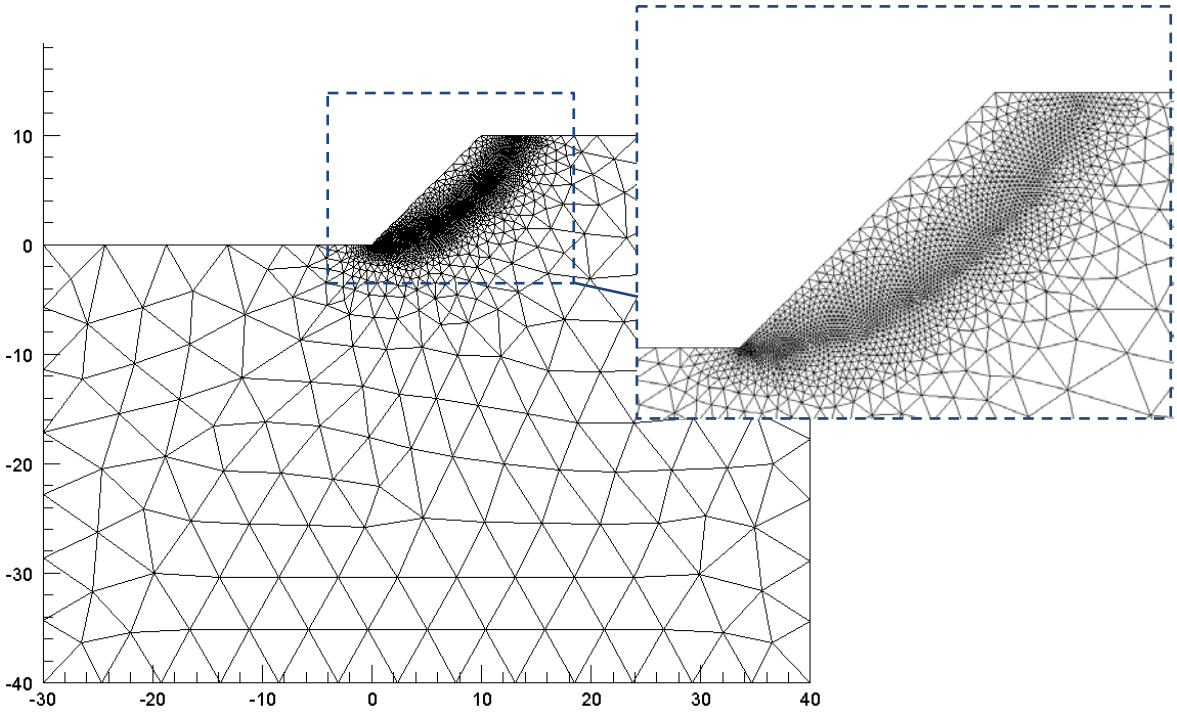

Figure 22: LFEA upper bound mesh for the homogeneous slope ($D = 4$, $\beta = 45°$, drained_2)

Figure 23 and Table 7 show results obtained with different element numbers. The procedure, once more, clearly indicates the mesh influence on accuracy. The Error between the bounds decreases the better the discretization becomes. However, at some point additional elements do not lead to more accurate results and an adequate mesh is found.

The underlying meshes for this analysis are all produced with adaptive remeshing (three steps). Therefore, relatively low element numbers (>500) achieve already moderate results. The standard element number for the LFEA of the slope derived from the procedure is 3000. The benefit of the slightly better results of higher element numbers is offset by the additional calculation time.

Table 7: LFEA results from different element numbers. ($D = 4$, $\beta = 45°$, drained_2)

Elements	Lower Bound	Upper Bound	max. Error
50	1.03	1.69	64.9%
100	1.18	1.65	39.8%
250	1.35	1.58	17.0%
500	1.41	1.57	11.3%
1000	1.45	1.54	6.4%
2000	1.45	1.53	5.5%
3000	1.46	1.52	4.1%
4000	1.46	1.51	3.3%
5000	1.46	1.51	3.3%

The blue line in Figure 23 is the mean value of the lower and upper bound (3000 elements). The two other lines represent the bounds for different element numbers and the gap between the lines is the corresponding maximal error.

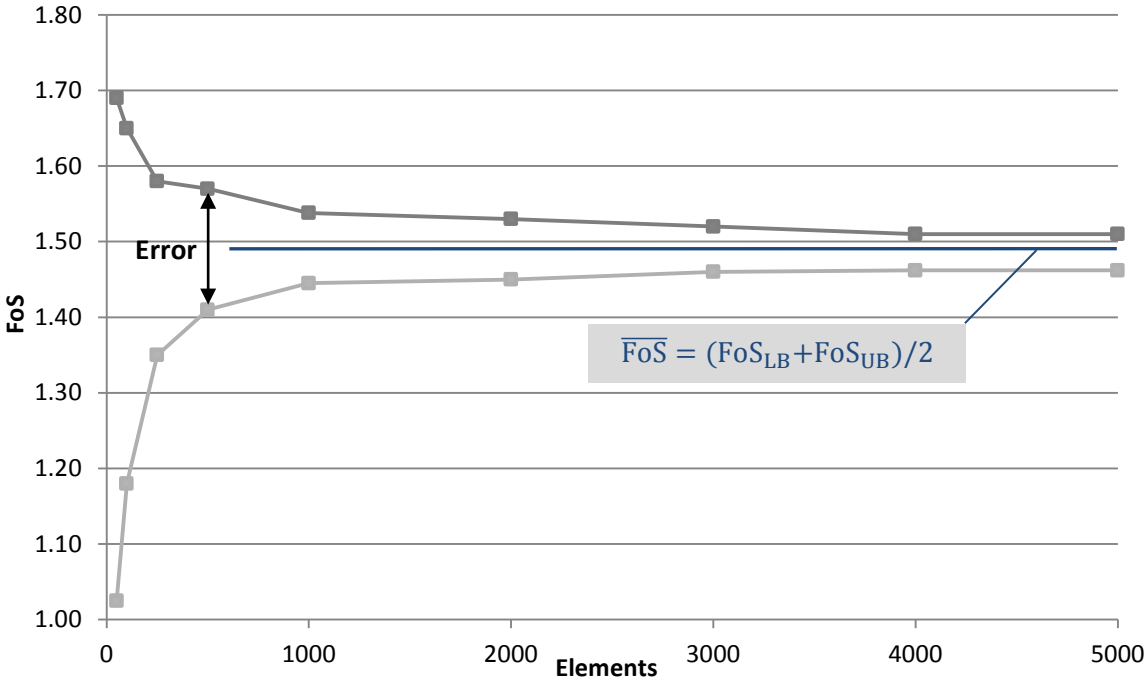

Figure 23: LFEA results from different element numbers. ($D = 4$, $\beta = 45°$, drained_2)

6.4.3 FoS estimation for the frictional material (no cohesion)

A homogeneous slope consisting of cohesion less soil creates a relatively unique problem for LFEA. The stability of the slope is virtually load independent. Depending on the length of the slope this statement becomes more apparent. Assume for example an infinitely long slope. Its stability is solely governed by the relation between the slope angle and the friction angle of the material. In the limit case, the slope angle equals the friction angle and a greater slope angle than friction angle is impossible.

However, LFEA optimises the loads in upper and lowered bound analysis until the least and greatest limit load for the problem are found. To calculate a FoS in terms of material strength, various strength parameters are entered to determine the state where the limit load over actual load equals 1 (See section 4.7 for more detail on the general FoS estimation). The general estimation procedure is not applicable since there is no limit load for this case, the load is either 0 or ∞. However, the limit state relation between friction and slope angle ($\varphi = \beta$) must hold.

Although a practicable application of LFEA on such a problem is questionable, it is important to evaluate its functionality. Consequently, the following approach can be used

to estimate limit strength parameters of a slope consisting of purely frictional soil. Similar to the general FoS procedure, several trials with adjusted strength parameters are required. However, while the limit strength itself cannot be found, the procedure eventually provides an accurate figure of the limit strength. This is possible because the bearing load of the single trails is either 0 or ∞ and the limit case must be between the 2 closest trails of 0 (unstable) and ∞ (stable). The procedure is illustrated in Figure 24.

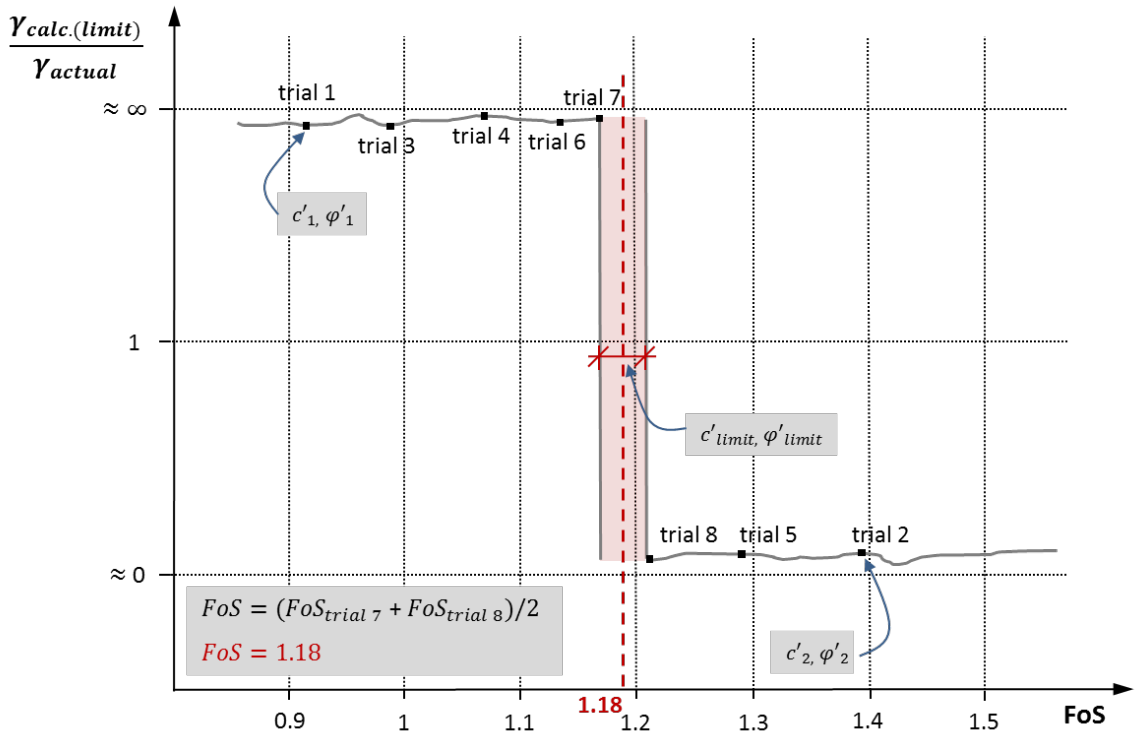

Figure 24: FoS estimation of a load independent stability problem

The limit strength parameters are bracketed between trial 7 and trail 8. The closer they lie to together the more accurate is the result.

6.5 Results

6.5.1 Failure Mechanisms

In general, both methods achieve similar failure mechanisms. However, note that a comparison of the frictional material without cohesion is excluded since limit analysis is unable to obtain the actual state of failure. The method can only obtain, as explained above, either a stable (FoS $= \infty$) or unstable state (FoS $= 0$). The following figures show generic results of the case $D = 4,\ \beta = 45°$ and the material drained 2_A.

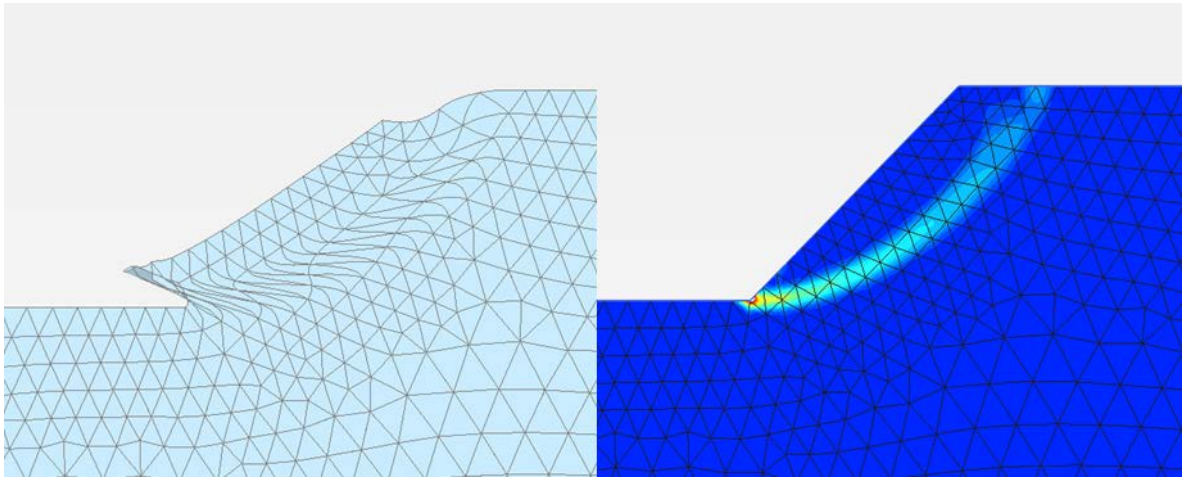

Figure 25: Plaxis failure mechanism for $D = 4,\ \beta = 45°$, drained 2_A (Deformed mesh on the left side and deviatoric strains on the right side).

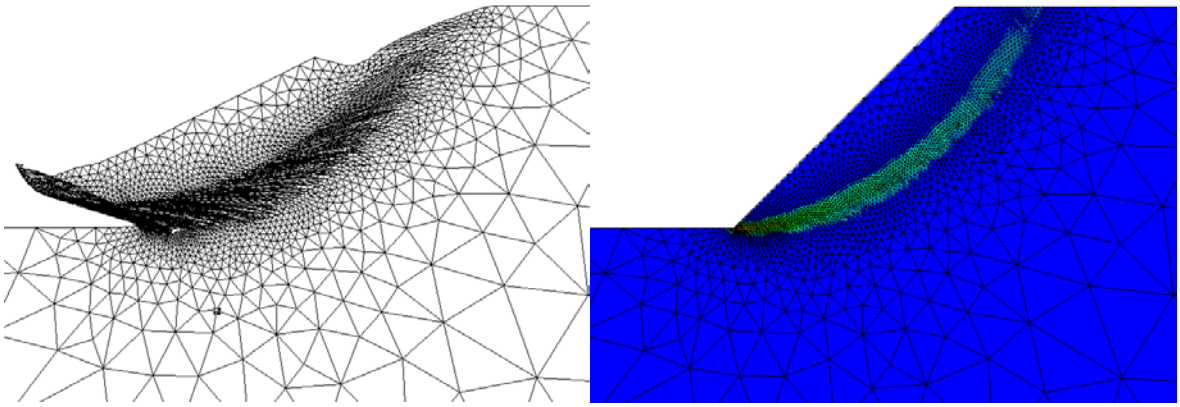

Figure 26: LFEA upper bound results for $D = 4,\ \beta = 45°$, drained 2_A (Deformed mesh on the left side and power dissipation on the right side).

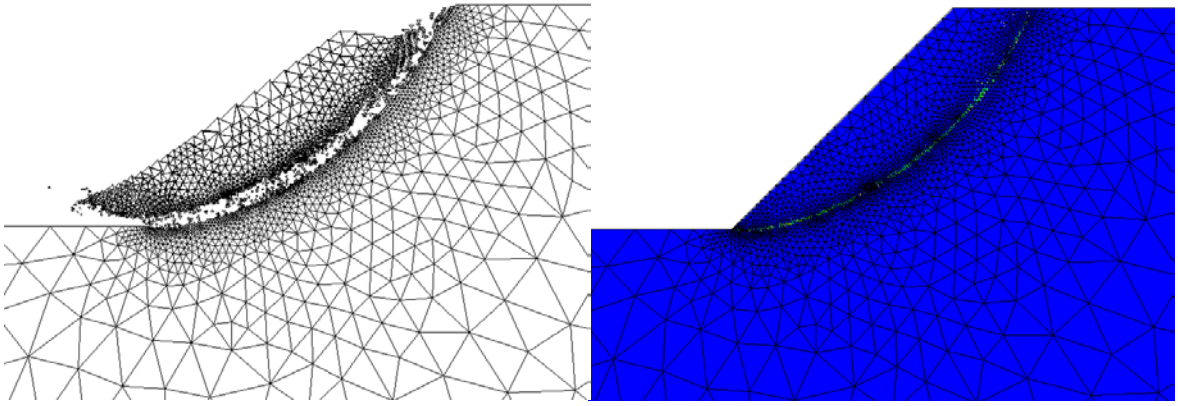

Figure 27: LFEA lower bound results for $D = 4,\ \beta = 45°$, drained 2_A (Deformed mesh on the left side and plastic multiplier on the right side).

6.5.2 Frictional material

The stability of slopes consisting of solely frictional soil is not an easy issue in numerical analysis. In Nature, a strength reduction would lead to a failure mechanism that begins at the upper edge of the slope and is very shallow. The soil grains at the top of the slope would start to roll down until the new slope angle is at least equal to the friction angle. Hence, natural slopes of purely frictional soil, such as sand or gravel, have a friction angle equal or greater than the slope angle. However, addressing this issue in numerical simulations can lead to singularities or difficulties in finding the true failure mechanism.

The results of the drained analysis are shown in the following tables and figures. Both cases, $D = 1$ and $D = 4$ are demonstrated. The non-associated approach of Plaxis is compared with the adjusted LFEA results after Davis (Davis E. H., 1968). The associated approach on the other hand, is compared with the standard (associated) LFEA outcomes.

Table 8: LFEA (standard) and SRM-FEA (associated) results for the frictional material - $D = 1$

β	drained_1_A	Lower Bound	Upper Bound
15	2,64	2,61	2,65
30	1,23	1,21	1,25
45	0,70	0,70	0,72
60	0,41	0,40	0,42

Table 9: LFEA (standard) and SRM-FEA (associated) results for the frictional material - $D = 4$

β	drained_1_A	Lower Bound	Upper Bound
15	2,64	2,62	2,63
30	1,23	1,21	1,24
45	0,71	0,70	0,73
60	0,39	0,40	0,45

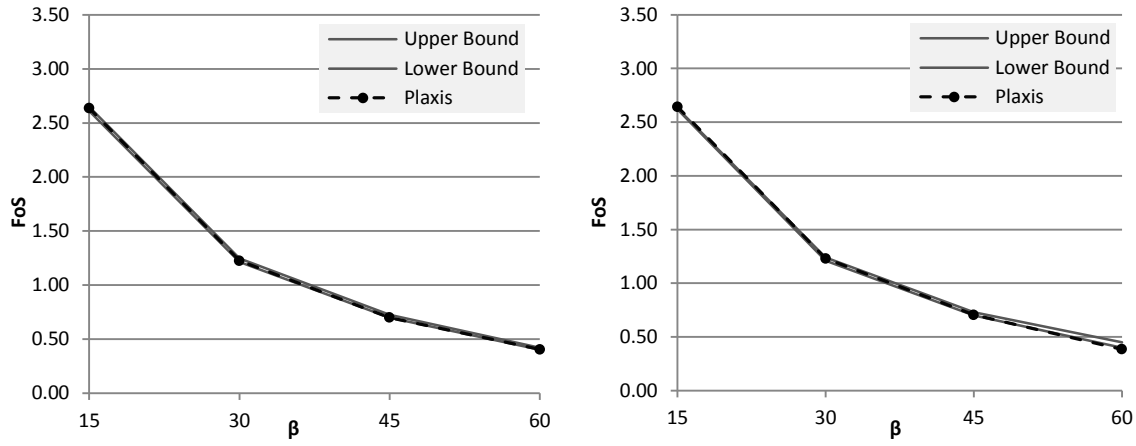

Figure 28: FLEA (standard) and SRM-FEA (associated) for the frictional material ($D = 1$ on the left side and $D = 4$ on the right side).

Table 10: LFEA (Davis approach) and SRM-FEA (non-associated ($\psi = 0$) and Davis approach) results for the frictional material - $D = 1$

β	drained_1_NA	drained_1 (Davis)	Lower Bound (Davis)	Upper Bound (Davis)
15	2,54	2,16	2,13	2,17
30	no solution	1,00	0,99	1,02
45	no solution	0,57	0,57	0,59
60	no solution	no solution	0,33	0,35

Table 11: LFEA (Davis approach) and SRM-FEA (non-associated ($\psi = 0$) and Davis approach) results for the frictional material - $D = 4$

β	drained_1_NA	drained_1 (Davis)	Lower Bound (Davis)	Upper Bound (Davis)
15	2,62	2,16	2,14	2,15
30	1,16	1,00	0,97	1,02
45	no solution	0,58	0,57	0,60
60	no solution	no solution	0,33	0,37

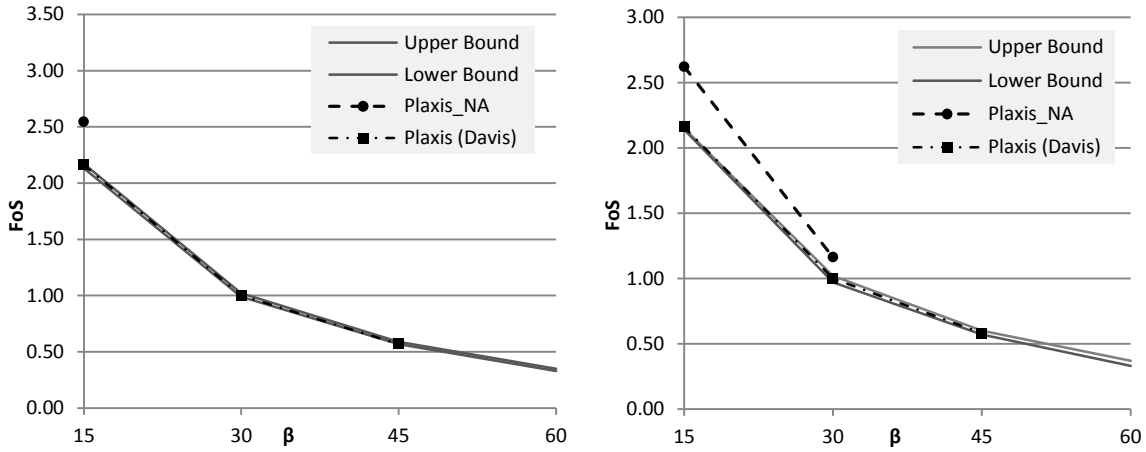

Figure 29: FLEA (Davis approach) and SRM-FEA (non-associated $\psi = 0$) for the frictional material ($D = 1$ on the left side and $D = 4$ on the right side).

The results show a tendency that the non-associated approach with $\psi = 0$ does not perform as well as the associated approach. Fortunately, the associated SRM-FEA results are either in between the lower and upper bounds or closely outside the bounds. The non-associated approach on the other hand, did not find a clear solution in more than half of the cases. A definite reason for this behaviour remains vague. However, it seems that the method struggles to find the true failure mechanism if the dilatancy angle is set to 0. The closer the friction angle is to the slope angle the more apparent the problem becomes. Section 6.6 shows a more detailed study of this issue.

Apart from this, it is important to note that the limit friction angles obtained with associated

flow rules are practically in line with the slope angle. Table 12 and Table 13 show the slope angles versus the limit friction angles. Although the dilatancy angle is set equal to the friction angle, the results coincide with the slope angles. This might lead to the conclusion that the associated approach provides precise results for a slope of frictional material. Furthermore, the poor performance of the non-associated approach underlines that the associated approach might be more favourable for such an unconstraint problem.

Table 12: φ_{limit} vs. slope angle - LFEA (standard) and associated approach in SRM-FEA ($D = 1$)

β	drained_1_A	Lower Bound	Upper Bound
15	14.85	15.02	14.80
30	29.65	29.98	29.35
45	44.60	45.01	44.04
60	60.88	60.08	58.95

Table 13: φ_{limit} vs. slope angle - LFEA (standard) and associated approach in SRM-FEA ($D = 4$)

β	drained_1_A	Lower Bound	Upper Bound
15	14.85	14.96	14.91
30	29.65	30.06	29.45
45	44.60	45.01	43.81
60	60.88	60.26	57.27

Finally, there are only small differences between the cases of $D = 1$ and $D = 4$. This is favourable since the depth of the bedrock should not affect the stability of the solely frictional material. The occurred differences are likely to be caused by the discretisation influence.

6.5.3 Cohesive-frictional material (drained)

The results of the stability analysis of the cohesive–frictional material under drained conditions are shown in this section. The SRM-FEA non-associated approach is compared to the adjusted LFEA results after Davis. The associated approach on the other hand is directly compared with the LFEA results.

In general, the obtained SF's of the 2 methods coincide well. However, in some cases the Plaxis results are below the lower bound. Fortunately, the percentage value of these differences is only small. The failure mechanisms of the cohesive frictional and purely frictional material differ. This is basically due to the fact that a higher degree of stress independent strength (cohesion) causes a deeper failure mechanism in slopes.

While the depth of the bedrock had no influence on the stability of the solely frictional soil, it affects the results of the cohesive-frictional material.

Table 14: LFEA (standard) and SRM-FEA (associated) results for cohesive-frictional material under drained conditions - $D = 1$

β	drained_2_A	Lower Bound	Upper Bound
15	3,32	3,31	3,36
30	1,95	1,97	2,01
45	1,44	1,46	1,50
60	1,13	1,16	1,21

Table 15: LFEA (standard) and SRM-FEA (associated) results for cohesive-frictional material under drained conditions - $D = 4$

β	drained_2_A	Lower Bound	Upper Bound
15	3,12	3,08	3,16
30	1,94	1,88	1,94
45	1,44	1,39	1,45
60	1,13	1,07	1,12

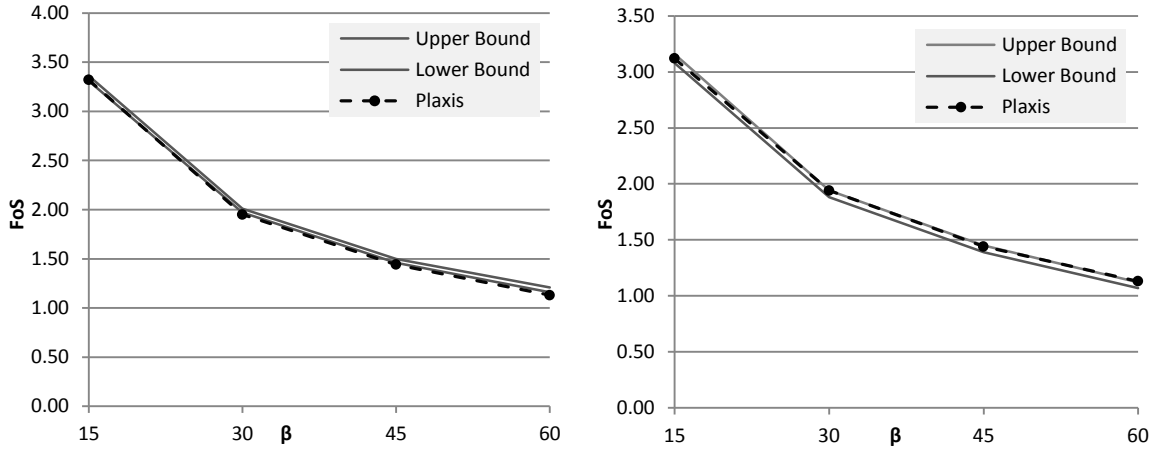

Figure 30: FLEA (standard) and SRM-FEA (associated) for the cohesive-frictional material under drained conditions ($D = 1$ on the left side and $D = 4$ on the right side).

The difference between the associated and non-associated approaches is smaller than determined for the frictional material. Furthermore, the SRM-FEA had no difficulties in finding the failure mechanisms.

Table 16: LFEA (Davis approach) and SRM-FEA (non-associated) results for cohesive-frictional material under drained conditions - $D = 1$

β	drained_2_NA	drained_2 (Davis)	Upper Bound (Davis)	Upper Bound (Davis)
15	3,30	3,00	3,00	3,05
30	1,92	1,76	1,78	1,82
45	1,38	1,30	1,32	1,36
60	1,07	1,02	1,05	1,10

Table 17: LFEA (Davis approach) and SRM-FEA (non-associated) results for cohesive-frictional material under drained conditions - $D = 4$

β	drained_2_NA	drained_2 (Davis)	Lower Bound (Davis)	Upper Bound (Davis)
15	3,10	2,83	2,82	2,89
30	1,90	1,75	1,76	1,81
45	1,41	1,31	1,32	1,38
60	1,08	1,02	1,05	1,09

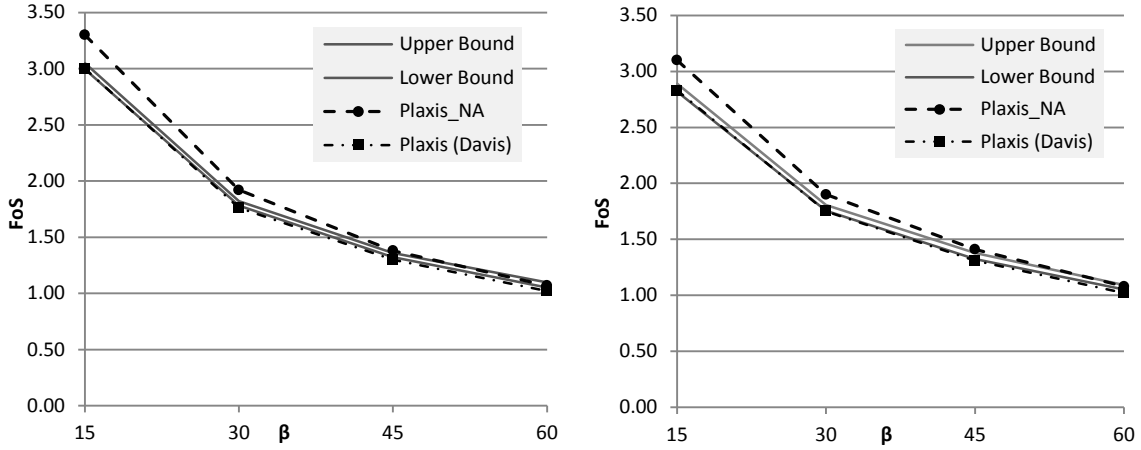

Figure 31: FLEA (Davis approach) and SRM-FEA (non-associated) for the cohesive-frictional material under drained conditions ($D = 1$ on the left side and $D = 4$ on the right side).

6.5.4 Cohesive-frictional material (undrained)

The results of the undrained analysis are summarised in the following tables and figures. The tables show all 3 calculation methods performed with Plaxis whereas the figures only illustrate the results of Method A and B versus LFEA.

The results of the total stress calculations (Method B, C and LFEA) show only small differences. In fact, the difference between Plaxis - Method B and the corresponding mean value of the lower and upper bounds, is less than 1% for all cases. The FoS's of Method C are slightly lower, however they are still close to the bounds.

Method A, on the other hand, generally obtained higher Factors of Safety, with apart from that similar failure mechanism. Furthermore, the limit strength resistance along the failure surfaces are likely to be similar as well. The discrepancy of the Safety Factor is, as explained in section 5.6, assumed to be due to the different Factor of Safety definition. Further information and more detailed undrained stability analyses are shown in sections 5.6 and 7 respectively.

Table 18: LFEA (standard) and SRM-FEA (Methods A/B/C) results for the cohesive-frictional material under undrained conditions - $D = 1$

β	undrained_A	undrained_B	undrained_C	Lower Bound	Upper Bound
15	4.20	3.96	3.92	3.92	3.99
30	2.74	2.56	2.54	2.53	2.59
45	2.13	1.96	no solution	1.96	1.99
60	1.71	1.60	no solution	1.59	1.63

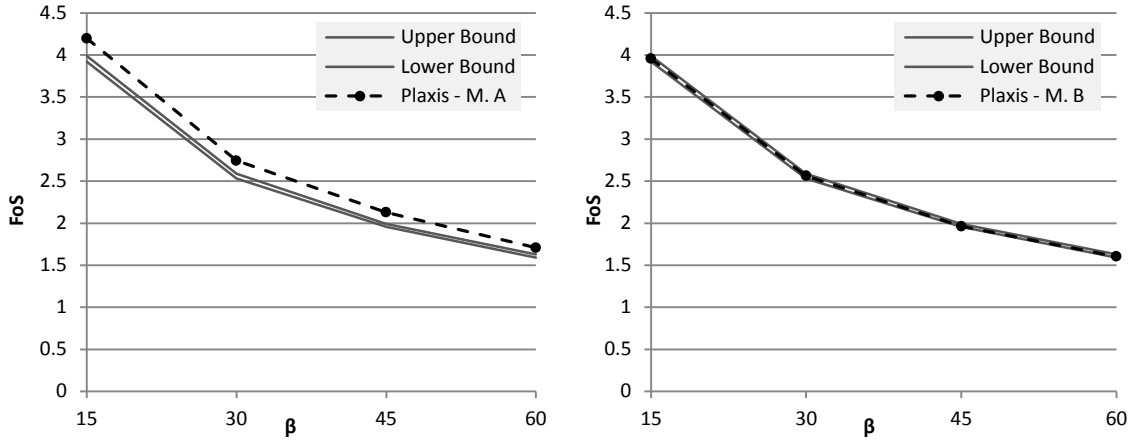

Figure 32: LFEA (standard) and SRM-FEA (Method A and B) results for the cohesive-frictional material under undrained conditions - $D = 1$ (Method A on the left side and Method B on the right side).

Table 19: LFEA (standard) and SRM-FEA (Methods A/B/C) results for the cohesive-frictional material under undrained conditions - $D = 4$

β	undrained_A	undrained_B	undrained_C	Lower Bound	Upper Bound
15	3.82	3.63	3.62	3.60	3.69
30	2.68	2.50	2.49	2.47	2.54
45	2.16	1.98	1.95	1.95	2.01
60	1.72	1.61	1.58	1.59	1.64

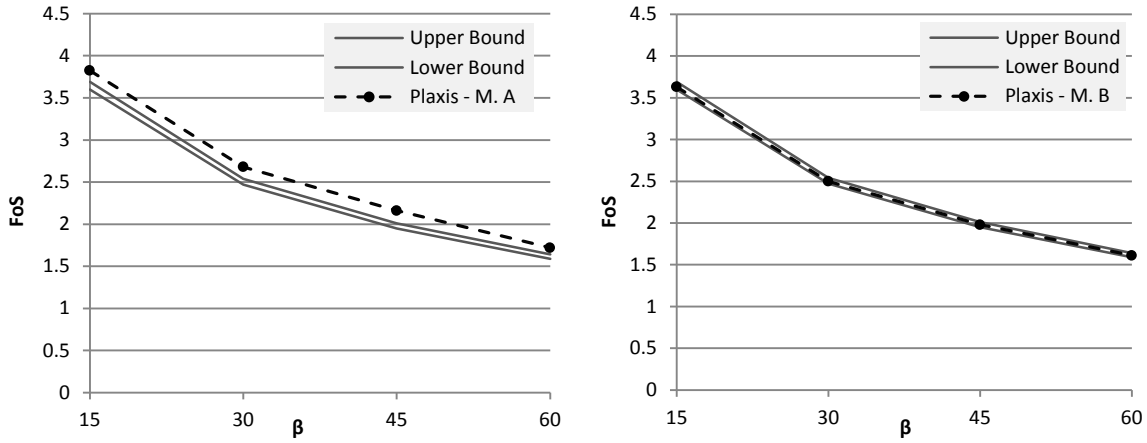

Figure 33: LFEA (standard) and SRM-FEA (Method A and B) results for the cohesive-frictional material under undrained conditions - $D = 4$ (Method A on the left side and Method B on the right side).

6.6 Extended analysis of the purely frictional material

6.6.1 Analysis description

This additional analysis considers a purely frictional material in more detail. The problem is reduced to one case and only a PLAXIS 2D 2010 analysis is performed. The slope angle is 30° and the bedrock stands at the bottom of the slope ($D = 1$). The emphasis of the study is put on the influence of the flow rule. Therefore, the dilatancy angle is set to different values, ranging from 0 up to the value of the friction angle. The SRM-FEA model and mesh are illustrated in Figure 34.

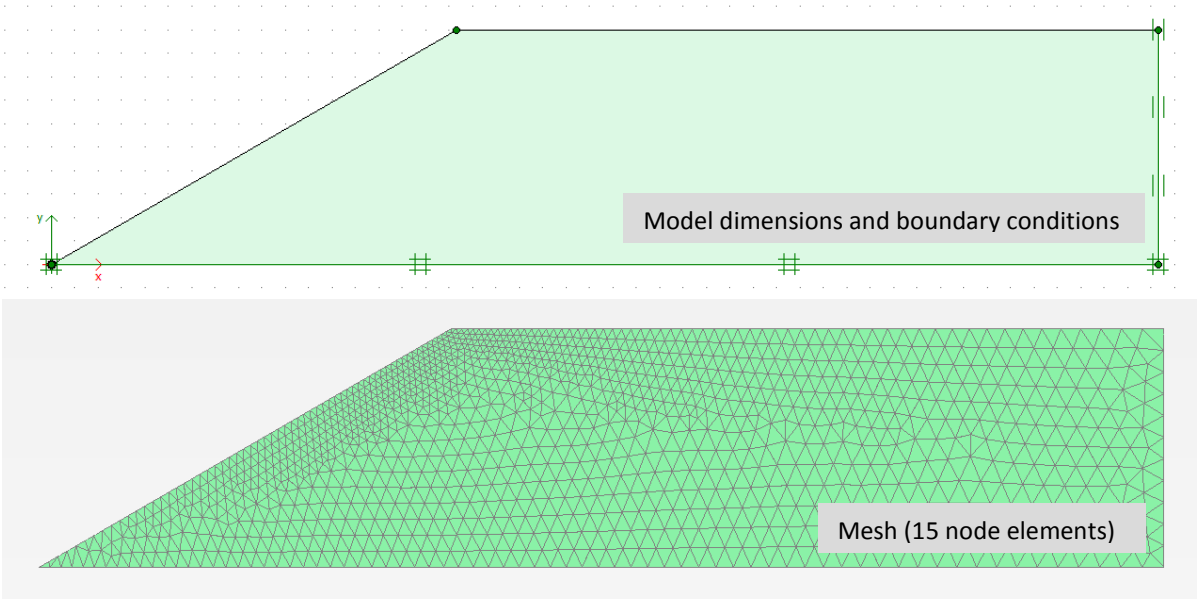

Figure 34: Homogenous slope model and mesh for the additional analysis with the purely frictional material - $D = 1$ and $\beta = 30°$.

Table 20 shows the strength parameters. The analysis includes 5 friction angles with 5 corresponding dilatancy angles each. All other material parameters are equal to the frictional material (drained_1) parameters.

Table 20: Strength parameters for the additional homogeneous slope analysis

φ	Dilatancy angle ψ				
30	0.00	5.00	10.00	15.00	30.00
32.5	0.00	5.00	10.00	15.00	32.50
35	0.00	5.00	10.00	15.00	35.00
37.5	0.00	5.00	10.00	15.00	37.50
40	0.00	5.00	10.00	15.00	40.00

6.6.2 Results

Figure 35 illustrates the strength reduction outcomes of the non-associated (ψ = 0) approach (dashed lines) compared to the associated ($\psi = \varphi$) approach (solid lines). The associated outcomes show clear strain occurring after a few steps, whereas the non-associated results show a relatively unstable figure.

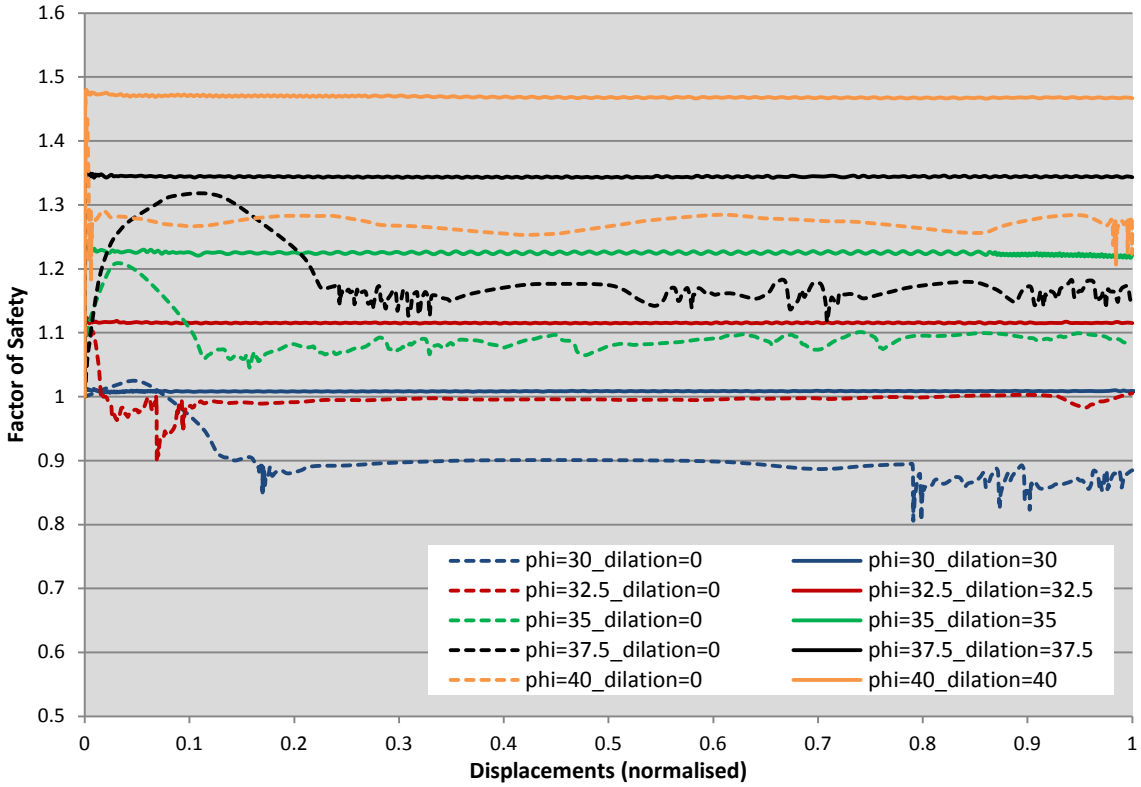

Figure 35: Summarised Plaxis - strength reduction outcomes of the of the extended analysis with the purely frictional material

The following figures show the outcomes of one friction angle with the according dilatancy angle variations. The outcomes indicate that higher dilatancy angles lead to more stable results. Furthermore, the limit friction angles obtained with associated flow rules coincide most with the slope angles.

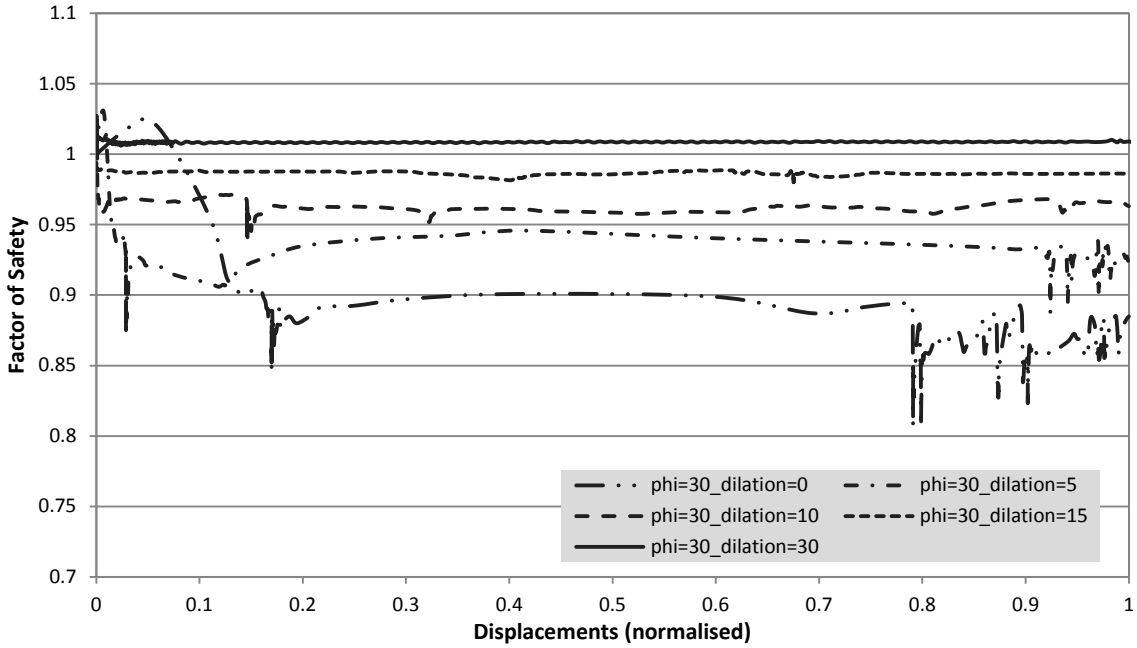

Figure 36: Plaxis – strength reduction outcomes of the frictional material with $\varphi = 30°$ and different dilatancy angles ($D = 1$ and $\beta = 30°$)

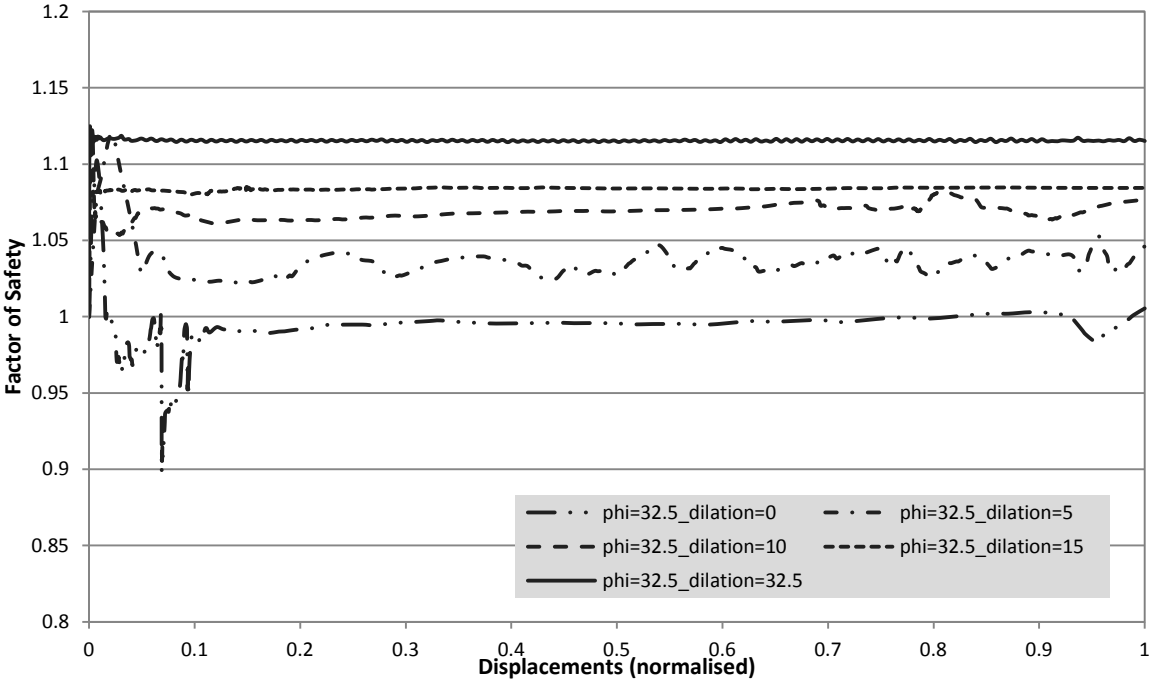

Figure 37: Plaxis – strength reduction outcomes of the frictional material with a friction angle $\varphi = 32.5°$ and different dilatancy angles ($D = 1$ and $\beta = 30°$)

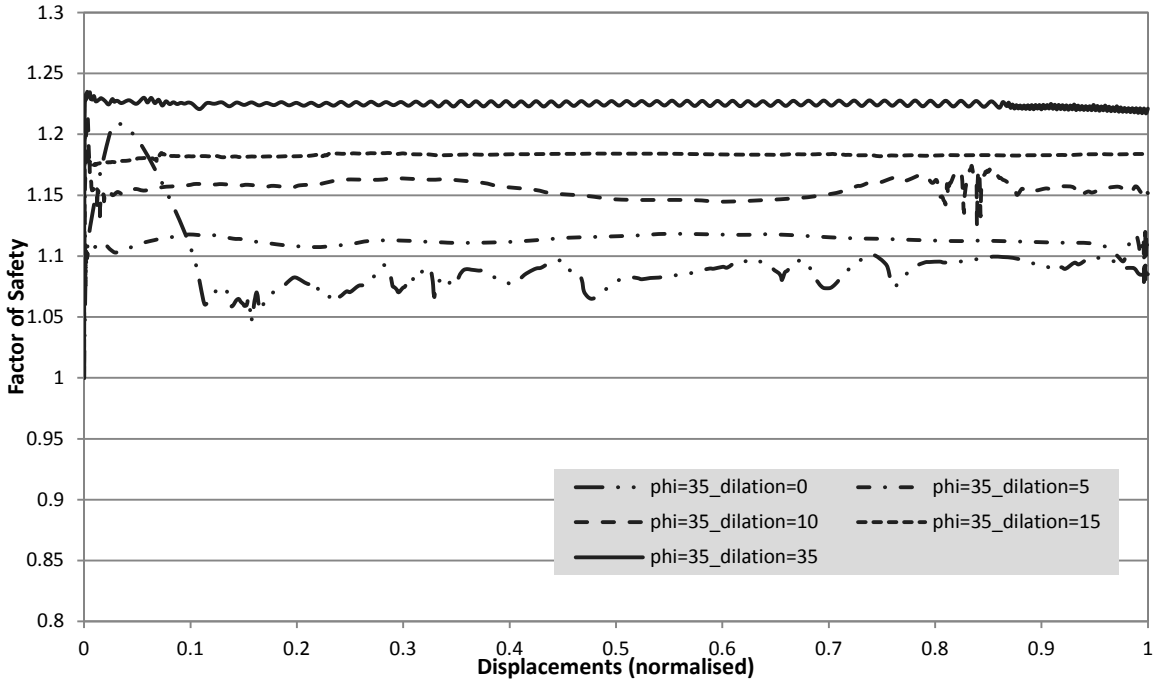

Figure 38: Plaxis – strength reduction outcomes of the frictional material with a friction angle $\varphi = 35°$ and different dilatancy angles ($D = 1$ and $\beta = 30°$)

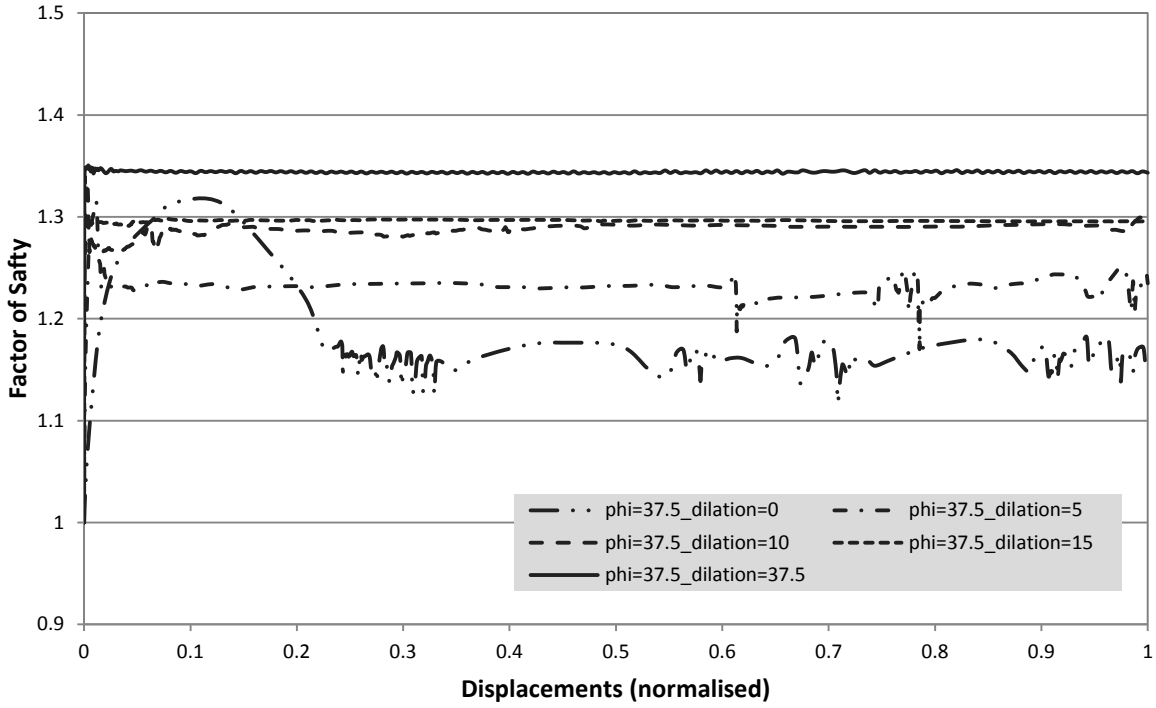

Figure 39: Plaxis – strength reduction outcomes of the frictional material with a friction angle $\varphi = 37.5°$ and different dilatancy angles ($D = 1$ and $\beta = 30°$)

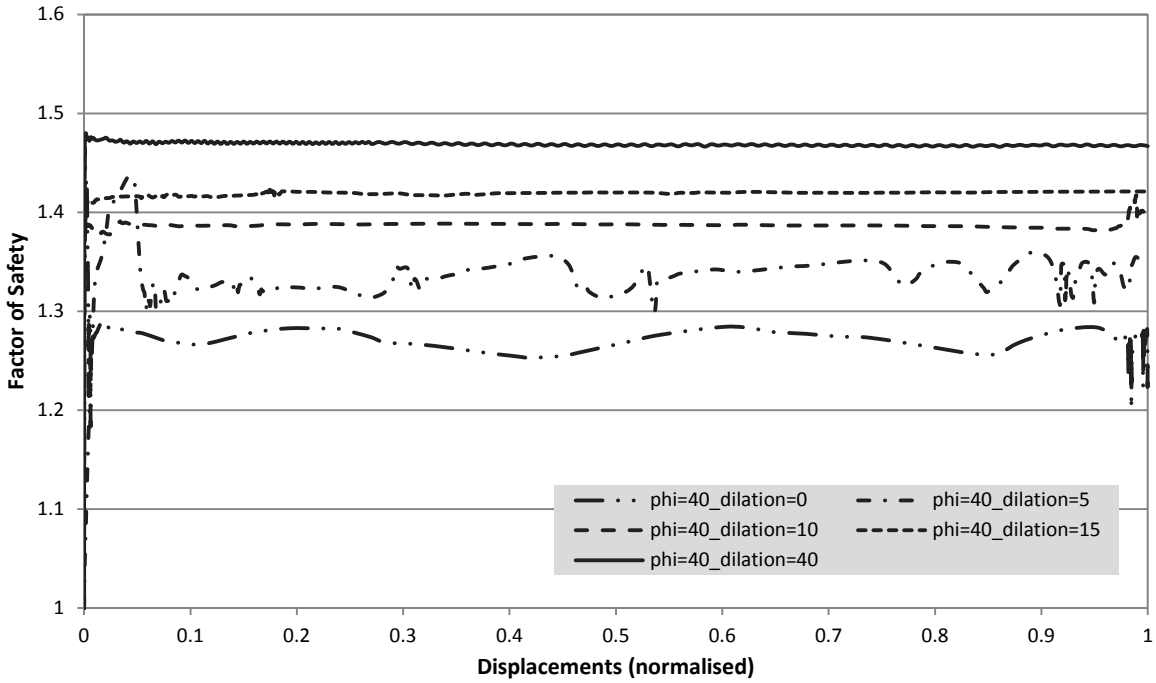

Figure 40: Plaxis – strength reduction outcomes of the frictional material with a friction angle $\varphi = 40°$ and different dilatancy angles ($D = 1$ and $\beta = 30°$)

7 Tunnel face

7.1 Problem description

This Example considers a plane strain stability analysis of a tunnel face. The tunnel has an overburden H and a diameter D. The face of the tunnel is stabilised with a pressure σ_T and its side walls are supported with a rigid smooth lining. The analysis includes various soil parameter sets under undrained conditions. The layout of the problem is shown in Figure 41. The focus in this example is to analyse the differences between the undrained calculation methods of Plaxis in more detail.

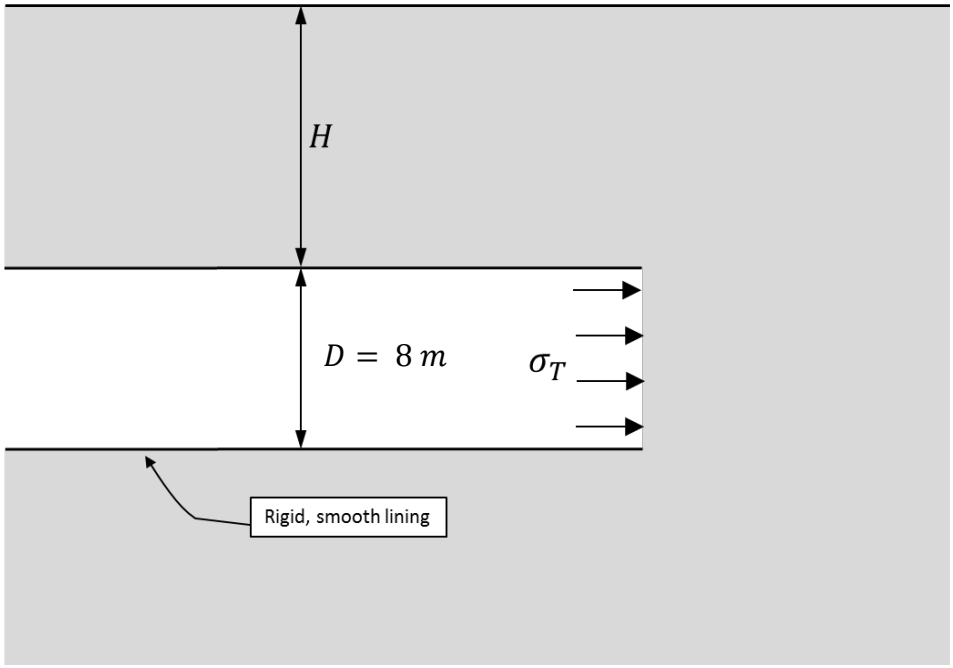

Figure 41: Plane strain tunnel face stability geometry

Therefore, two different overburdens H $(8\,m$ & $24\,m)$ are considered. In the first case the ratio of $H/D = 1$ and in the second case $H/D = 3$. Additionally, the supporting pressure σ_T is set to 25 kPa and 75 kPa respectively. This provides lower and higher Factors of Safety under apart from that similar (soil and geometry) conditions.

7.2 Parameter description

The undrained shear strength profiles range from constant to highly depth dependent. However, regardless of the profile, the initial undrained shear strength at the top of the

tunnel is fixed at a constant value. The value at this point is $\gamma * H * 0.4$ and the various strength profiles are governed by different $s_{u,inc}/s_{u,ref}$ ratios. The constant value ensures Factors of Safety above 1 and no large values for high $s_{u,inc}/s_{u,ref}$ ratios. Table 21, Table 22 and Table 23 show the parameters for Method A, B and C respectively. The LFEA strength parameters are equivalent to the strength parameters of Method B and C.

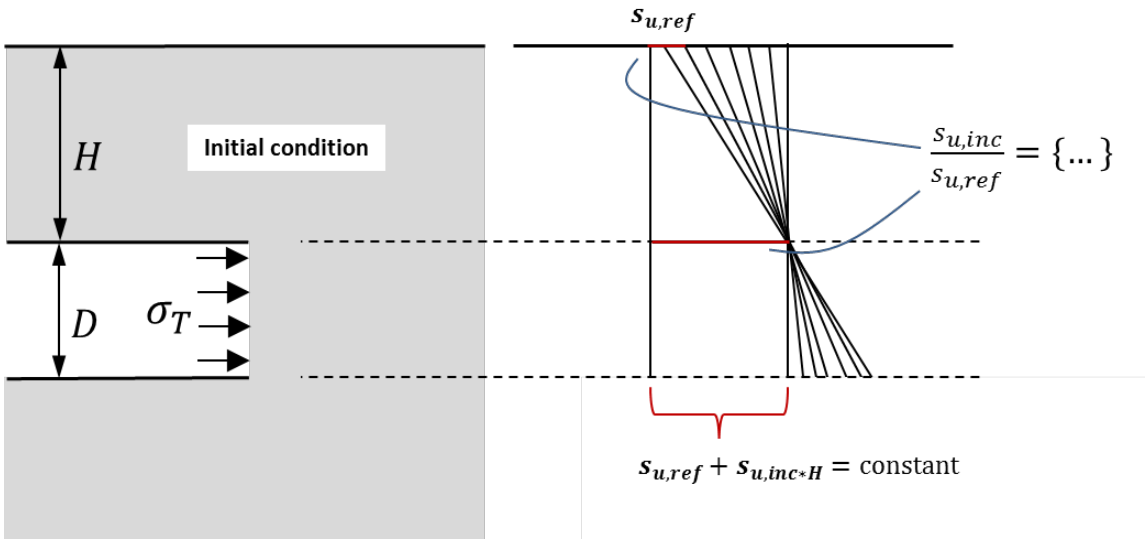

Figure 42: Undrained shear strength profile concept

Table 21: Effective shear strength parameters and corresponding E-moduli (Method A)

Su,inc/Su,ref		0.00	0.05	0.15	0.25	0.50	0.75	1.00	1.50
H/D=1	c'	60.80	43.75	28.54	21.37	13.27	9.67	7.62	5.36
	φ'	0.00	6.99	14.43	18.48	23.58	26.06	27.55	29.25
	E	18240	13029	8291	6080	3648	2606	2027	1403
	E,inc	0	651	1244	1520	1824	1954	2027	2105
H/D=3	c'	182.40	85.61	43.03	29.01	16.08	11.14	8.53	5.81
	φ'	0.00	14.43	22.86	26.06	29.25	30.53	31.22	31.96
	E	54720	24873	11896	7817	4209	2880	2189	1479
	E,inc	0	1244	1784	1954	2105	2160	2189	2218

The soil stiffness is coupled with the undrained shear strength. Thus, it has a fixed and an increasing component. The relation between the stiffness and undrained shear strength is $E = s_u * 300$. Furthermore, the possion ratio v is 0.3 [-] and the soil weight γ is $19\ kN/m^3$ for all parameter sets.

Table 22: Undrained shear strength parameters and E-moduli (Method B)

$s_{u,inc}/s_{u,ref}$		0.00	0.05	0.15	0.25	0.50	0.75	1.00	1.50
H/D=1	$s_{u,ref}$	60.800	43.429	27.636	20.267	12.160	8.686	6.756	4.677
	$s_{u,inc}$	0.000	2.171	4.145	5.067	6.080	6.514	6.756	7.015
	E	18240	13029	8291	6080	3648	2606	2027	1403
	$E_{,inc}$	0	651	1244	1520	1824	1954	2027	2105
H/D=3	$s_{u,ref}$	182.400	82.909	39.652	26.057	14.031	9.600	7.296	4.930
	$s_{u,inc}$	0.000	4.145	5.948	6.514	7.015	7.200	7.296	7.395
	E	54720	24873	11896	7817	4209	2880	2189	1479
	$E_{,inc}$	0	1244	1784	1954	2105	2160	2189	2218

Table 23: Undrained shear strength parameters and undrained E-moduli (Method C)

$s_{u,inc}/s_{u,ref}$		0.00	0.05	0.15	0.25	0.50	0.75	1.00	1.50
H/D=1	$s_{u,ref}$	60.800	43.429	27.636	20.267	12.160	8.686	6.756	4.677
	$s_{u,inc}$	0.000	2.171	4.145	5.067	6.080	6.514	6.756	7.015
	Eu	21046	15033	9566	7015	4209	3007	2338	1619
	$E_{u,inc}$	0	752	1435	1754	2105	2255	2338	2428
H/D=3	$s_{u,ref}$	182.400	82.909	39.652	26.057	14.031	9.600	7.296	4.930
	$s_{u,inc}$	0.000	4.145	5.948	6.514	7.015	7.200	7.296	7.395
	Eu	63138	28699	13726	9020	4857	3323	2526	1706
	$E_{u,inc}$	0	1435	2059	2255	2428	2492	2526	2560

7.3 SRM – FEA Properties

7.3.1 Model

Figure 43 shows the model dimensions and boundary conditions of the tunnel face. The boundary conditions are defined by standard fixities plus additional fixed vertical displacements along the tunnel lining. The overburden of the model is equal to the tunnel diameter. For the case $H/D = 3$, the model is extended to the top with otherwise similar dimensions.

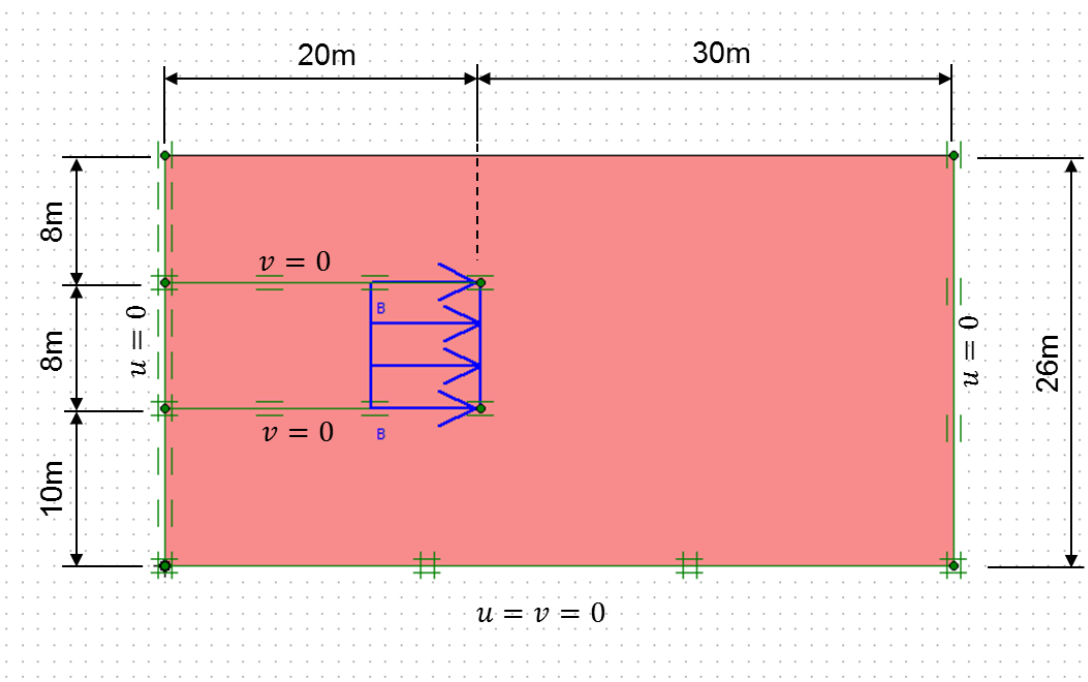

Figure 43: Tunnel face model dimensions in Plaxis (H/D=1)

7.3.2 Stage construction

The initial conditions are determined by the Ko-procedure. The next step is the application of the supporting pressure σ_T followed by the excavation of the tunnel. Ultimately, the strength reduction is performed.

7.3.3 Mesh

The mesh influence is evaluated to minimise the discretization error. The summarised results of the procedure are shown in Table 24. The determined mesh properties are as follows. The total element number is 2260. The global coarseness is set to fine. Furthermore, a cluster and 2 lines are introduced to increase the mesh density only where necessary. The refined cluster reaches from underneath the tunnel up to the soil surface. It covers the area where failure primarily occurs. Additional refinement emphasis is put on the top and bottom corner of the tunnel face. The 2 lines are placed at the corners to increase the mesh density where the largest strains are expected. The lines are slightly inclined upwards and run roughly 2-3 m into the soil cluster. Figure 44 illustrates the mesh for the case $H/D = 1$. Similar mesh properties are used for $H/D = 3$.

Table 24: FoS and calculation time with different element numbers

Elements	FOS	Time (sec)
152	1.275	20
270	1.260	28
597	1.255	46
1224	1.244	119
1420	1.238	94
2260*	**1.232**	**146**
3330	1.236	217

*Defined Element number for the analysis. Figure 44 shows the Mesh and its properties

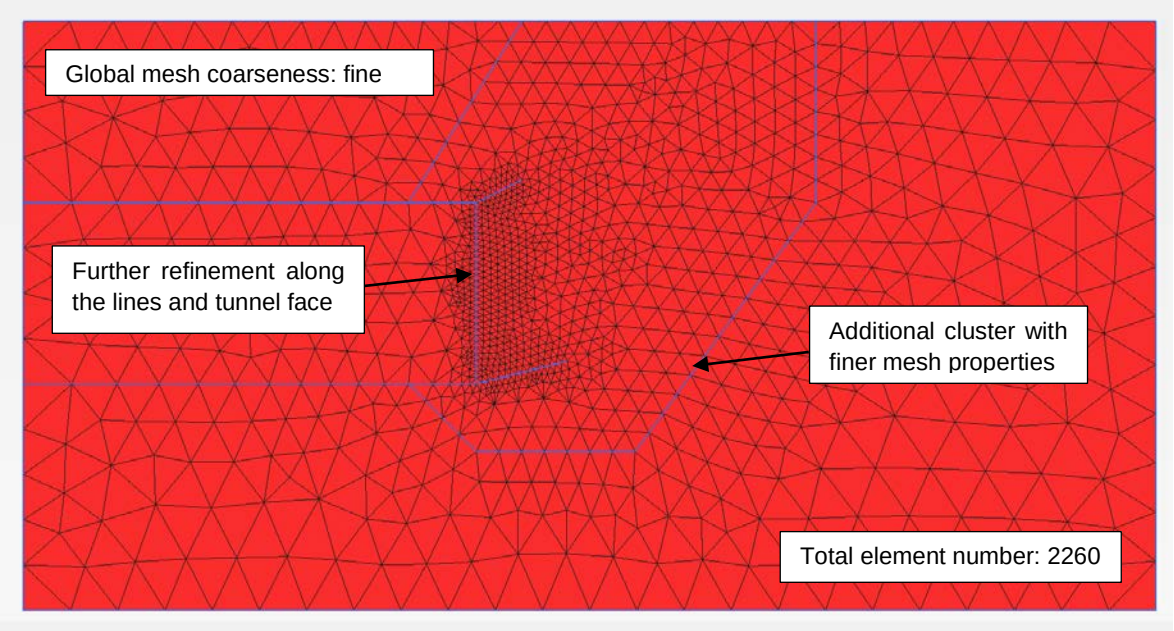

Figure 44: Mesh properties of the tunnel face model (H/D=1)

7.4 LFEA properties

7.4.1 Model

The LFEA model dimensions are equal to the SRM-FEA model dimensions and basically the same is applicable for the boundary conditions. However, the boundary formulation itself differs between the 2 approaches. The boundaries in the UB method require velocity assumptions whereas otherwise displacements are considered.

7.4.2 Mesh

The adaptive mesh refinement procedure is used for this problem. The initial element number is 1000 and the final element number is 3000 for $H/D = 1$ and 4000 for $H/D = 3$. Three calculation steps are considered in this process. Figure 45 shows the evolution of

the mesh with the initial, intermediate and final mesh.

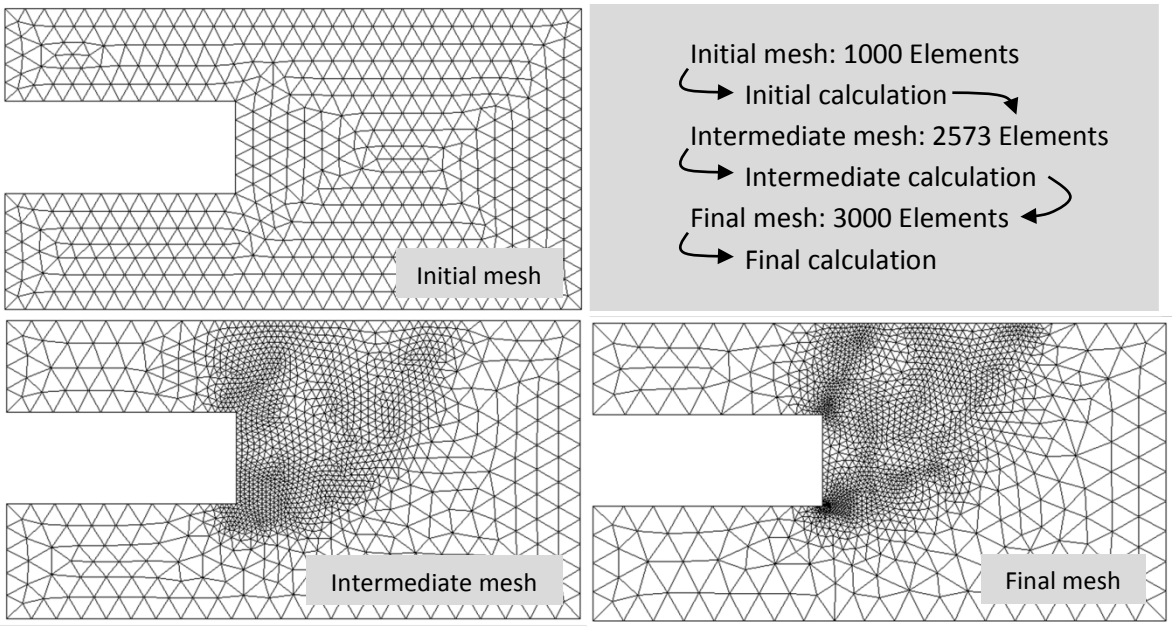

Figure 45: Mesh refinement procedure for the tunnel face (LFEA)

A mesh evaluation, regarding the final element number, is not explicitly shown in this section. However, the determined mesh provides adequate results. The errors between the lower and upper bound are smaller than 5% for all cases.

7.5 Results

7.5.1 General

Overall, the calculation methods with undrained strength parameters, namely LFEA and Plaxis – Method B and C, practically produce identical Factors of Safety. The mean value of the lower and upper bound differs less than 1% from Plaxis Method B and the results obtained with Method C are almost in line as well. However, Method C's outcomes are slightly lower. The Calculation in effective stresses only coincides in the 4 cases ($s_{u,inc}/s_{u,ref} = 0$) where the strength is constant throughout the problem area. For all other cases, where the soil has a friction angle (stress increase with depth) the results differ from the total stress calculations. This is primarily due to the different FoS definition and not due to failure occurring at a different limit strength (see section 5.6 for more information). Therefore, Plaxis – Method A achieves equal or higher Factors of Safety. The difference ranges from 0 – 10%. It is 0 for the constant case ($s_{u,inc}/s_{u,ref} = 0$) and increases the higher the ratio of $s_{u,inc}/s_{u,ref}$ becomes.

The results are summarised and illustrated in the following parameter configurations.

- Parameter set 1: $\boldsymbol{H/D = 1}$ and $\boldsymbol{\sigma_T = 25\ kPa}$
- Parameter set 2: $\boldsymbol{H/D = 1}$ and $\boldsymbol{\sigma_T = 75\ kPa}$
- Parameter set 3: $\boldsymbol{H/D = 3}$ and $\boldsymbol{\sigma_T = 25\ kPa}$
- Parameter set 4: $\boldsymbol{H/D = 3}$ and $\boldsymbol{\sigma_T = 75\ kPa}$

The lower pressure at the tunnel face results in lower Factors of Safety and the higher pressure leads to higher Safety Factors respectively. Furthermore, the 2 depth ratios $H/D = 1$ and $H/D = 3$ create different relations between stress dependent and stress independent strength at the depth of the tunnel. The stress dependent component at the deeper tunnel $H/D = 3$ adds a larger degree to the overall shear strength compared to the case $H/D = 1$. Thus, any existing trends, whether caused by the magnitude of strength reduction (FoS) or depth should be noticeable.

However, the results show no clear influence regarding these 2 issues. The only key element seems to be the ratio between the constant ($s_{u,ref}$) and increasing part ($s_{u,inc}$) of the undrained shear strength. A higher Factor of Safety might only multiply this effect by a small extend. Parameter set 2, for example, shows higher differences between the total and effective stress calculations than parameter set 1. However, the same should apply for parameter set 4 compared to 3. Though, these results (percentage difference %) are almost equivalent.

7.5.2 Failure mechanisms

Both approaches, LFEA and SRM-FEA, obtain similar failure mechanisms. Figure 46 shows the results for the case $H/D = 1$ and $\sigma_T = 25\ kPa$. Illustrated are the Methods A and B of Plaxis and the lower and upper bound outcomes.

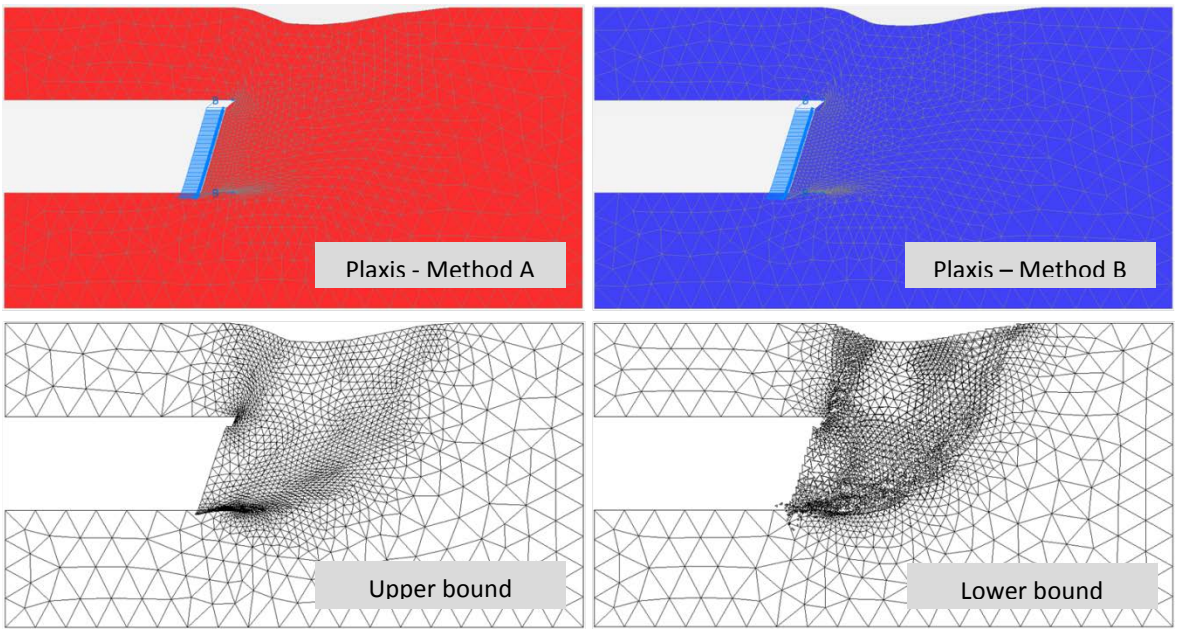

Figure 46: Failure mechanisms of the tunnel face ($H/D = 1$ and $\sigma_T = 25\ kPa$).

7.5.3 Parameter set 1: $H/D = 1$ and $\sigma_T = 25\ kPa$

Table 25: FoS from different calculation methods ($H/D = 1$ and $\sigma_T = 25\ kPa$)

$s_{u,inc}/s_{u,ref}$	Method A	Method B	Method C	Lower Bound	Upper Bound
0.00	1.23	1.23	1.19	1.21	1.25
0.05	1.30	1.29	1.27	1.27	1.34
0.15	1.35	1.31	1.31	1.29	1.36
0.25	1.37	1.34	1.33	1.31	1.37
0.50	1.40	1.35	1.34	1.32	1.37
0.75	1.42	1.35	1.34	1.33	1.38
1.00	1.43	1.35	1.35	1.33	1.38
1.50	1.44	1.35	1.35	1.33	1.38

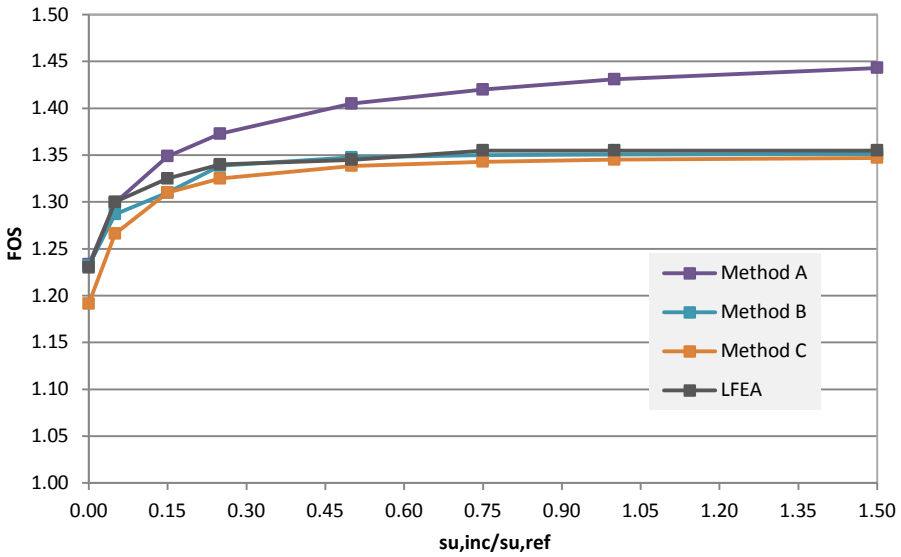

Figure 47: FoS from different calculation methods ($H/D = 1$ and $\sigma_T = 25\ kPa$)

Table 26: Comparison between Plaxis - Method A, B and LFEA$_{mean}$ ($H/D = 1$ and $\sigma_T = 25\ kPa$)

$s_{u,inc}/s_{u,ref}$	Method A	Method B	LFEA $_{mean}$	Diff. A/B	Diff. LFEA/B
0.00	1.23	1.23	1.23	0%	0%
0.05	1.30	1.29	1.30	1%	1%
0.15	1.35	1.31	1.33	3%	1%
0.25	1.37	1.34	1.34	3%	0%
0.50	1.40	1.35	1.35	4%	0%
0.75	1.42	1.35	1.36	5%	0%
1.00	1.43	1.35	1.36	6%	0%
1.50	1.44	1.35	1.36	7%	0%

7.5.4 Parameter set 2: $H/D = 1$ and $\sigma_T = 75\ kPa$

Table 27: FoS for the tunnel face from different calculation methods ($H/D = 1$ and $\sigma_T = 75\ kPa$)

$s_{u,inc}/s_{u,ref}$	Method A	Method B	Method C	Lower Bound	Upper Bound
0.00	1.60	1.60	1.55	1.58	1.62
0.05	1.69	1.68	1.65	1.66	1.70
0.15	1.77	1.74	1.72	1.72	1.76
0.25	1.82	1.75	1.74	1.73	1.78
0.50	1.88	1.77	1.76	1.74	1.79
0.75	1.91	1.77	1.77	1.75	1.80
1.00	1.93	1.77	1.77	1.75	1.80
1.50	1.94	1.78	1.77	1.75	1.81

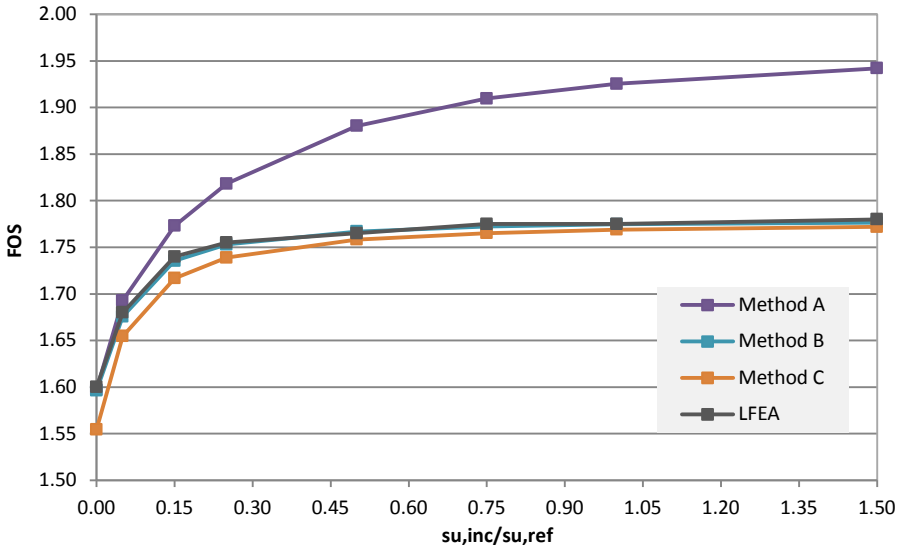

Figure 48: FoS for the tunnel face from different calculation methods ($H/D = 1$ and $\sigma_T = 75\ kPa$)

Table 28: Comparison between Method A, B and LFEA$_{mean}$ ($H/D = 1$ and $\sigma_T = 75\ kPa$)

$s_{u,inc}/s_{u,ref}$	Method A	Method B	LFEA $_{mean}$	Diff. A/B	Diff. LFEA/B
0.00	1.60	1.60	1.60	0%	0%
0.05	1.69	1.68	1.68	1%	0%
0.15	1.77	1.74	1.74	2%	0%
0.25	1.82	1.75	1.76	4%	0%
0.50	1.88	1.77	1.77	6%	0%
0.75	1.91	1.77	1.78	8%	0%
1.00	1.93	1.77	1.78	8%	0%
1.50	1.94	1.78	1.78	9%	0%

7.5.5 Parameter set 3: $H/D = 3$ and $\sigma_T = 25\ kPa$

Table 29: FoS for the tunnel face from different calculation methods ($H/D = 3$ and $\sigma_T = 25\ kPa$)

$s_{u,inc}/s_{u,ref}$	Method A	Method B	Method C	Lower Bound	Upper Bound
0.00	2.00	2.00	1.98	1.97	2.03
0.05	2.09	2.05	2.04	2.02	2.07
0.15	2.14	2.02	2.01	1.98	2.05
0.25	2.14	1.99	1.98	1.96	2.03
0.50	2.14	1.97	1.96	1.93	2.00
0.75	2.14	1.96	1.95	1.92	1.99
1.00	2.14	1.95	1.95	1.92	1.98
1.50	2.14	1.95	1.94	1.91	1.97

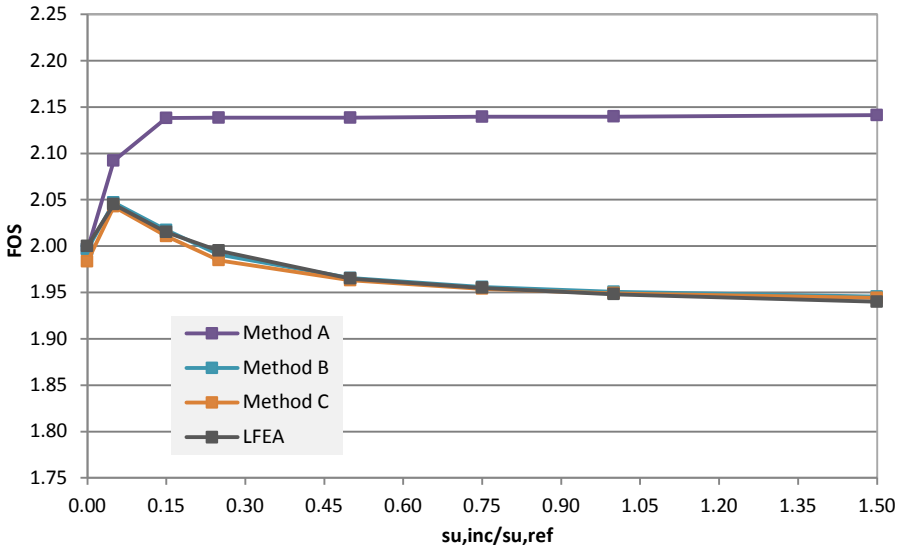

Figure 49: FoS for the tunnel face from different calculation methods ($H/D = 3$ and $\sigma_T = 25\ kPa$)

Table 30: Comparison between Method A, B and LFEA$_{mean}$ ($H/D = 3$ and $\sigma_T = 25\ kPa$)

$s_{u,inc}/s_{u,ref}$	Method A	Method B	LFEA $_{mean}$	Diff. A/B	Diff. LFEA/B
0.00	2.00	2.00	2.00	0%	0%
0.05	2.09	2.05	2.05	2%	0%
0.15	2.14	2.02	2.02	6%	0%
0.25	2.14	1.99	2.00	7%	0%
0.50	2.14	1.97	1.97	9%	0%
0.75	2.14	1.96	1.96	9%	0%
1.00	2.14	1.95	1.95	10%	0%
1.50	2.14	1.95	1.94	10%	0%

7.5.6 Parameter set 3: $H/D = 3$ and $\sigma_T = 75\ kPa$

Table 31: FoS for the tunnel face from different calculation methods ($H/D = 3$ and $\sigma_T = 75\ kPa$)

$s_{u,inc}/s_{u,ref}$	Method A	Method B	Method C	Lower Bound	Upper Bound
0.00	2.21	2.21	2.20	2.19	2.23
0.05	2.32	2.27	2.26	2.25	2.30
0.15	2.37	2.24	2.23	2.20	2.26
0.25	2.37	2.21	2.20	2.17	2.24
0.50	2.37	2.18	2.18	2.14	2.22
0.75	2.37	2.17	2.17	2.13	2.20
1.00	2.37	2.16	2.16	2.12	2.19
1.50	2.37	2.16	2.16	2.11	2.19

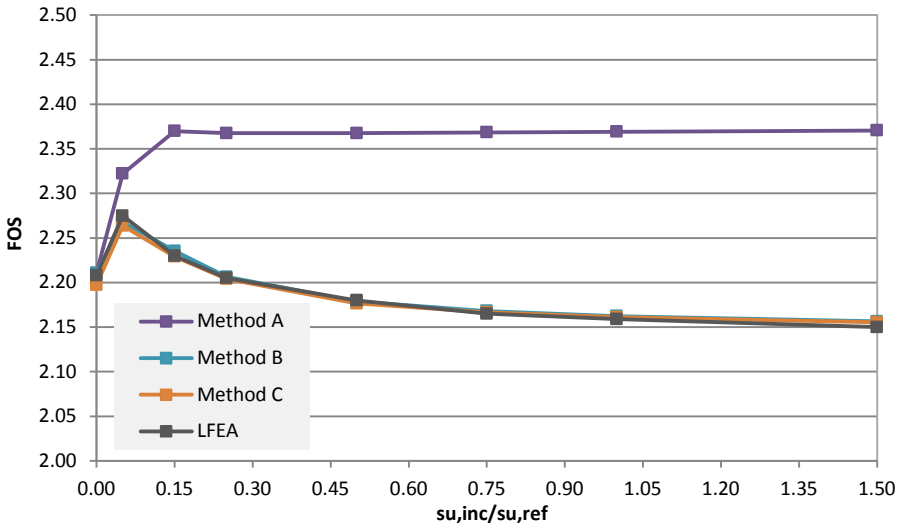

Figure 50: FoS for the tunnel face from different calculation methods ($H/D = 3$ and $\sigma_T = 75\ kPa$)

Table 32: Comparison between Method A, B and LFEA$_{mean}$ ($H/D = 3$ and $\sigma_T = 75\ kPa$)

$s_{u,inc}/s_{u,ref}$	Method A	Method B	LFEA $_{mean}$	Diff. A/B	Diff. LFEA/B
0.00	2.21	2.21	2.21	0%	0%
0.05	2.32	2.27	2.28	2%	0%
0.15	2.37	2.24	2.23	6%	0%
0.25	2.37	2.21	2.21	7%	0%
0.50	2.37	2.18	2.18	9%	0%
0.75	2.37	2.17	2.17	9%	0%
1.00	2.37	2.16	2.16	10%	0%
1.50	2.37	2.16	2.15	10%	0%

8 Pile

8.1 Problem description

This last example is a pile in a homogenous frictional soil under drained conditions. The pile has a height H of 10 m and a diameter D of 1 m. The loads acting on it are 800, 1600, 2400 and 3200 kN respectively. The friction between the material and the pile is 80% ($\tan\varphi * 0.8$) at the sides and a 100% at the bottom of the pile. The geometry of the stability problem is shown in Figure 51.

The primary objective of this stability analysis is to provide a comparison of FELA and SRM-FEA outcomes of a constraint problem with a relatively high friction angle and varying dilatancy angle. In case of LFEA, Davis approach is used to derive Factors of Safety for the materials where the dilatancy angle is less than the corresponding friction angle.

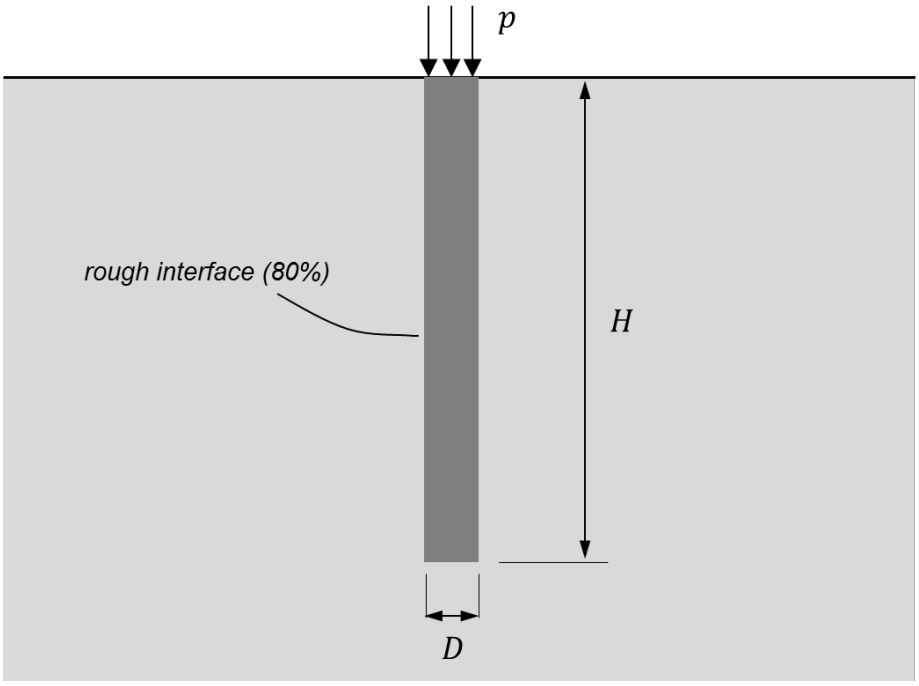

Figure 51: Pile geometry

Note that the problem is modelled in plane strain conditions and not in an axial symmetric manner as one would expect it. This is due to the current limitations of the limit finite element analysis codes, where so far no axisymmetric modelling is possible. Also, the resulting failure mechanism is of little practical importance, since the required deformation is very large. However, the example is still valid to compare and evaluate the results of the methods for a constraint stability problem.

8.2 Parameter description

Table 33 shows the material parameters. 4 different friction angles and 5 different dilatancy angles (each) are considered. The dilatancy angles are set to 0°, 5°, 10°, 20° and in the associated cases equal to the friction angles. Basically, the interface properties are similar to the material properties, though the strength parameters are reduced to 80% of the material values.

Table 33: Material properties

		drained_30_ψ_i	**drained_35_ψ_i**	**drained_40_ψ_i**	**drained_42.5_ψ_i**
γ_{unsat}	[k/m^3]	18	18	18	18
γ_{sat}	[k/m^3]	20	20	20	20
E	[k/m²]	30000	30000	60000	60000
ν '	[-]	0.3	0.3	0.3	0.3
c'	[k/m²]	0	0	0	0
φ'		30	35	40	42.5
ψ_1	[°]	0	0	0	0
ψ_2	[°]	5	5	5	5
ψ_3	[°]	10	10	10	10
ψ_4	[°]	20	20	20	20
ψ_5	[°]	30	35	40	42.5

Table 34: Interface properties

		int_30_ψ_i	**int_35_ψ_i**	**int_40_ψ_i**	**int_42.5_ψ_i**
γ_{unsat}	[k/m^3]	18	18	18	18
γ_{sat}	[k/m^3]	20	20	20	20
E	[k/m²]	30000	30000	60000	60000
ν '	[-]	0.3	0.3	0.3	0.3
c'	[k/m²]	0	0	0	0
φ'		24.79	29.26	33.87	34.34
ψ_1	[°]	0	0	0	0
ψ_2	[°]	4	4	4	4
ψ_3	[°]	8.03	8.03	8.03	8.03
ψ_4	[°]	16.23	16.23	16.23	16.23
ψ_5	[°]	24.79	29.26	33.87	34.34

The reduced values after Davis are not shown explicitly. However, the can be derived using Equations 8 and 9 on the parameters from the above illustrated tables.

8.3 SRM – FEA Properties

8.3.1 Model

Figure 52 shows the SRM-FEA model of the pile. Only one side of the problem is modelled since an axis of symmetry exists. The boundary conditions are determined by standard fixities. The model dimensions measure 25 m in height and 20/ 30 m in width. 20 m for the 2 lower loads and 30 m for higher loads.

The pile itself is 10 m long and 0.5 wide. An interface element is used to model the interaction between pile and material. The interface runs an additional 0.5m from the bottom of the pile into the soil. This is sought to reduce the development of very high stresses beneath the edge of the pile.

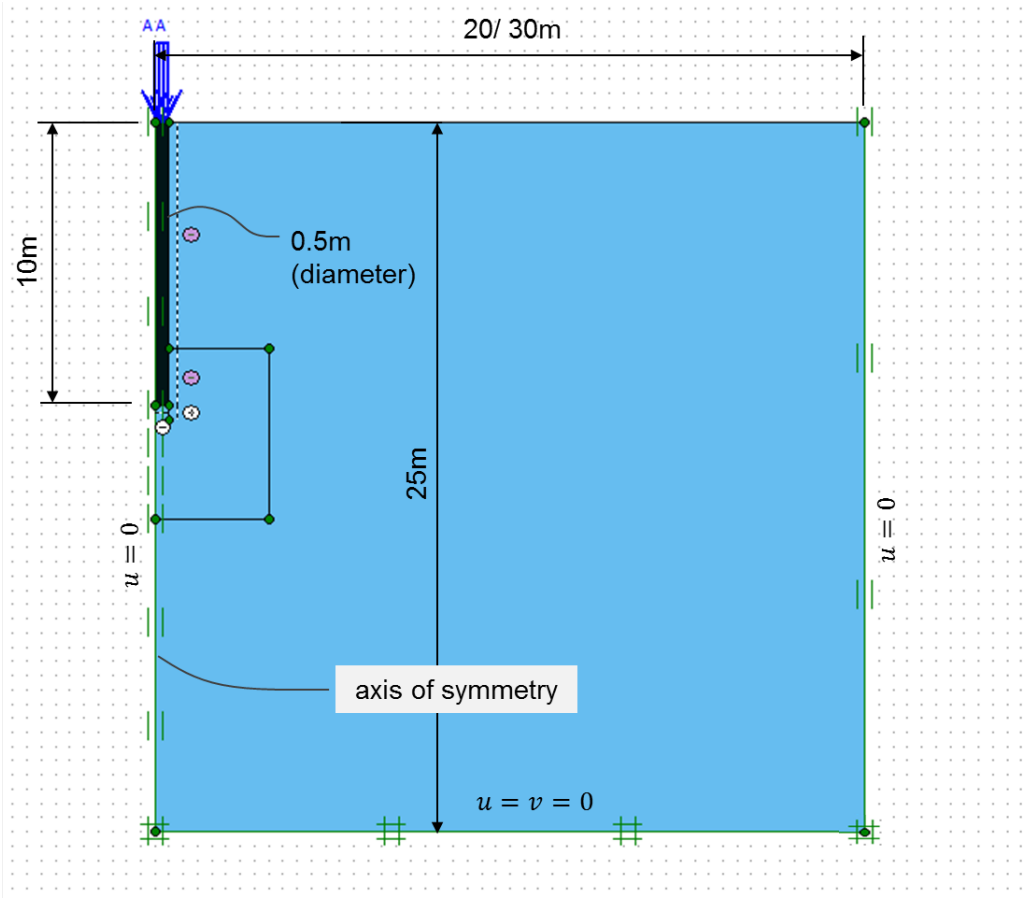

Figure 52: Pile model dimensions in Plaxis

8.3.2 Mesh

The mesh is shown in Figure 53. The elements are 15-noded with a total element number of 3240. The global coarseness is set to *medium* and an additional cluster with finer mesh properties is defined around the bottom of the pile, where large strains are anticipated. Further refinement is done along the sides of the pile for similar reasons.

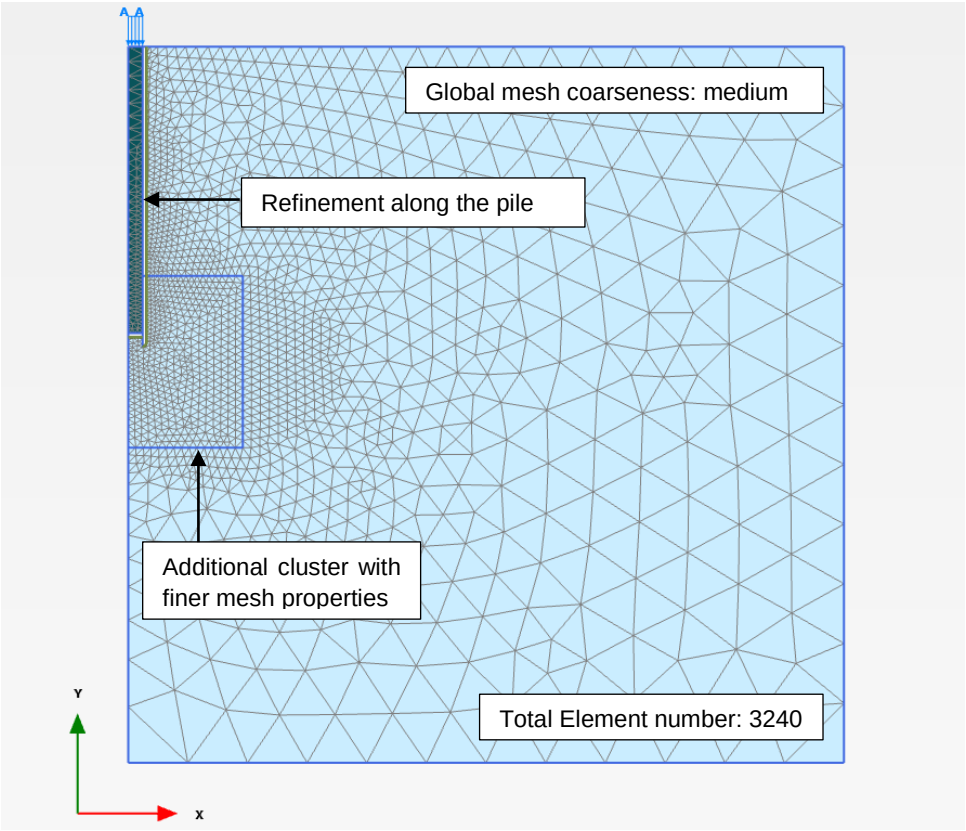

Figure 53: Pile geometry (larger model for the cases $\varphi = 40° \; and \; 42.5°$)

8.3.3 Calculation phases

The initial stress distribution is determined by the *Ko-procedure.* The next stage is the loading stage of the pile, ultimately followed by the strength reduction (safety analysis). The additional calculation steps in the safety analysis are increased to at least 500 steps. The calculation settings of the loading phase are, in some cases, slightly modified to be able to apply the full load on the pile. The modifications are an increased tolerated error of 2% and a switch off of the arc-length control.

8.4 LFEA Properties

8.4.1 Model

The model represents one side of the problem (due to the symmetry). The whole model has a height of 30 m and a width of 40 m. The boundary conditions are both directions fixed at the bottom and the direction normal to the boundary fixed at the sides. Besides that, a fan point is introduced to better cope with possible stress singularities occurring at the edge of the pile.

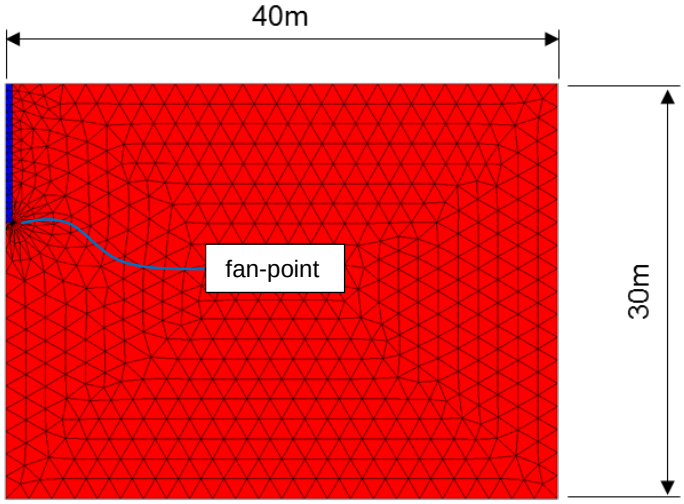

Figure 54: Pile model dimensions for LFEA

8.4.2 Mesh

The meshes (LB and UB) of this stability analysis are generated with the adaptive mesh refinement procedure. The initial mesh has 1000 elements and the final mesh number is 6000. The procedure uses 3 steps. The evolution of the mesh is depending on the resulting failure mechanism (loads and the material). An example is shown in Figure 55.

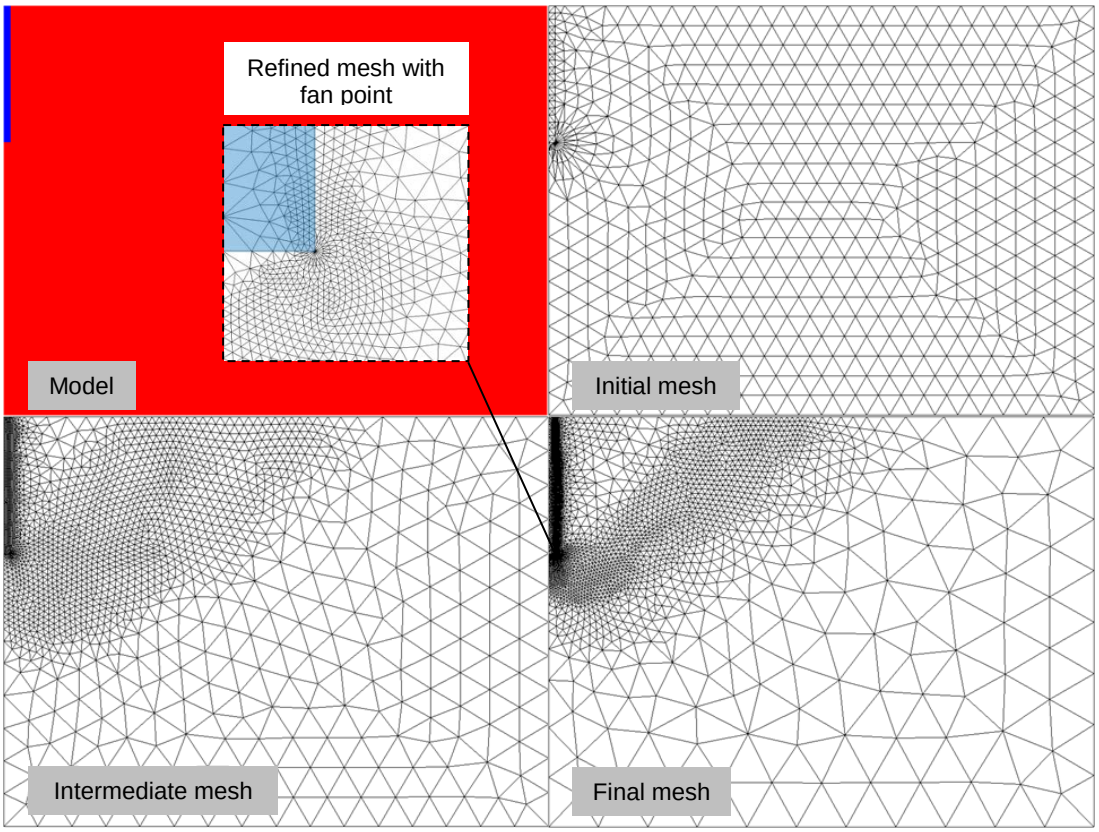

Figure 55: Mesh refinement procedure for the pile (LFEA, P= 1600 kN)

The gaps between the lower and upper bound outcomes (obtained with the final mesh) are smaller than 3% for all cases.

8.5 Results

8.5.1 General

The following table shows the complete list of Factors of Safety obtained with LFEA and Plaxis. In general, the LFEA (standard) outcomes are higher than the Plaxis results. The range is about 10%, but differs slightly depending on the applied load. The non-associated Plaxis results compared to the LFEA outcomes with reduced strength parameters show a different figure. Especially, in case of high friction angles, Davis approach provides lower Safety Factors than obtained with Plaxis. The Plaxis results with low dilatancy angles are similar to the associated outcome, whereas the reduction after Davis leads to considerably different SF´s from LFEA.

Table 35: Factors of Safety obtained with LFEA and Plaxis – Pile stability analysis

		Load= 800 kN			Load= 1600 kN		
φ	ψ	Plaxis	LFEA	diff. %	Plaxis	LFEA	diff. %
30	0	3.15	3.17	1%	2.03	2.05	1%
30	5	3.23	3.30	2%	2.12	2.14	1%
30	10	3.25	3.42	5%	2.15	2.21	3%
30	20	3.25	3.59	10%	2.16	2.33	8%
30	30	3.25	3.66	13%	2.16	2.37	10%
35	0	3.82	3.64	-5%	2.46	2.35	-4%
35	5	3.90	3.81	-0.02	2.56	2.47	-4%
35	10	3.94	3.98	0.01	2.60	2.58	-1%
35	20	3.94	4.25	8%	2.62	2.75	5%
35	35	3.94	4.44	13%	2.62	2.87	10%
40	0	4.58	4.08	-11%	2.95	2.64	-
40	5	4.69	4.30	-8%	3.07	2.78	-9%
40	10	4.72	4.52	-4%	3.12	2.93	-6%
40	20	4.72	4.91	4%	3.14	3.18	1%
40	40	4.72	5.31	13%	3.14	3.44	10%
42.5	0	no solution	4.28	-	no solution	2.77	-
42.5	5	no solution	4.53	-	3.35	2.94	-12%
42.5	10	5.16	4.78	-7%	3.41	3.09	-9%
42.5	20	5.16	5.23	1%	3.43	3.39	-1%
42.5	42.5	5.16	5.81	13%	3.43	3.76	10%

		Load= 2400 kN			Load= 3200 kN		
φ	ψ	Plaxis	LFEA	diff. %	Plaxis	LFEA	diff. %
30	0	no solution	1.65	-	no solution	1.43	-
30	5	1.69	1.71	1%	no solution	1.49	-
30	10	1.73	1.77	2%	1.51	1.54	2%
30	20	1.75	1.87	7%	1.52	1.62	7%
30	30	1.75	1.90	9%	1.52	1.65	9%
35	0	no solution	1.89	-	no solution	1.64	-
35	5	2.06	1.98	-4%	no solution	1.72	-
35	10	2.10	2.06	-2%	1.82	1.80	-1%
35	20	2.12	2.21	4%	1.85	1.92	4%
35	35	2.12	2.3	8%	1.85	2.01	9%
40	0	no solution	2.12	-	no solution	1.84	-
40	5	2.49	2.23	-10%	no solution	1.94	-
40	10	2.52	2.34	-7%	2.20	2.04	-7%
40	20	2.54	2.55	0%	2.22	2.22	0%
40	40	2.54	2.76	9%	2.22	2.4	8%
42.5	0	no solution	2.22	-	no solution	1.93	-
42.5	5	2.69	2.35	-13%	no solution	2.05	-
42.5	10	2.74	2.48	-9%	2.39	2.16	-10%
42.5	20	2.78	2.72	-2%	2.42	2.36	-2%
42.5	42.5	2.78	3.02	9%	2.42	2.62	8%

In some cases, Plaxis could not obtain a solution. This happened only with no or very low dilatancy angles. However, the actual reason is not straight forward. Sometimes, the full load could not be applied. In other instances, the strength reduction resulted in an unrealistic deformation field. Figure 56 shows the plastic point output of Plaxis at failure. On the left side the material with a dilatancy angle of 0 failed during the loading stage whereas the right side shows the outcome of the strength reduction of the similar material with an associated flow rule and a Factor of Safety of 1.65.

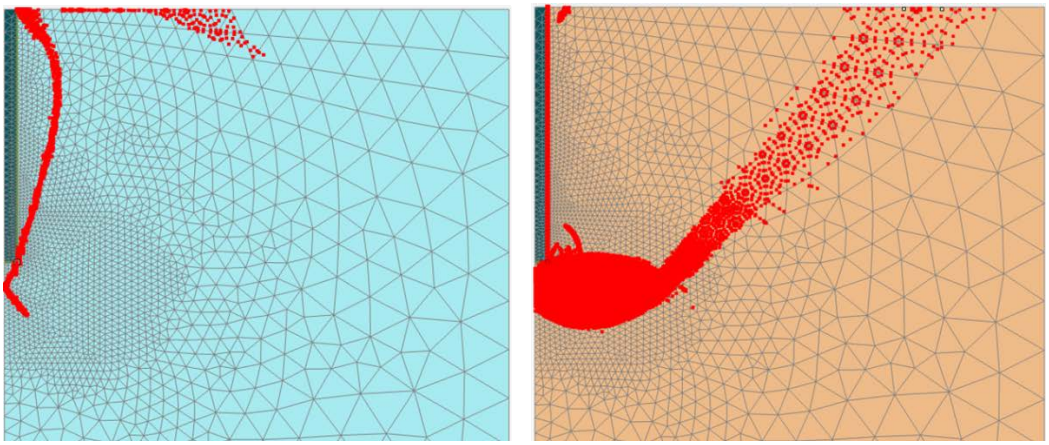

Figure 56: Plastic point outputs at failure during the load stage and after the strength reduction.

Figure 57 shows the Safety Factor vs. displacements obtained from a strength reduction with 500 steps. The behaviour looks abnormal and is in this case due to an error occurring at the top of the pile, where a few points show unrealistic excessive displacements.

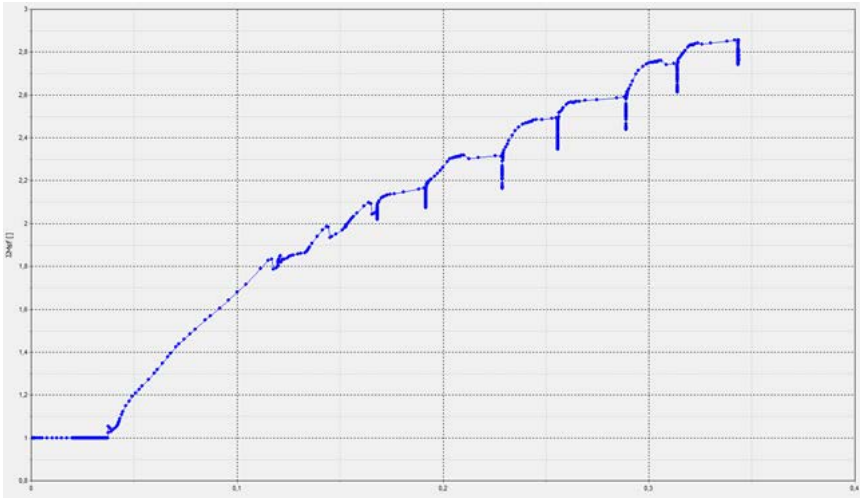

Figure 57: Strength reduction output where no true failure mechanism could be obtained

8.5.2 Failure mechanisms

Basically the failure mechanisms coincide well, as shown in Figure 58. However, LFEA can only obtain the ultimate soil failure, which is in case of the pile, from a practical point of view of little importance, since the deformation required to produce this kind of failure is simply too large for most structures. Plaxis on the other hand, would be apple to consider a certain deformation as the limiting case. However, in this stability analysis only the ultimate case is compared.

The outputs A to F in Figure 58 are the following:

- A: Plaxis – deformed mesh
- B: Plaxis – plastic points
- C: LFEA – velocity field (upper bound)
- D: Plaxis – deviatoric strains
- E: LFEA – failure mechanism with plastic contours (upper bound)
- F: LFEA – failure mechanism with plastic contours (lower bound)

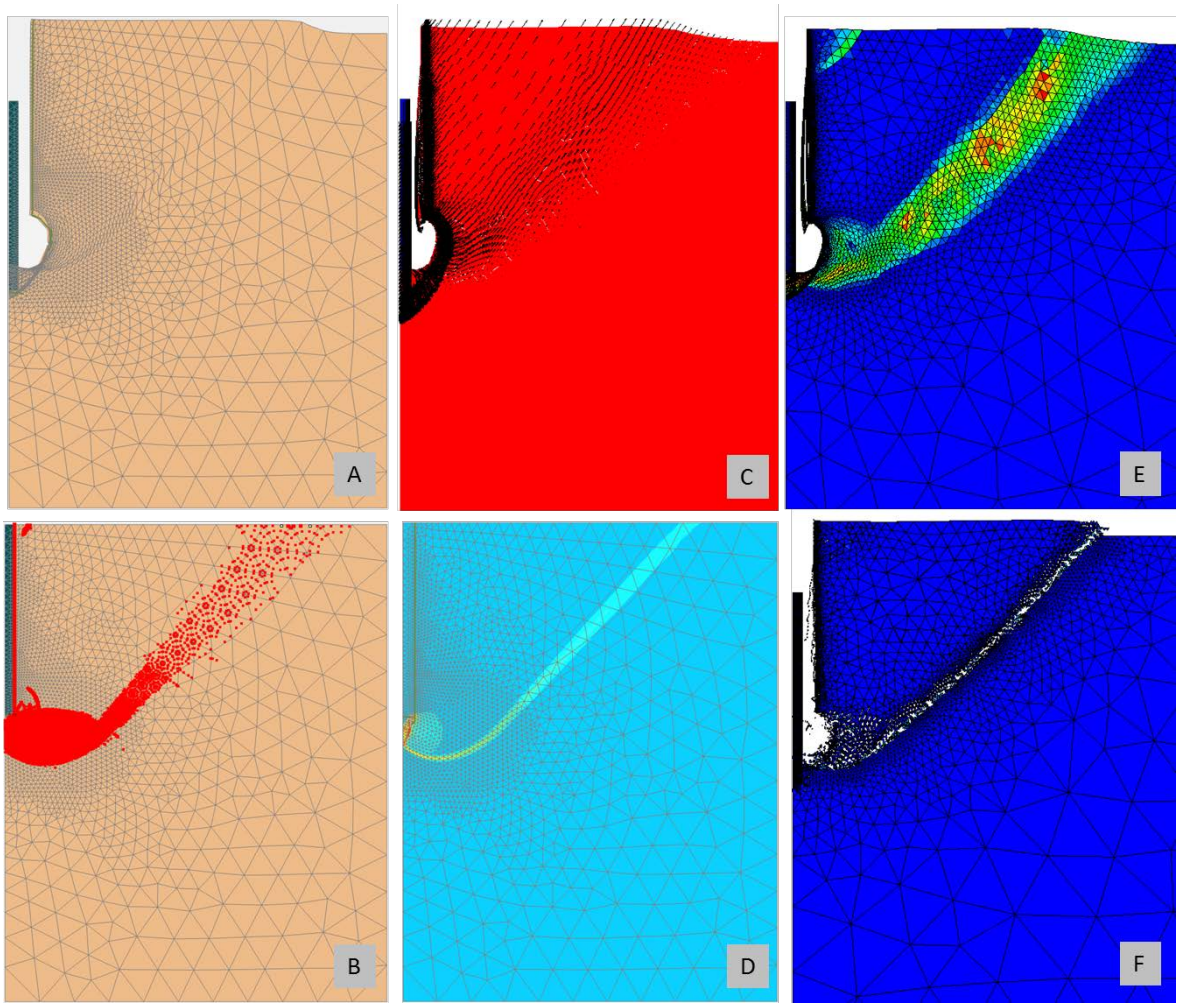

Figure 58: Pile – Comparison of failure the failure mechanisms

It is important to note that, there are 4 limit strength parameters according to the 4 applied loads under LFEA and 4*5 with Plaxis due to the different dilatancy angels. The various friction angles only represent different starting points in the strength reduction procedure.

An favourable aspect, is the fact that the Plaxis outcomes $\varphi = 30\_\psi_i$, $\varphi = 35\_\psi_i$, $\varphi = 40\_\psi_i$ and $\varphi = 42.5\_\psi_i$ of one load should all yield similar limit strength parameters. Thus, the results can be double checked. The outcomes are shown below in the following sections of each load.

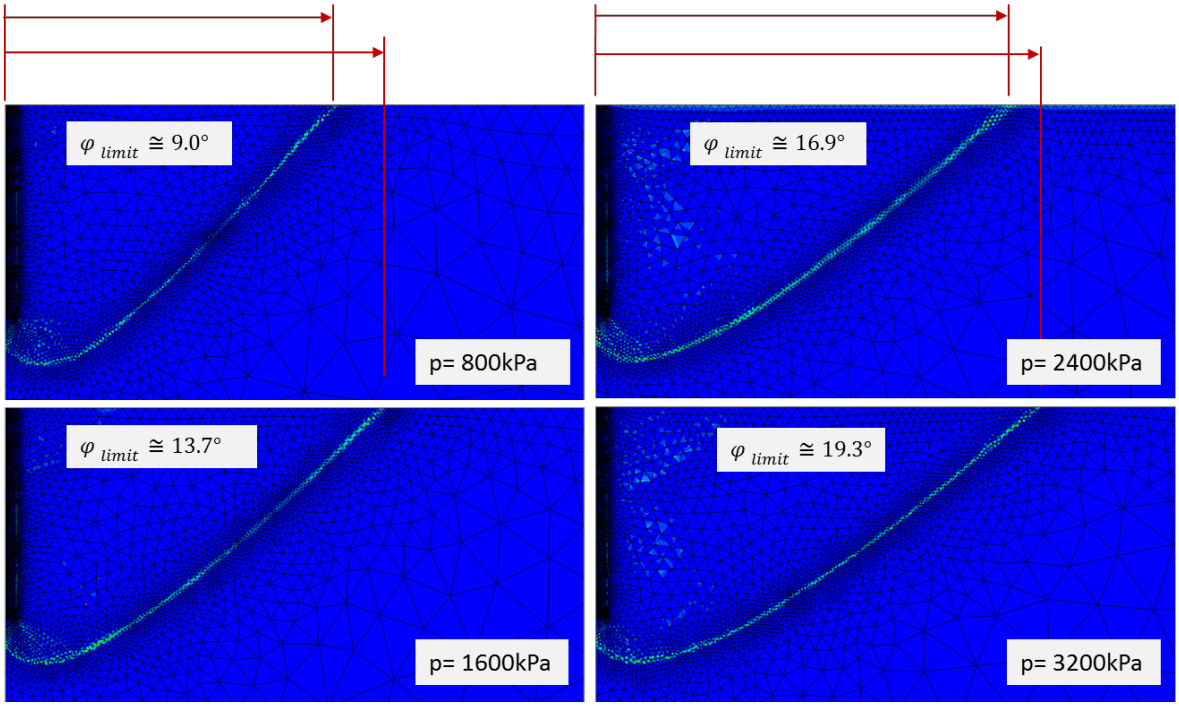

Figure 59: Comparison between the failure mechanisms of the 4 different loads (LFEA)

Figure 59 illustrates the 4 different failure mechanism obtained with LFEA. The smallest load provides the least limit friction angle and therefore the shortest failure surface through the soil. Accordingly, the higher loads result in higher limit friction angles and different failure characteristics.

Lastly, before the Factors of Safety and limit friction angles are shown individually for each load, one interesting aspect about the strength reduction procedure in Plaxis should be pointed out again. As explained in section 5.5 the dilatancy angle is kept constant during the strength reduction until the reduced friction angle is equal to it. As a result, the ratio between dilatancy angle and friction angle changes. A problem with an initially defined non-associated flow rule can become a problem with an associated flow rule in the limit case. The following results show this feature clearly, since all Factors of Safety where the limit friction angle is below the initial dilatancy angle are equal to the associated outcomes.

8.5.3 Load 800 kN

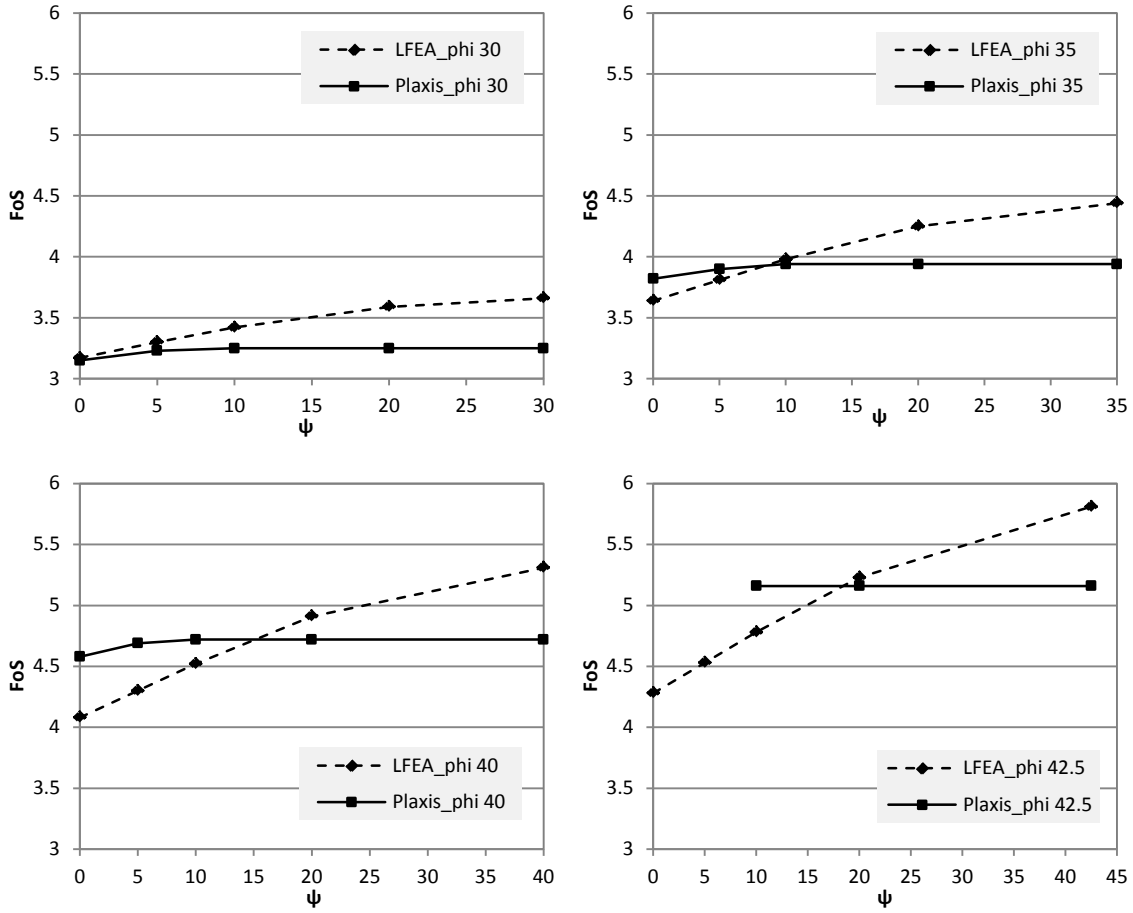

Figure 60: LFEA and Plaxis SF´s obtained with different friction and dilatancy angles (Load= 800kN)

Table 36: Limit friction angles calculated with LFEA and Plaxis (Load= 800kN)

φ	ψ	Plaxis - φ_{limit}	LFEA - φ_{limit}	φ	ψ	Plaxis - φ_{limit}	LFEA - φ_{limit}
30	0	10.39	10.32	40	0	10.38	11.62
30	5	10.13	9.92	40	5	10.14	11.04
30	10	10.07	9.58	40	10	10.08	10.52
30	20	10.07	9.14	40	20	10.08	9.70
30	30	10.07	8.96	40	40	10.08	8.98
35	0	10.39	10.89	42.5	0	no solution	12.08
35	5	10.18	10.41	42.5	5	no solution	11.44
35	10	10.08	9.98	42.5	10	10.07	10.85
35	20	10.08	9.36	42.5	20	10.07	9.94
35	35	10.08	8.96	42.5	42.5	10.07	8.96

8.5.4 Load 1600 kN

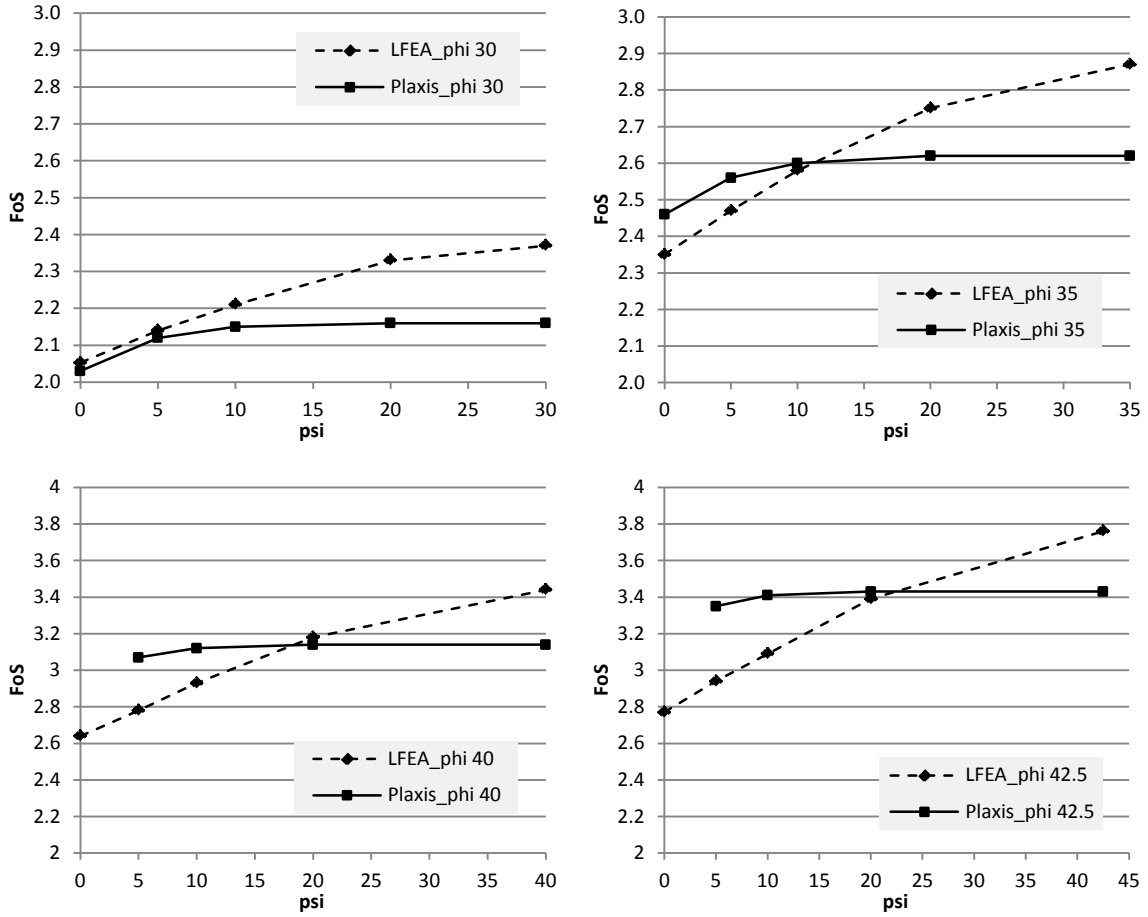

Figure 61: LFEA and Plaxis SF´s obtained with different friction and dilatancy angles (Load= 1600kN)

Table 37: Limit friction angles calculated with LFEA and Plaxis (Load= 1600kN)

φ	ψ	Plaxis - φ_{limit}	LFEA - φ_{limit}	φ	ψ	Plaxis - φ_{limit}	LFEA - φ_{limit}
30	0	15.88	15.71	40	0	no solution	17.63
30	5	15.23	15.10	40	5	15.29	16.80
30	10	15.03	14.64	40	10	15.05	15.98
30	20	14.96	13.92	40	20	14.96	14.78
30	30	14.96	13.69	40	40	14.96	13.71
35	0	15.89	16.59	42.5	0	no solution	18.30
35	5	15.30	15.83	42.5	5	15.30	17.31
35	10	15.07	15.18	42.5	10	15.04	16.52
35	20	14.96	14.29	42.5	20	14.96	15.13
35	35	14.96	13.71	42.5	42.5	14.96	13.70

8.5.5 Load 2400 kN

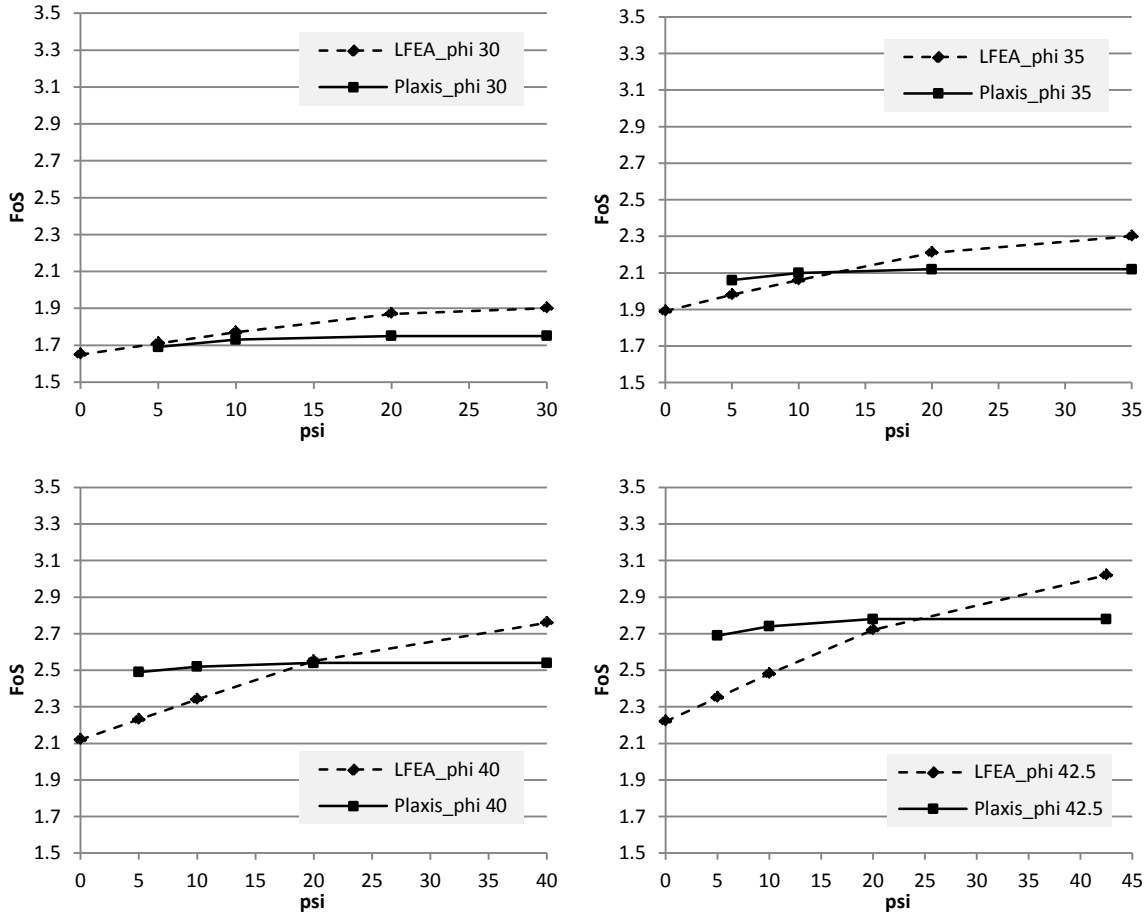

Figure 62: LFEA and Plaxis SF´s obtained with different friction and dilatancy angles (Load= 2400kN)

Table 38: Limit friction angles calculated with LFEA and Plaxis (Load= 2400kN)

φ	ψ	Plaxis - φ_{limit}	LFEA - φ_{limit}	φ	ψ	Plaxis - φ_{limit}	LFEA - φ_{limit}
30	0	no solution	19.29	40	0	no solution	21.59
30	5	18.86	18.66	40	5	18.62	20.62
30	10	18.46	18.07	40	10	18.42	19.73
30	20	18.26	17.16	40	20	18.28	18.21
30	30	18.26	16.90	40	40	18.28	16.91
35	0	no solution	20.33	42.5	0	no solution	22.43
35	5	18.77	19.48	42.5	5	18.81	21.30
35	10	18.44	18.77	42.5	10	18.49	20.28
35	20	18.28	17.58	42.5	20	18.24	18.62
35	35	18.28	16.93	42.5	42.5	18.24	16.88

8.5.6 Load 3200 kN

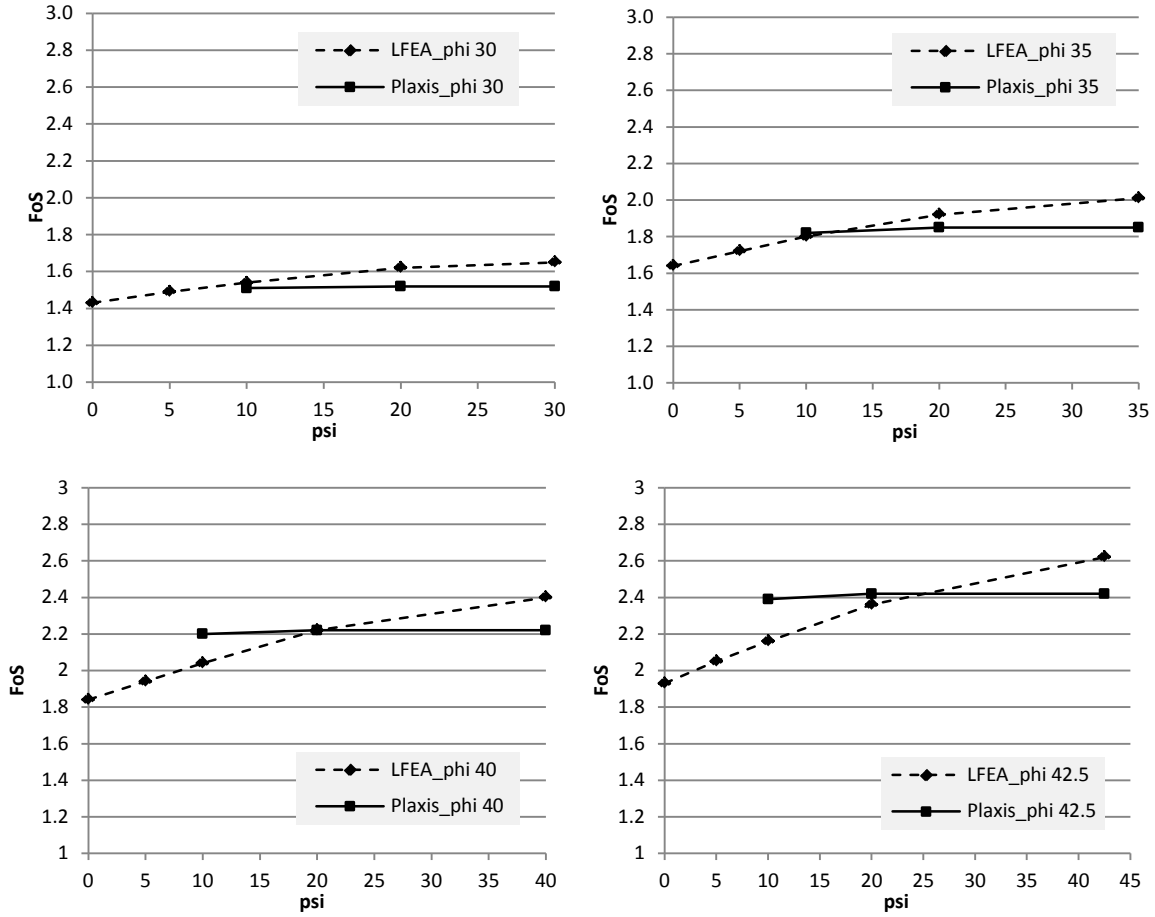

Figure 63: LFEA and Plaxis SF´s obtained with different friction and dilatancy angles (Load= 3200kN)

Table 39: Limit friction angles calculated with LFEA and Plaxis (Load= 3200kN)

φ	ψ	Plaxis - φ_{limit}	LFEA - φ_{limit}	φ	ψ	Plaxis - φ_{limit}	LFEA - φ_{limit}
30	0	no solution	21.99	40	0	no solution	24.51
30	5	no solution	21.18	40	5	no solution	23.39
30	10	20.92	20.55	40	10	20.88	22.36
30	20	20.80	19.62	40	20	20.71	20.71
30	30	20.80	19.29	40	40	20.71	19.27
35	0	no solution	23.12	42.5	0	no solution	25.40
35	5	no solution	22.15	42.5	5	no solution	24.08
35	10	21.04	21.26	42.5	10	20.98	22.99
35	20	20.73	20.04	42.5	20	20.74	21.22
35	35	20.73	19.21	42.5	42.5	20.74	19.28

References

A., C. C. (1773). Sur une application des regles de maximis et minimis a quelques problemes de statique relatifs a l'architecture. *Acad. R. Sci. Mem. Math. Phys. par divers savants, 7* , 343-382.

Augarde C. E., L. A. (2003). Stability of an undrained plane strain heading revisited. *Computers and Geotechnics, 30*, 419-430.

Brinkgreve R.B.J., S. W. (2010). *PLAXIS 2D 2010 - General Information.* Delft, Netherlands : Plaxis bv.

Chen W.F. (2008). *Limit Analysis and Soil Plasticity.* Fort Lauderdale: J.Ross Publisching.

Cheng Y. M., L. T. (2007). Two-dimensional slope stability analysis by limt equilibrium and strength reduction methods. *Computers and Geotechnics 34*, S. 137-150.

Davis E. H. (1968). Theory of Plasticity and Failure of Soil Masses. *Soil Mechanics Selected Topics*, pp. 341-354.

Donald I.B., G. P. (1989). *Soil slope stability programs review.* Melbourne: Association for Computer Aided Design (ACADS).

Drucker D.C., G. H. (1951). The safety factor of an elastic-plastic body in plane strain. *Appl. Mechanics*, 371-378.

Drucker D.C., G. H. (1952). Extended limit design thoerems for continuous media. *Appl. Math.*, 381-389.

H., T. (1868). Memoire sur l'ecoulement des corps solides. *Acd. R. Sci. Mem. Math. Phys. par divers savants, 18*, 733-799.

Lyamin A. V., S. S. (2002a). Lower bound limit analysis using nonlinear programming. *International Journal for Numerical Methods in Engineering*, 55(5), 573-611.

Lyamin A. V., S. S. (2002b). Upper bound limit analysis using linear finite elements and nonlinear programming. *International Journal for Numerical and Analytical Methods in Geomechanics*, 26(2), 181-216.

Lyamin A. V., S. S. (2005). Lower bound limit analysis with adaptive remeshing. *International Journal for Numerical Methods in Engineering 63*, S. 1961-1974.

Mohr O. (1882). Ueber die Darstellung des Spannungszustandes und des Deformationszustandes eines Körperelements. *Zivilingenieur*, 113-156.

R., V. M. (1928). Mechanik der plastischen Formaenderung von Kristallen. *Z. Angew. Math. Mech, 8*, 161-185.

Sloan S. W. (2004). *Geotechnical stability analysis: new methods for an old problem .* Australian Geomechanics Society, Australia.

Sloan S., L. A. (2006). 1D, 2D and 3D computer codes for quasi-upper bound and quasi-

lower bound shakedown analysis using nonlinear programming. Geosential Software Pty Ltd.

Sloan S., L. A. (2007). 1D, 2D and 3D programs for upper and lower bound limit analysis using nonlinear programming. Geosential Software Pty Ltd.

Terzaghi K. (1943). *Theoretical Soil Mechanics.* New York: Wiley.

Terzaghi K., P. R. (1996). *Soil Mechanics in Engineering Practice.* John Wiley & Sons, Inc.

Yamamoto K., L. A. (2011). Stability of circular tunnel in cohesive-frictional soil subjected to surcharge loading. *Computers and Geotechnics, 38*, 504 - 514.

Yu H. S., S. R. (1988). Limit analysis versus limit equilibrium for slope stability. *Journal of Geotechnical and Geoenvironmental engineering, 124, No. 1*.

Figures